Deciphering the Molecular Nexus: RNF20 as a Critical Mediator at the Epigenetics-Metabolism Interface in Driving Lung Cancer Progression

INAUGURALDISSERTATION

zur Erlangung des Doktorgrades der Naturwissenschaften

- Doctor rerum naturalium -

(Dr. rer. nat.)

eingereicht am Fachbereich Biologie und Chemie der

Justus-Liebig-Universität Giessen

vorgelegt von

Anshu Singh

Mannheim, 2023

Die vorliegende Arbeit wurde am Max-Planck-Institut für Herz- und Lungenforschung Bad Nauheim und Centrum für Biomedizin und Medizintechnik Mannheim der Abteilung **"Anatomie und Entwicklungsbiologie"** unter der leitung von **Frau Prof. Dr. Gergana Dobreva** angefertigt.

Erstgutachter:
Prof. Dr. Reinhard Dammann
Institut für Genetik
Justus-Liebig-Universität Giessen
Heinrich-Buff-Ring 58, 35392 Giessen
Germany

Zweitgutachter:
Prof. Dr. Gergana Dobreva
Department of Anatomy and Developmental Biology
Medical Faculty of Mannheim, University of Heidelberg
Ludolf-Krehl-Str. 7-11
68167 Mannheim
Germany

Disputation am 06/03/2024

DEDICATED TO MY

PARENTS, HUSBAND AND DAUGHTER

Who inspired and believed in me for higher ambition in life

Table of Contents

List of Figures

ABSTRAKT

Lungenkrebs ist die häufigste Krebserkrankung und die Hauptursache für krebsbedingte Todesfälle bei Männern und Frauen in der ganzen Welt. Trotz der Fortschritte bei den Behandlungsmöglichkeiten von Lungenkrebs verläuft die Sterblichkeitsrate parallel zur Inzidenzrate. Lungenkrebs ist eindeutig ein globaler Notfall, der sofortige Aufmerksamkeit erfordert.

In Säugetierzellen ist das Ringfingerprotein 20 (RNF20) die wichtigste H2B-spezifische Ubiquitin-Ligase. Seine Hauptfunktion ist die Monoubiquitinierung von Histon H2B an Lysin 120 (H2Bub). Auf zellulärer Ebene unterdrückt RNF20 die Expression mehrerer Proto-Onkogene, die sich bevorzugt in geschlossenem Chromatin befinden und nur in geringem Maße transkribiert werden. Einerseits haben Zellkulturstudien gezeigt, dass eine Reduktion von RNF20 die Transkriptionseffekte des epidermalen Wachstumsfaktors (EGF) verstärkt, die Zellmigration fördert und Transformation und Krebs induziert [1]. Andererseits hat sich herausgestellt, dass RNF20 für MLL-veränderte Leukämie erforderlich ist. Trotz mehrerer Fortschritte bei der Erforschung der Funktion von RNF20 bei der Krebsentstehung ist seine Rolle nach wie vor umstritten. Daher habe ich versucht, Licht in die Krebsentwicklung und -progression zu bringen.

Um die Rolle von RNF20 bei der Krebsentwicklung zu untersuchen, habe ich ein genetisches Mausmodell für den Funktionsverlust von Rnf20 (LOF) verwendet. Die globale Ablation von Rnf20 führte zur embryonalen Letalität vor der Implantation. Interessanterweise waren Rnf20+/- Mäuse lebensfähig und fruchtbar, wiesen aber eine signifikant höhere Inzidenz von spontanen Tumoren in der Lunge auf. Die immunhistochemische Analyse ergab, dass diese spontanen Lungentumore dem Phänotyp des kleinzelligen Lungenkrebses (SCLC) und des Adenokarzinoms angehörten. SCLCs waren am häufigsten. Für die mechanistische Charakterisierung verwendete ich ein in vitro Zellkulturmodell. Ich habe MLE-12-Zellen mit Rnf20-Funktionsverlust durch crispr-Cas9 sowie siRNA-vermittelte Ausschaltung von Rnf20 in NCL-H82-Zellen hergestellt. In Zellkulturtests entdeckte ich, dass die Deletion von RNF20 einen epithelial-mesenchymalen Übergang (EMT) auslöste und die Zellmigration und -

invasion erleichterte. In Rnf20-depletierten Zellkulturmodellen stellte ich eine Zunahme von DNA-Schäden und eine verzögerte DNA-Schadensreparatur fest, was auch in den Lungen von Rnf20+/- Mäusen bestätigt wurde. Tests zur Glukoseaufnahme, Laktatsekretion und extrazellulären Säuerungsrate (ECAR) in RNF20-depletierten Zellen ergaben, dass eine RNF20-Depletion die glykolytische Aktivität in Lungenzellen erhöht. Darüber hinaus ergab die Erstellung von Metabolomics-Profilen einen signifikanten Anstieg der Metaboliten nach RNF20-depletion.

Neueste Forschungen haben gezeigt, dass die Überexpression von HIF1a eine wichtige Rolle beim Tumorwachstum und bei der Metastasierung spielt, indem sie die Angiogenese initiiert und den Zellstoffwechsel reguliert, um Hypoxie zu überwinden. In meiner Forschung habe ich herausgefunden, dass die Abreicherung von RNF20 die HIF1a-Konzentration in Lungenzellen deutlich erhöht. Darüber hinaus wird der HIF1a-Signalweg aktiviert, wenn RNF20 entfernt wird. Infolgedessen verändert sich das Stoffwechselprofil von Rnf20-LOF-Zellen drastisch, ebenso wie ihre Invasions- und Migrationsfähigkeit. Nachdem ich Hif1a ausgeschaltet hatte, konnte ich den glykolytischen und invasiven Phänotyp der Rnf20-LOF-Zellen teilweise wiederherstellen.

Zusammenfassend lässt sich sagen, dass meine Studie eine wichtige Rolle für die RNF20-HIF1a-Achse bei der kritischen metabolischen Umprogrammierung im Lungenkarzinom aufgedeckt hat, was darauf hindeutet, dass diese Proteine potenzielle Ziele für therapeutische Maßnahmen bei Lungenkrebs sind.

ABSTRACT

Lung cancer is the most common cancer and the leading cause of cancer-related deaths in both men and women around the world. Despite advances in lung cancer treatment options, the mortality rate closely parallels the incidence rate. Lung cancer is clearly a global emergency that requires immediate attention.

In mammalian cells, the ring finger protein 20 (RNF20) is the major H2B-specific ubiquitin ligase. Its primary function is to monoubiquitinate histone H2B on lysine 120 (H2Bub). On a cellular level, RNF20 suppresses the expression of several proto-oncogenes, which reside preferentially in closed chromatin and are modestly transcribed. On one hand cell culture based studies have shown that, RNF20 reduction enhanced the transcriptional effects of epidermal growth factor (EGF), boost cell migration, and induced transformation and cancer [1]. On the other hand, RNF20 is found to be required for MLL-rearranged leukemia. Despite several advancements in the study of RNF20 function in cancer development, its role is still debatable. As a result, I sought to shed light on the cancer development and progression.

To study the role of RNF20 in cancer development, I used a genetic mouse model of *Rnf20* loss of function (LOF). Global ablation of *Rnf20* caused pre-implantation embryonic lethality. Interestingly, *Rnf20*+/- mice were viable and fertile but had a significantly higher incidence of spontaneous tumors in the lungs. Immunohistochemical analysis revealed that these spontaneous lung tumors belonged to the small cell-like lung cancer (SCLC) phenotype and adenocarcinoma. SCLCs were more common. For the mechanistic characterization, I used an *in vitro* cell culture model. I made *Rnf20* loss of function MLE-12 cells by crispr-Cas9 as well as siRNA mediated silencing of *Rnf20* in NCL-H82 cells. In cell culture assays, I discovered that RNF20 depletion induced epithelial-mesenchymal transition (EMT) and facilitated cell migration and invasion. I noticed an increase in DNA damage in *Rnf20*-depleted cell culture models and delayed DNA damage repair, which was also confirmed in the lungs of *Rnf20*+/- mice. Glucose uptake, lactate secretion, and extracellular acidification rate (ECAR) assays in RNF20 depleted cells revealed that RNF20 depletion increased glycolytic activity in lung cells. Furthermore, metabolomics

profiling revealed a significant increase in the level of metabolites following RNF20 depletion.

Recent research has shown that HIF1a overexpression plays a significant role in tumor growth and metastasis by initiating angiogenesis and regulating cellular metabolism to overcome hypoxia. In my research, I discovered that RNF20 depletion significantly increased the level of HIF1a in lung cells. Furthermore, when RNF20 is depleted, the HIF1a signaling pathway is activated, and as a result, the metabolic profile of *Rnf20* LOF cells is dramatically altered, as is their invasive and migratory ability. After knocking down *Hif1a*, I was able to partially rescue the glycolytic and invasive phenotype of *Rnf20* LOF cells.

In conclusion, my study revealed an important role for the RNF20-HIF1a axis for critical metabolic reprogramming in lung carcinoma, pointing to these proteins as potential targets for lung cancer therapeutic intervention.

Chapter 1: INTRODUCTION

1.1 Lung cancer

The latest World Health Organization (WHO) cancer report predicts a dramatic rise in cancer incidence, doubling within the next two decades. Lung cancer is the most frequent cancer and the leading cause of cancer related deaths in men and women worldwide. Globocan estimated 2.09 million new cases and 1.76 million deaths due to lung cancer in 2018. The main risk factors for lung cancer include lifestyle factors (e.g. tobacco smoking), genetic factors, lung infections, chronic lung disease (e.g. fibrosis), as well as environmental and occupational exposures (e.g. air pollution, asbestos) [2]. Currently lung cancer patients are treated with surgery, chemotherapy, radiation therapy, targeted therapy, or combinations of these treatments [3]. Despite advances in treatment options for lung cancer, the mortality rate closely parallels the incidence rate. It is clear that lung cancer is an urgent global challenge and requires immediate attention.

1.2 Classification of Lung cancer

Histopathologically, lung tumors are classified as non-small cell lung cancer (NSCLC) and small cell carcinoma (SCLC). The most common type of lung cancer, accounting for 85 percent of cases, is NSCLC [4]. Squamous cell carcinoma (SSC), adenocarcinoma, and large cell carcinoma are the three types of NSCLC.

Adenocarcinoma is divided into five subtypes: acinar, papillary, bronchioloalveolar, solid adenocarcinoma with mucin, and adenocarcinoma with mixed subtypes [5]. They are mostly found on the periphery. Endobronchial tumor that arises from the central portion of the respiratory tree is extremely rare [6]. Furthermore, Squamous cell carcinomas can be classified as keratinizing, non keratinizing, or basaloid types, and these tumors are unambiguously positive for P40 and P63 by immunohistochemical analysis [7]. Pathologists have recently begun to reclassify large cell carcinoma into adenocarcinoma, small cell carcinoma, and other subtypes as a result of the inclusion of TTF1, P40, and other genes into diagnosis [8].

SCLC, large cell neuroendocrine tumors (LCNEC), and carcinoids are all classified as neuroendocrine tumors due to their neuroendocrine cells of origin. Carcinoid tumors have

fewer genetic abnormalities and a lower rate of mitosis and necrosis than SCLC and LCNEC [7].

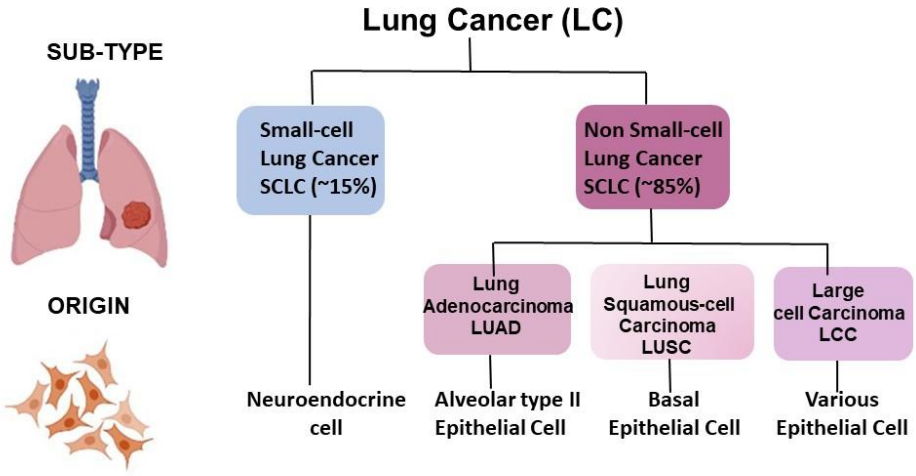

Figure 1. Classification of Lung cancer (Adapted from Ortega et al. Cells. 2021. Small cell lung cancer (SCLC; 15% of cases) and Non small cell lung cancer (NSCLC; 85% of cases) are the two most common types of lung cancer. The neuroendocrine cell lineage gives rise to SCLC tumors. The origin of tumor cells in NSCLC, on the other hand, is categorized into three sub-types. Adenocarcinoma (LUAD; alveolar type II epithelial cell), Squamous cell Carcinoma (LUSC; basal epithelial cell), and Large-cell Carcinoma (LUSC; basal epithelial cell) (LCC; various epithelial cells).

1.2.1 Non-small cell lung cancer

Non-small-cell lung cancer (NSCLC) accounts for over 85% of cases, and despite advances in treatment, the majority of patients are detected at an advanced stage, with a five-year survival rate of roughly 15% [9], [10], [11]. The greatest risk factor for developing this disease is tobacco smoking, but radon exposure and air pollution also play a role. Management strategies for NSCLC includes surgery, radio chemotherapy, immunotherapy and targeted approaches with anti angiogenic monoclonal antibodies or Tyrosine kinase inhibitors if tumors harbor oncogenic mutations. Several driver mutations have been identified in for example epidermal growth factor receptor (EGFR) and anaplastic lymphoma kinase (ALK) genes, and therapy to combat acquired resistance

continues to advance [12]. EGFR belongs to a receptor tyrosine kinase family that also includes human epidermal growth factor receptor 2 (HER2, HER3 and HER4) Gefitinib and erlotinib, epidermal growth factor receptor tyrosine kinase inhibitors (EGFR TKIs), are reversible competitive inhibitors of EGFR's tyrosine kinase domain that attach to its adenosine-5' triphosphate-binding site. In patients with NSCLC, somatic activating mutations in the EGFR gene, increased gene copy number, and specific clinical and pathological characteristics have been linked to dramatic tumor responses and improved clinical outcomes with these medicines (NSCLC) [13]. Around 5-7% of NSCLC cases harbor an ALK fusion gene and may benefit from ALK inhibitor therapy [14]. KRAS mutations is the most frequent molecular alterations found in advanced NSCLC. In non-small cell lung cancer (NSCLC), KRAS is the most prevalent oncogenic driver, found in up to 30% of lung adenocarcinoma [15]. In NSCLC, KRAS mutations have been shown to be very difficult to cure. KRAS has resurfaced as one of the most promising oncogenic drivers with therapeutic potential in NSCLC, thanks to recent treatment advances, and efforts to specifically target KRAS oncoproteins are becoming clinically relevant. KRAS has a reputation for being undruggable for many years, however multiple ongoing clinical trials are redefining the efficacy of various direct and indirect KRAS inhibitors by properly stratifying patients and identifying subgroup mutations [16]. The P53 gene (also known as T53) is widely considered to be the most frequently altered tumor suppressor gene in humans. T53 mutation elevated the expression of immunological checkpoints, activated T-effectors, and interferon-signatures considerably. More interestingly, the TP53/KRAS comutated subgroup had the largest number of PD-L1+/CD8A+ and unique enhanced expression of PD-L1. TP53 and KRAS mutation status have predictive value for response to PD-1 Blockade immunotherapy in lung adenocarcinoma [17].

1.2.2 Small cell lung cancer

Small cell lung cancer (SCLC) is a highly aggressive neuroendocrine cancer, It accounts for 15% of all lung malignancies and is distinguished by a high proliferative rate, a proclivity for early metastasis, and poor prognosis. SCLC genomic analysis revealed a high mutation burden and widespread chromosomal rearrangements, nearly usually all cases with functional inactivation of the tumor suppressor genes *TP53* and *RB1* [18].

In a mouse model established by Meuwissen et al. [19] for conditional inactivation of RB1 and P53 in lung epithelial cells revealed that the mouse develop tumor with morphological and immunophenotypic similarity to SCLC, suggesting that inactivation of these two gene is prerequisite of developing SCLC in mice. Moreover, structural abnormalities in RB1 were observed in SCLC but were not observed in other types of lung cancer [20].

In cell culture studies in SCLC cells notch is found to have role in cell cycle arrest. Mechanistically, active NOTCH proteins resulted in a significant decrease in hASH1 expression and a significant activation of phosphorylated extracellular signal- regulated kinase (ERK)1 and ERK2, both of which have been linked to cell cycle arrest in SCLC [21]. However other studies involving mouse models and human patient study indicated that role of notch in SCLC can be both tumor suppressive and protumorogenic. In a mouse model of small cell lung cancer and in human tumors, endogenous stimulation of the Notch system causes a neuroendocrine fate transition in 10-50% of tumor cells [22]. REST (also known as NRSF), a transcriptional repressor that decreases neuroendiocrine gene expression, plays a role in this switch. Slow-growing non-neuroendocrine Notch activated small-cell lung cancer cells are consistent with a tumor suppressive role for Notch, but they are also chemo resistant and offer trophic support to neuroendocrine tumor cells, suggesting a pro-tumorigenic role for Notch [22].

In a patient derived xenograft (PDX) model system for SCLC, increased expression of DLL3, one of the notch ligands, was observed. Since DLL3 is present on the surface of tumor cells but not in normal lung tissue, treatment with a humanized anti-DLL3 monoclonal antibody conjugated to a DNA-damaging pyrrolobenzodiazepine (PBD) dimer toxin induced tumor regression in multiple PDX models [23].

1.3 Genomic instability in lung cancer

Genomic instability is a feature of almost all human malignancies, but we are only now beginning to understand when it occurs and what is molecular foundation [24]. Aneuploidy is described as chromosomal numerical anomalies, and it is common (>90 percent) in solid tumors. With tumor growth, tumor cells become progressively aneuploid. It has been proposed that increased genomic instability has a role in tumor progression, if not necessitates it. Microsatellite instability (MIN) and chromosomal instability are two major

types of genomic instability (CIN) [25]. CIN – the most common kind of genomic instability has been found in sporadic cancers. Two distinct models are proposed for causing CIN, first is mutator theory [26], and the second is the oncogene-induced DNA replication stress concept for cancer progression. CIN in sporadic malignancies, according to the latter paradigm, is caused by the oncogene-induced collapse of DNA replication forks, which leads to DNA DSBs and genomic instability [27]. Oncogene activation disrupts replication regulation, resulting in slow and stalled replication forks, hyper-activation and/or a lack of origin activation. Such deregulation replication causes DNA damage.

To ensure the fidelity of DNA replication, organisms have devised a variety of processes that can be divided onto two categories. The first group of mechanisms includes those that prevent premature DNA replication and ensure that the genome is fully copied only once each division cycle. Key players in this context are cyclin-dependent kinase (CDK)-dependent and CDK-independent are among them. In higher eukaryotes there are additional mechanisms that seem to play a larger role in preventing abberant DNA replication and genomic instability. The second class ensures that cells can respond to a variety of stimuli that constantly threaten the genome's integrity by triggering DNA-damage-dependent checkpoints and coordinating DNA damage repair systems [28].

1.3.1 The role of H2Bub in orchestrating DNA damage response

Histone modifications, such as H2Bub, play pivotal roles in regulating diverse cellular processes, including gene expression and DNA repair. Specifically, double-strand breaks (DSBs) trigger monoubiquitylation of histone H2B in human cells, a modification intricately linked to transcription elongation in undamaged cells. This process hinges on the E3 ubiquitin ligase responsible for recruiting the RNF20-RNF40 heterodimer to DSB sites, along with ATM-dependent phosphorylation.

For DNA repair, two primary pathways exist: non-homologous end-joining (NHEJ) and homologous recombination repair (HRR). Monoubiquitylation is crucial for swiftly recruiting repair machinery, as highlighted in [29].

Addressing clinical implications, a notable study unveiled the clinical significance of H2B monoubiquitination and its modulation in lung cancer, revealing the role of the tumor

necrosis factor receptor-associated factor interacting protein (TRAIP). In lung adenocarcinoma, H2B monoubiquitination was markedly reduced compared to adjacent normal tissues, as indicated by immunohistochemistry. The downregulation was linked to TRAIP, as TRAIP-specific siRNA treatment significantly diminished H2B monoubiquitination triggered by ionizing radiation. This study established TRAIP's role in regulating Histone H2B monoubiquitination within DNA damage response pathways [30]. Furthermore, the E3 ubiquitin ligase RNF20 orchestrates chromatin structure through histone H2B monoubiquitination during transcription. This modification affects DNA end resection and the recruitment of repair factors like RAD51 and BRCA1, as demonstrated by studies cited in [31]. Cells lacking RNF20 or expressing a mutant H2B incapable of ubiquitination exhibit impaired homologous recombination repair (HRR) and heightened radiation sensitivity. Chromatin relaxation partially compensates for RNF20's role in HRR, emphasizing the impact of DSB-induced H2B ubiquitination on chromatin remodeling and DNA repair.

DNA damage-bypass systems are vital for countering mutation induction, genomic instability, and cancer. They aid in resolving replication blockades in proliferating cells during and after S phase. Research highlighted in [32] illuminates that H2Bub presence is crucial for replication fork passage through lesions that cause stalling. Deficient H2Bub leads to accumulation of RPA foci, implicating disrupted DNA damage tolerance (DDT) and homologous recombination (HR) pathways. Notably, Rad51 recruitment during S phase hinges on H2Bub for template switching and HR. H2Bub's importance extends to G2/M phase, aiding chromatin restoration post bulk DNA synthesis.

A related study suggests that RNF20 and RNF40 influence the DNA damage response by influencing the choice between NHEJ and HR pathways. Interestingly, H2AX and γH2AX, despite their importance in the DNA damage response, are not essential for RNF20/RNF40-mediated H2B ubiquitination. This study also points to a cooperative role of ATM and ATR in controlling H2B ubiquitination post ionizing radiation, suggesting a redundant function for these kinases in the potential H2Bub pathway [33].

1.4 Metabolic landscape of Lung cancer

To meet the demands of the growing cancer cell, the cancer cell requires nutrient acquisition and metabolic reprogramming. Changes in cell metabolism, such as increased glycolysis, glutaminolytic flux, induction of the pentose phosphate pathway, upregulation of amino acid and lipid metabolism, enhancement of mitochondrial biogenesis, and macromolecule biosynthesis, are also characteristics of cancer cells. Reprogrammed metabolism is considered a hallmark of cancer [34] [35]. The rewiring of tumor cells' energy production networks promotes rapid proliferation, continuous growth, survival, invasion, and metastasis. In cancer cells, oxidative phosphorylation is inhibited, and the cells generate energy through glycolysis. Glycolysis is an inefficient method of producing energy (only 2 ATP molecules are produced per glucose molecule) and generates lactate as a byproduct [34] [35]. Lactate encourages cancer cell survival, invasion, and metastasis by regulating the tumour microenvironment. Cancer cells upregulate glucose transporters, such as Glut1, Glut2, Glut3, and Glut4 to increase the glucose uptake, and thereby compensating the dramatically lower efficacy of energy generation. In fact, increased glucose uptake in cancer cells are exploited to visualize tumours in Positron Emission Tomography (PET) imaging using radiolabelled analogs of glucose as a tracer, such as 18F-fluorodeoxyglucose. Cancer cells also upregulate the expression of the majority of glycolytic enzymes, primarily through increased transcriptional activity of two glycolysis master inducers, c-Myc and HIF1α, and insufficient p53-mediated control. Both c-Myc and HIF1α directly bind to the promoters of a large number of glycolytic genes. HIF1α is primarily active in hypoxia, while c-Myc promotes the expression of its glycolytic target genes in normoxia as well. Thus, the dynamic interplay of key master regulators of glycolysis continuously drive glycolysis to support rapid proliferation and accelerated biosynthesis of cancer cells [36] [37] [38].

In case of normal cell glucose is converted to pyruvate in the presence of oxygen by the process of glycolysis and if oxygen is limited glucose is converted to lactate. However in case of cancer cell most of the glucose is converted to lactate irrespective of the presence or absence of oxygen widely due to dysfunction of mitochondria, this phenomenon has been described by Otto Warburg. However, this lead to lot of

misconception that glycolysis is the only source of ATP generation in case of cancer cells. From recent studies, it is clear that loss of function of tumor suppressors, activation of oncogenes and alteration in signaling pathways for example P13K pathway can lead to upregulation in glycolysis and advantage of increased glycolysis is the generation of metabolic intermediates. Interestingly, most of the energy demand of the cancer cell is met by mitochondrial respiration even in case of impairment of enzymes of mitochondria by metabolic rewiring by generating necessary metabolic intermediates and ROS (reactive oxygen species). However, a great majority of tumors generate ATP through glucose oxidation since the metabolic intermediates of glycolysis enter the TCA cycle and generate energy through oxidative phosphorylation [39].

Cancer cells are highly proliferative cells which require a constant supply of molecules such as glucose, amino acids etc from the extracellular space. To compensate for the increasing demand of the nutrients there is elevated expression of nutrient transporters and thereby ATP is generated in these cells as well as lipids, nucleic acid and non essential amino acids are generated as metabolic intermediates and acquired from extracellular space. However the acquisition of nutrient transporters is important but not the sole criterion for the proliferative nature of these cells. Among different kinds of transporters, glucose is transported through passive diffusion or through facilitated transport by certain glucose transporters and also via active transport by certain transporters such as SGLTs (Sodium linked glucose transporters). In addition to these glucose transporters, there are some net amino acid importers such as SNATs (Sodium coupled neutral amino acid transporter) and amino acid exchangers such as glutamine transporter ASCT2 (solute carrier family 1 member 5, SLC1A5) and amino acid transporter LAT1 (SLC7a5) [40].

Metabolic alterations promotes redox changes in cancer cells. Generation of reactive oxygen species is among them the most important of all. ROS are radical species generated during the course of normal metabolism in cells. At low level, ROS can activate growth and survival of cells. At moderate level, ROS can activate stress responsive genes such as Hif1a and proteins providing prosurvival signals such as Glut1 and VEGF. At higher level ROS can damage DNA, induce senescence and cause

permeablisation of mitochondria. In order to compensate for the detrimental effect of high ROS levels cells cells produce antioxidant molecules such as GSH and TRX [41].

Several of the metabolic liability of cancer cells have been translated into clinic. Asparginase, an enzyme which converts aspargine into aspartic acid and ammonia is essensial for the treatment of ALL (Acute lymphoblastic leukemia) [42]. In an early attempt of sequencing TCA cycle genes, IDH1 and IDH2 in 445 central nervous tumors and 494 non CNS tumors concludes that mutations of $NADP^+$ dependent isocitrate dehydrogenase encoded by IDH1 and IDH2 in majority of the malignant gliomas [43]. Another interesting study unveils the role of mitochondrial enzyme succinate dehydrogenase and fumerate dehydratase linking mitochondrial dysfunction and cancer. Inactivation of isocitrate dehydrogenase and fumerase leads to accumulation of the substrates of these enzymes isocitrate and fumerate in the mitochondria and further leakage in the cytosol leading where they inhibit family of prolyl hydroxylase enzymes (PHDs), depending on the type of PHD either the cell become resistant to apoptotic signal or activate a pseudohypoxic responses that enhances glycolysis via HIF [44]. Another important discovery deciphers selective killing of oncogenic transformed cells by β-phenylethyl isothiocynate (PEITC) through a ROS mediated mechanism [45]. In addition to this drug, an advanced novel ROS modulating agent LBL21, which inhibit cancer growth in vitro and in vivo and also with ability to eliminate stem-like cancer cells have been discovered [46]. In yet another study stromal control of cystine metabolism promote cancer cell survival in case of chronic lymphocytic leukemia (CLL). Mechanistically they exploited the property of stromal cells to import cystine and convert it into cysteine which is released into the microenvironment for uptake by the CLL cells which induced leukemia cell survival and further protected them from drug induced cytotoxicity. Disabling the protecting mechanism of stromal cells makes CLL cells more sensitive to drug treatment in the stromal cell microenvironment [47].

1.4.1 Glycolysis

Reprogramming glucose metabolism not only involves glycolysis but also several different pathways such as pentose phosphate pathway, hexosamine pathway and one carbon metabolism cycle.

Glycolysis has broadly three steps, first step involves conversion of glucose into glucose 6 phosphate by enzyme hexokinases. This step is really important since it involves trapping the glucose inside the cell which would otherwise be transported by glucose transporters. The second committed step is catalysed by phosphofructokinase (PFK1) and involves the conversion of fructose 6 phosphate (F6P) into fructose-1,6-bisphosphate (F1,6BP). And the third committed step involves the conversion of phosphoenol pyruvate to pyruvate by enzyme pyruvate kinase. The first two committed steps involves the consumption of ATP whereas the third committed step generates ATP. In many cases, cancer cells have attenuated last step of glycolysis. The attenuation is achieved partly achieved by low affinity isoform PKM2, which catalyses the reaction. Although there is attenuation of the third committed step in case of cancer cells, the conversion of pyruvate to lactate is higher in cancer cells. Interestingly, in an early attempt to study the relationship between glycolysis, mitochondrial function and tumor maintenance, LDHA levels were knockdown by means of short hairpin RNA in tumor cells, reduction of LDHA activity resulted in stimulation of mitochondrial respiration and decrease of mitochondrial membrane potential which resulted in drastically decreased tumorigenesis of these cells. [48].

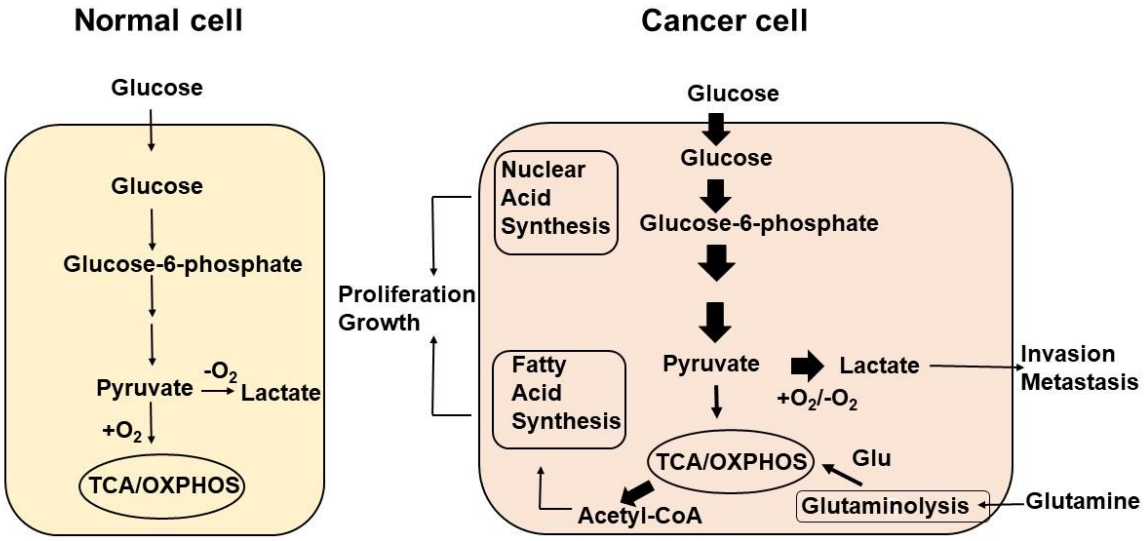

Figure 2. Metabolic differences between normal and malignant cells (Adapted from Jóźwiak, et al. Front endocrinol (Lausanne). 2014. PMID: 25250015). Glucose is converted to pyruvate in normal cells, which is then oxidized to CO_2 through the TCA cycle and the oxidative phosphorylation process in the mitochondria. Pyruvate is converted to lactate when oxygen is limiting. Cancer cells convert majority of the glucose to lactate regardless of the presence or absence of oxygen. Lactate secretion promotes tumor development. Increased glucose utilization via the glycolytic pathway produces metabolic intermediates such as glucose-6-phosphate, which is used in the pentose phosphate pathway to synthesize nucleic acids. The principal substrate for refueling the TCA cycle is glutamate, which is created during glutaminolysis. For lipid synthesis, citrate-derived acetyl CoA is employed **[49].**

1.4.2 Metabolic pathways emerging from glycolysis

The metabolic pathways emerging from glycolysis are essential for cellular energy production and various biochemical processes. Glycolysis leads to the production of pyruvate, which serves as a critical branching point. In aerobic conditions, pyruvate enters the citric acid cycle for ATP generation via oxidative phosphorylation. In anaerobic conditions, pyruvate is converted to lactate, replenishing NAD+ for continued glycolysis. Additionally, glycolytic intermediates contribute to biosynthetic pathways for nucleotide and amino acid synthesis. These interconnected pathways exemplify glycolysis' central role in cellular homeostasis and adaptation, influencing cell function and maintaining energy balance.

1.4.2.1 The Pentose Phosphate Pathway (PPP)

Pentose phosphate pathway is comprised of two different pathways, oxidative and non-oxidative pathways. The oxidative pathway generates Ribulose 5 phosphate and NADPH and the non-oxidative pathway generates pentose phosphate for ribonucleotide synthesis and some other metabolites such as Fructose 6 phosphate and Glyceraldehyde 3 phosphate. In proliferating cancer cells both the oxidative and non-oxidative pathways are increased by specific oncogenic drivers. PPP pathway generates NADPH which is required for intracellular redox balance and fatty acid synthesis and pentose phosphate required for RNA and DNA synthesis, therefore has very important role in cancer metabolism [50]. A study on human clear cell –renal cell carcinoma looked at the metabolic profiles of glycolysis and the pentose phosphate pathway (PPP), in human clear cell-renal cell carcinoma (ccRCC) to see how these pathways affect cell proliferation, NADPH levels, and the production of reactive oxygen species (ROS). In ccRCC tumor samples, metabolomics analysis revealed increased glucose uptake and utilization. Inhibiting Glucose-6-phosphate dehydrogenase, an enzyme that connects glycolysis to the PPP pathway along with other PPP metabolites, resulted in a significant decrease in cancer cell survival, a decrease in NADPH levels, and an increase in ROS production, indicating that PPP is important in the regulation of ccRCC redox homeostasis [51].

1.4.2.2 The Serine-Glycine Pathway and One-carbon metabolism

Serine is required for the synthesis of amino acids such as glycine and cysteine and also production of sphingolipids and phospholipids. Serine is also a major donor of one carbon units to folate cycle through one carbon metabolism. One carbon units derived from serine is used for de novo synthesis of adenosine, guanosine etc. These one carbon units are also utilized in remethylation of homocysteine and thus supporting methionine cycle. Since glycine and cysteine derived from serine is required for the synthesis of glutathione, it also contributes to the redox balance in the cell. Therefore, serine metabolism may have an important role in cancer development as well as to other pathological conditions [52].

1.4.2.3 TCA cycle and Oxidative phosphorylation

Among the currently recognized oncometabolites D-2-hydroxygluterate, L-2-hydroxygluterate, succinate and fumerate are the most common. Oncometabolites play an important role in tumorigenesis. The upstream pathways responsible for generation of oncometabolites and downstream pathways that are activated by oncometabolites can be potential therapeutic target.

It is well established that cancer associated IDH1 mutation results in the conversion of α-ketogluterate to 2-Hydroxygluterate (2-HG) and excess accumulation of 2HG results in formation and progression of gliomas [53]. Mutation of IDH1 and IDH2 are frequently found in several different types of gliomas [43]. In all cases mutation of arginine 132 has been observed in case of IDH1, tumors which do not have this mutation had mutation in analogous amino acid R172 of IDH2 gene [43]. During oxidative phosphorylation IDH leads to conversion of isolcitrate to α-ketogluterate. Mutation in IDH results in reduced affinity of these enzyme for isocitate and increased affinity for α-ketogluterate and reduced NADPH which implicates in novel enzymatic activity resulting in conversion of α-ketogluterate to 2-hydroxygluterate [53]. IDH1 and IDH2 mutations is also found in subset of patients with Acute myeloid leukemia (AML) and Myelodysplastic syndromes (MDS). 2HG accumulation is found to be dramatically increased in sera, marrow and urine of IDH1/2 mutant AML patients and levels of this oncometabolite correlate with the disease burden and therapeutic response [54]. Others have reported that IDH1 and IDH2 mutations promote oncogenesis. Therefore, taken together IDH mutations are drivers of malignant transformation.

Interestingly, oncometabite succinate is accumulated in Succinate dehydrogenase (SDH) deficient cells. SDH is an enzyme of TCA cycle involved in conversion of succinate to fumerate and key component of mitochondrial respiratory chain. Mutation in SDH gene is found in familial paraganglioma, pheochromocytoma, renal carcinoma and T cell leukemia (PCC) [55] [56] [57]) [58]. Succinate is multifunctional and acts as a competitive inhibitor of α-ketogluterate dependent dioxygenases (aKGDD). For instance succinate inhibits prolyl hydroxylases (PHDs), a KGDD involved in degradation of hypoxia inducing factor Hif1a leading to aberrant stablisation of Hif1a mimicking hypoxia [59]. Succinate also inhibits Ten eleven translocating proteins (TETs) enzyme involved in DNA

methylation and CpG island hypermethylation. [59]. In addition, succinate also inhibits KDMs, aKGDDs involved in histone demethylation [60]. Epigenetic changes leading to DNA hypermethylation are involved in dedifferentiation and invasion in case of SDH deficient tumors [61]. Yet another oncometabolite, fumerate hydratase mutations, causes renal cell cancer and leiomyomatosis. Fumerate, a small molecule metabolite accumulated in fumerate hydratase deficient cells, has been shown to play key role in cell transformation. Fumerate also inhibits aKGDDs that are involved in DNA and histone demethylation leading to epigenetic changes. However the link between fumerate accumulation, epigenetic changes and tumorigenesis is unclear. It has been shown that fumerate inhibits TET mediated demethylation of a regulatory region of antimetastatic miRNA cluster mir-200ba429 leading to expression of EMT related transcription factors and in turn leading to enhanced migratory property. Loss of fumarate hydratase and subsequent accumulation of fumarate leads to epithelial mesenchymal transition, which is associated with tumor initiation, progression and metastasis [62].

1.4.2.4 TCA cycle and Oxidative phosphorylation

The synthesis of glucose from non-carbohydrate substrates is known as gluconeogenesis. The liver, kidney, gut, and skeletal muscle are the most common sites. Though many of the steps in gluconeogenesis are glycolytic reactions in reverse, three of them are solely mediated by gluconeogenesis enzymes. PEPCK, the first enzyme in gluconeogenesis, is a bottleneck in cell metabolism that connects the TCA cycle to glycolysis/gluconeogenesis. PCK1 is a cytosolic isoform of PEPCK, and PCK2 is a mitochondrial isoform (PEPCK-M, PEPCK2). Oxaloacetate (OAA) and GTP are converted to phosphoenolpyruvate. (PEP), CO_2, and GDP by PCK1 and PCK2. PCK1 and PCK2 have been demonstrated to be important in the progression of some malignancies. Fructose-1,6-bisphosphatase 1 (FBP1), on the other hand, is a downstream gluconeogenesis enzyme that inhibits glycolysis and tumor growth, partly through non-enzymatic methods [63]. Another study discovered that PCK2 was expressed selectively in lung adenocarcinoma subtypes. PCK2 expression was associated with considerably increased overall survival in lung adenocarcinoma, and

PCK1/2 expression was higher in metastasized tumors than in primary tumors, probably due to the distinct environment. [64].

1.5 The role of epigenetics and metabolism in tumorigenesis

The two fields of epigenetics and metabolic reprogramming are inextricably linked. The metabolic state of the cell influences the function of chromatin modifying enyzmes, and epigenetic processes regulate the expression of metabolic genes, thereby altering cell metabolism. As a result, identifying key players at the crossroads of cancer metabolism and epigenetics may lead to the development of a novel therapeutic approaches.

1.5.1 The effect of metabolites on epigenetic state of chromatin

Acetyl CoA is a key metabolite that fuels the TCA cycle and is an intermediate molecule in glycolysis, glutaminolyis, and fatty acid metabolism in mitochondria. Histone acetylation is the process of adding an acetyl group to the lysine residues. The acetyl group counteracts the positive change in lysine residues and thus reduces the ionic interaction between histones and DNA, resulting in open chromatin structure, which is associated with positive transcriptional regulation. Acetyl CoA is an intermediate metabolite that serve as a substrate for histone acetylation. Histone acetylation is controlled by the opposing actions of histone acetyl transferases (HATs) and histone deacetyltransferases (HDACs), which catalyze the addition or removal of acetyl group from histones. The activity of HATs is determined by the intracellular level of acetyl CoA. Acetyl CoA is a key regulator of histone acetylation levels in cancer [65]. Furthermore, histone acetylation is dependent on ATP citrate lyase (ACL), an enzyme that converts citrate derived from glucose to acetyl CoA [66]. ACL activity is required for growth factor-induced increases in nutrient metabolism regulation to histone acetylation. Overall, a high level of acetyl CoA leads to more open chromatin via histone acetylation, which promotes gene expression and cell growth.

SAM and SAH are intermediate metabolites of a pathway that is part of the subset of one carbon metabolism pathways. SAM is produced by methionine adenosyl transferase (MAT), which uses methionine and ATP as substrates. SAM donates a methyl group, and SAH is the product. SAH is a strong methyltransferase inhibitor,

particularly of DNA histone methyl transferases (DNMTs) and histone methyl transferases (HMTs). There is evidence that monitoring methionine metabolism and sensing methionine availability is sufficient to determine histone methylation levels by modulating SAM and SAH [67]. A high SAM level could contribute to DNA hypermethylation at CpG sites and inappropriate gene silencing. An intriguing clinical study elucidates SAM overproduction in the case of a rare disease caused by a lack of Glycine N-methyl transferases (GNMT). GNMT deficiency activates oncogenic pathways and increases the risk of hepatocellular carcinoma [67]. Furthermore, in the case of cancer, the ratio of SAM and SAH has a significant impact on aberrant histone methylation. Nicotinamide N-methyl transferases (NNMTs) have been found to be overexpressed in a number of human cancers. NNMT reduces cancer cells methylation potential by consuming methyl units from SAM to produce the stable metabolic product 1-methylnicotinamide. As a result, NNMT acts a SAM sink, severely depleting the SAM/SAH ratio and rending SAM unavailability for Histone methyl transferases (HMTs). NNMT knockdown increases histone methylation, but NNMT overexpression or knockdown has no effect on DNA methylation, possibly due to varying km values of DNMTs and HMTs for SAM. Overall, SAM deregulation in cancer is context dependent and needs to be investigated further [68].

1.5.2 The effect of epigenetic processes on metabolic state

The activity of DNA and histone demethylases regulates DNA and histone demethylation. TETs catalyze the conversion of (5m-C) to 5 hydroxymethyl (5-hMC), which is followed by cytosine reversion by oxidation and base repair by thymine DNA glycosylase (TDG). TET mutations have been linked to myeloid malignancies and may play a role in AML prognosis [69]. TET downregulation has also been observed in a variety of human tumors [70]. Thus, active methylation and deactive demethylation collaborate to cause promoter hypermethylation in cancer. Histone demethylation of lysine residues, on the other hand, is carried out by the lysine specific protein demethylases KDM1 and jumonji C domain containing (JMJD) enzymes. However, the role of histone demethylases in cancer is unknown; some of them are downregulated by mutation, deletion, or amplification. TET and JMJDs are aKGDDs that are inhibited in cancer by the accumulation of oncometabolites fumarate and succinate. [60].

Sirtulin deacetylase activity requires NAD+, and the NAD+/NADH ratio correlates with sirtuin activity. Several studies have shed light on sirtuins vritical role in responding to nutrient signals [71]. High energy levels result in a lower NAD+/NADH ratio and sirtuin activity inhibition. In cancer, increased glycolysis reduces the NAD+/NADH ratio and sirtuin activity inhibition. In cancer, increased glycolysis reduces the NAD+/NADH ratio, which inhibits sirtuins. Hyperacetylation of histones and abnormal gene transcription are caused by repressed sirtuins and increased histone acetylase HAT activity. The relationship between increased sirtuin activity and abnormal metabolism is not well established [71].

Histones are primarily phosphorylated at the serine and threonine residues by various kinases. Because the intracellular concentration of ATP is higher than the Km of most kinases, metabolic changes are unlikely to have a direct effect on histone phosphorylation. However, some kinases, such as AMPK, can phosphorylate histone H2B at position 36 in response to a low ATP/AMP ratio, which indicates metabolic stress. The phosphorylation of H2B Ser36 by AMPK is a direct transcriptional and chromatin regulatory pathway that leads to cellular adaptation to stress [72].

Approximately 5% of the glucose enters the Hexosamine Biosynthestic Pathway (HBP), where GlcNac is formed as an end product that is used for various protein glycosylation. In cell culture studies, researchers discovered that Histone H2B is GlcNacylated at residue S112 by OGT. Furthermore, they show that H2BS112 GlcNacylation is a histone modification that promotes H2BK120 monoubiquitination, which is well known for transcriptional activation [73]. GlcNAc regulates the expression of growth factor receptors, which help cells coordinate their glucose and glutamine metabolism [74]. GlcNAc regulates the expression of growth factor receptors, which help cells coordinate their glucose and glutamine metabolism. [74]. The role of histone GlcNAcylation in transcriptional regulation is still unknown. [75] [76]. [77].l

DNA methylation is known to directly regulate the expression of metabolic genes or indirectly regulate via misregulation of oncogenes eg. Hif1a, AKT etc. DNA methylation can induce overexpression of Glut1 by epigenetic silencing of promoter of DERL3, gene which acts upstream and involved in proteasomal degradation of Glut1 [75]. DNA methylation mediates downregulation of Fructose 1, 6 bisphosphatase (FBP1) in human

hepatocellular carcinoma and colon cancer [76]. Also loss of FBP1 by Snail mediated repression leads to metabolic advantages in basal like breast cancer [77]. However DNA hypomethylation leads to upregulation of pyruvate kinase gene 2 (PKM2) in human cancers [78]. DNA methylation also regulates tumor suppressor transcriptional silencing, which is part of a signaling cascade linked to metabolism. P13/AKT and Hif1a act as central regulators for the majority of glycolytic genes. Several tumor suppressors, including VHL, that inhibit P13/AKT/MTOR and Hif1a, are epigenetically silenced by promoter hypermethylation [79]. As a result, DNA methylation is important in the regulation of metabolic gene expression.

The role of sirtuins in histone modification is the most well studied of all histone modifying enzymes. Sirtuins have been linked to stress response and metabolism. They serve as an energy sensor and protect cells from metabolic stresses. Sirt6 knockout mice typically succumb to life's hypoglycemic environment. The mechanism underlying hyperglycemia, however, remains unknown. Surprisingly, Sirt6 is widely known as a histone deacetylase that regulates the expression of numerous glycolytic genes. Sirt6 is a master regulator of glucose homeostasis and a corepressor of Hif1a [80]. Sirt6 functions as a ribosome metabolism regulator. Sirt6 interacts with and represses myc transcriptional activity, making it a potent tumor suppressor in cancer metabolism. Furthermore, another sirtuin, Sirt2, promotes hepatic glucose uptake by deacyetylating the glucokinase regulatory protein [81]. Sirt7 regulates hepatic lipid metabolism via the ubiquitin proteasomal pathway.

1.6 Hif1a and intriguing links to DNA Damage Response

Hypoxia, a persistent condition within tumor microenvironments, arises from the rapid growth of tumor cells outpacing their blood supply. Emerging data underscores the significant role of hypoxia in shaping cancer metabolism and dormancy, promoting stemness, and driving cancer initiation and progression. Central to these effects is the induction of Hypoxia-Inducible Factor 1 alpha (HIF1A), a transcription factor that orchestrates diverse biological mechanisms, including angiogenesis and glycolytic metabolism [82]. Under normoxic conditions, prolyl hydroxylase domain (PHD) proteins hydroxylate HIF-subunits, marking them for polyubiquitination and proteasomal

degradation, thereby maintaining oxygen homeostasis [83]. Conversely, hypoxia stabilizes HIF1A, allowing it to accumulate and initiate downstream effects. Beyond oxygen-dependent control, instances like von Hippel-Lindau disease and TP53 mutations disrupt this balance, further contributing to HIF1A accumulation [84] [85] [86].

HIF1A is intricately regulated at the protein, transcriptional, and translational levels. Activation of the PI3K/AKT/mTOR pathway by growth stimuli, oncogenes, or mutations in genes like PTEN boosts HIF1A mRNA transcription and translation [87]. Furthermore, hypoxia induces mitochondrial production of reactive oxygen species (ROS), fostering HIF1A signaling [86]. This interplay links metabolic enzymes, oncometabolites, and Hif1a activation. Downregulation of enzymes, like succinate dehydrogenase, and mutations therein, as seen in gastric and colon carcinoma, contribute to HIF1A activation [88]. A novel nexus emerges with Histone H2AX, not only pivotal for DNA damage repair but also a critical regulator of HIF1 signaling. H2AX collaborates with HIF1 in curtailing nuclear export and degradation, bolstering VHL-independent HIF1 transcriptional activation. This alliance hinges on the hypoxia-induced E3 ligase activity of TRAF6 and ATM, which modulate HIF1A via mono-ubiquitylation and phosphorylation of H2AX [89] (PMID: 27918549). Remarkably, elevated TRAF6 and H2AX levels in breast cancer correlate with heightened HIF1 signaling and metastatic potential, underscoring their prognostic significance.

In summary, the intricate interplay between hypoxia and HIF1A casts a profound impact on cancer biology. From shaping metabolic adaptations to fueling tumorigenesis and influencing metastatic potential, these mechanisms underscore the significance of understanding the hypoxia-HIF1A axis in developing targeted therapies for cancer.

1.7 RNF20 [evolutionary conservation, enzymatic activity, substrates, mechanism of action]

BRE1 (Human homolog RNF20) was first discovered in yeast is a functional protein required for monoubiquitination of histone H2B. RNF20 has been known as a component of RNF20/40 E3 ubiquitin-protein ligase complex that mediates monoubiquitination of lys-120 of histone H2B (H2BK120ub1), gives a specific signature for epigenetic

transcriptional activation. Human RNF20 has 975bp residues, characterized by C-terminal ring domain and extended helical regions which are predicted to form coiled coil [90]**.** RNF20 is a classically known to be an E3 ubiquitin ligase which monoubiquitinates histone H2B. Ubiquitination is a cascade of events in which E1 activating enzyme activates the free ubiquitin by engaging ATP, which is transferred to the active site of E2 conjugating enzyme. E3 ubiquitin ligase works with E2 to transfer the ubiquitin to the target [91].

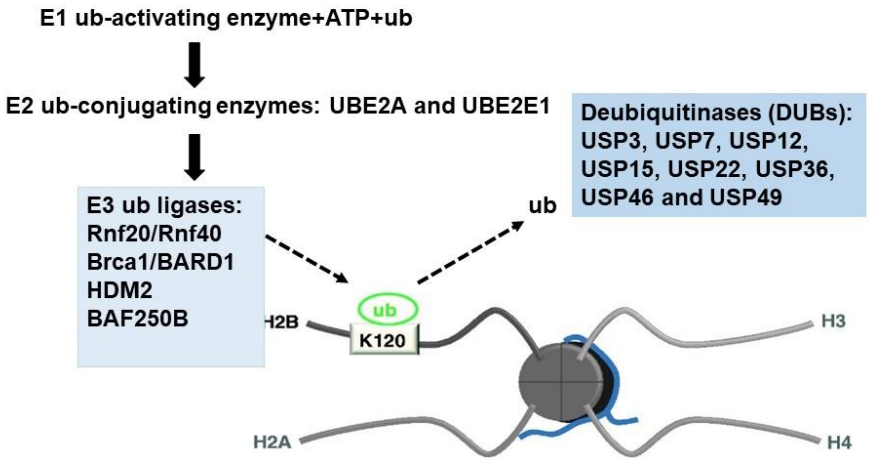

Figure 3. The ubiquitin enzyme cascade is connected to monoubiquitination of histone H2B at lysine K120 (H2Bub1) (Adapted from Cole et al. Endocr Relat Cancer. 2015)**.** ATP is used by an E1 ubiquitin (ub) – activating enzyme to activate free ubiquitin, which is subsequently transported to the active site of an E2 ubiquitin conjugating enzyme, of which H2Bub1 has been related to E3 ubiquitin ligases work with E2 ubiquitin ligases to transport ubiquitin to the target protein.

1.7.1 RNF20 acting as a tumor suppressor

Proliferation of cancer cells is linked to higher lipid levels. In recent study, it was discovered that RNF20 functions as a tumor suppressor in clear cell renal cell carcinoma. The authors discovered that knocking down or pharmacologically inhibiting sterol regulatory element binding protein 1c (SREBP1c) inhibits cell proliferation and cell cycle progression in these cells in cell culture tests. Furthermore, RNF20 overexpression

inhibits tumor development and lipid accumulation in xenograft models [92]. Another intriguing study suggests that RNF20 serves as a tumor suppressor by regulating gene expression selectively. Because H2B monoubiquitination is linked to gene transcription, they discovered that RNF20 affects just a handful of genes, primarily H2A, H2B, and the tumor suppressor P53. RNF20 also primarily affects EGF inducible genes. Furthermore, another very interesting study indicates that RNF20 acts as a tumor suppressor by regulating expression of selective genes. Since H2B monoubiquitination is associated with transcription of the gene, the study found that only a subset of genes are affected by RNF20-H2Bub1 axis. Importantly, RNF20 mainly affects EGF inducible genes. Moreover the authors found that *Rnf20* promoter is hyper methylated in case of breast cancer, they analyzed 56 cancer DNA samples and 12 normal DNA samples and found that *Rnf20* promoter is hyper methylated in significant number of cancer samples [93]. In yet another study, RNF20 was linked to reducing inflammation and cancer related with inflammation in both mice and humans. They discovered that *Rnf20+/-* mice develop colonic inflammation and inflammation-related colorectal cancer in their investigation [94] demonstrated that the P-63 containing nuclear factor B (NF -κB) is recruited to the P50 homodimer and that its expression is regulated by the reduction in the heterochromatin mark H3K79me3 on a subset of NF-κB target genes [94]. In cell biology, the role of transcriptional regulators during mitosis is a fundamental subject. RNF20 deletion causes cell cycle abnormalities, spindle assembly defects, and apoptosis, which is surprising because RNF20 and motor protein Eg5 interact in cell culture experiments, and RNF20 monoubiquitination stabilizes Rnf20. In vivo, both RNF20 and Eg5 depletion causes breast cancer [95]. Depletion of SMURF2 (smad ubiquitin regulatory factor 2), a HECT domain E3 ubiquitin ligase, leads to DNA damage and genomic instability, increasing susceptibility to several types of malignancies in old mice. SMURF2 and RNF20 are colocalized at the DNA damage site, and SMURF2 monoubiquitinates histone H2B and trimethylates lysine 4 and lysine 79 by directing RNF20 for proteasomal degradation, according to this study. As a result, through RNF20, SMURF2 protects genomic stability by altering the epigenetic landscape of histone modifications [96].

1.7.2 RNF20 acting as a tumor promoter

Mixed/lineage leukemia (MLL) fusions require RNF20. MLL fusions are potent oncogenes that induce leukemia that is aggressive. Suppressing *Rnf20* expression in cell culture and in vivo decreases cell proliferation in multiple MLL-rearranged leukemia models. The histone methyl transferase DOT1L is involved in cell proliferation, cell cycle progression, and cell death by using S-adenosyl-L-methionine as a cofactor to mono-, di-, and trimethylate H3K79: Prostrate, breast and ovarian cancers all have abnormalities in this enzyme's normal expression levels [97]. AF9 is another MLL-fusion partner involved in acute myeloid leukemia [98]. Also, Hoxa9 is another often disrupted gene in acute myeloid leukemia. *Rnf20* knockdown reduces the expression of MLL-AF9/Dot1I target genes. RNF20 is needed for local H3K79 methylation at *Hoxa9*, and H2Bub and H3K79me2 are enriched in the transcribed part of MLL-AF9 target genes. Overall, co-transcriptional recruitment of RNF20 at MLL-fusion target genes leads to Dot1l-mediated H3K79 methylation amplification, rendering leukemia cells reliant on RNF20 to maintain their oncogenic transcriptional program [99].

In vivo treatment with histone deacytylase inhibitor panobinostat (LBH5899 in a xenograft model of mixed lineage type leukemia (MLL)-rearranged aute lymphoblastic leukemia leads to antileukemic activity, overall survival, and lower tumor burden, shown by a recent study. The antileukemic activity is attributed to reduction of H2B monoubiquitination via the RNF20/RNF40/WAC E3 ligase complex according to in vitro investigations [100].

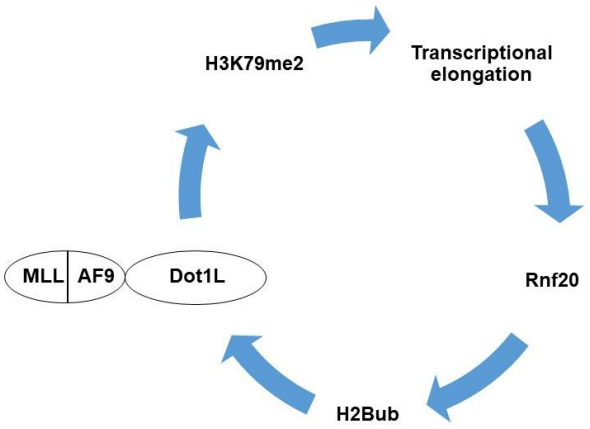

Figure 4. Model depicting the role of RNF20 in amplifying MLL-AF9-mediated transcriptional activation through cross-talk with Dot1l (Adapted from Wang et al. Proc Natl Acad Sci U S A. 2013. [99]**.**

1.7.3 RNF20 in chromatin remodeling

RNF20 regulates histone H2B monoubiquitination, which plays a function in chromatin architecture during gene transcription and has implications in cancer. Zhang et colleagues discovered WAC as a RNF20 interaction partner. RNF20 is targeted by WAC to form an association with the RNA polymerase II complex, which leads to H2B monoubiquitination at the active transcription start site, hence controlling transcription. WAC's N-terminal WW domain binds RNA polymerase II in a mechanism. WAC binds RNF20/RNF40 during gene transcription to engage with the RNA pol II complex for H2B ubiquitination at active transcription sites, which modulates transcription. [101].

RNF20 has also been shown to be present at the double strand break site and required for double strand break induced H2B monoubiquitination. In addition it is also shown that Rnf20 is required for methylation of H3K4 at double strand breaks and recruitment of chromatin remodeling factor SNF2h. As expected depletion of RNF20, SNF2h or cells expressing H2BK112R are highly sensitive to ionizing radiation [31].

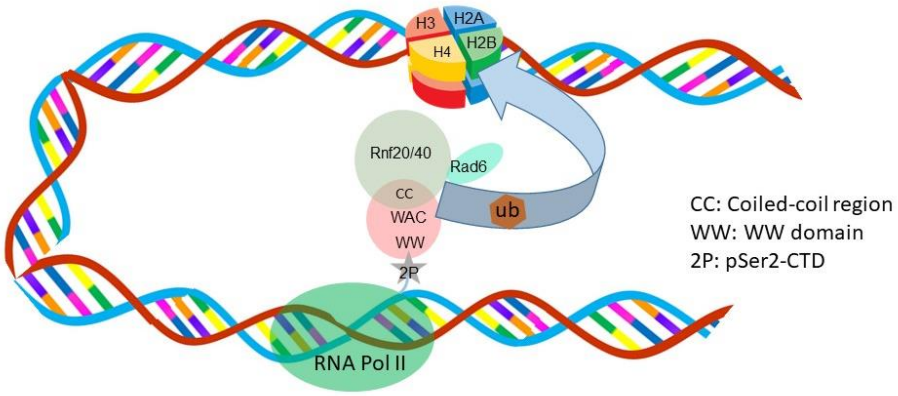

Figure 5. A model depicting WAC mediated transcription-coupled ubiquitination of H2B (Adapted from Zhang et al; Mol Cell. 2011). WAC binds to the C-terminal domain of RNA polymerase II and recruits RNF20/RNF40 and RAD6 to gene transcription sites for H2B ubiquitination [101].

1.7.4 Role of RNF20 in cancer metabolism

According to some research, RNF20 controls lipid metabolism in the liver and kidney. Rnf20 suppresses transcriptional activity of sterol regulatory element binding protein 1c (SREBP1c) and inhibits the expression of lipogenic genes that are targets of SREBP1c. In primary hepatocellular carcinoma cell, knocking out *Rnf20* activates the expression of SREBP1c and lipogenic genes, as well as lipogenic activity [102]. In contrast, another report suggests that RNF20 enhances the transcriptional activity of the peroxisome proliferator-activated receptor ($PPAR_{\gamma}$). *Rnf20* deficient (*Rnf20+/-*) mice had less fat mass and smaller adipocytes than wild type littermates when fed a standard chow. In addition, *Rnf20+/-* mice fed a high fat diet had less systemic insulin resistance and less fat tissue expansion. In conclusion, RNF20 stimulated $PPAR_{\gamma}$ transcriptional activity by promoting the proteasomal degradation of nuclear corepressor 1 (NCoR1) [102]. The most common subtype of kidney cancer is clear cell renal carcinoma (ccRCC), which is characterized by ectopic lipid accumulation. RNF20 overexpression suppresses lipogenesis and cell proliferation by inhibiting sterol regulatory element –binding protein 1c (SREBP1c). In Xenografts, RNF20 overexpression also inhibits tumor growth and lipid storage [92].

1.7.5 RNF20 role in Polymerase (PolII) pause, release and elongation

The transcription of RNA polymerase II is a strictly regulated process. This applies not just to the well-studied transcription initiation stage, but also to the elongation stage. RNF20 depletion lowers global levels of monoubiquitylated H2B (H2Bub) and raises the expression of growth-promoting proto-oncogenes. Those genes predominantly dwell in compact chromatin under basal conditions, and they are inefficiently transcribed. RNF20 preferentially represses those genes, according to this study, by interfering with TFIIS chromatin recruitment, likely via H2Bub [103]. Another study discovered parameters that allowed RNA polymerase II to catalyze the formation of an RNA transcript despite the presence of a contagious array of nucleosomes barriers. H2Bub1 is dependent on RNF20, RNF40, UBCH6, PAF and FACT for transcription for target genes, according to the researchers. FACT function is aided by H2B monoubiquitination, which promotes transcript elongation and the creation of longer transcripts [104].

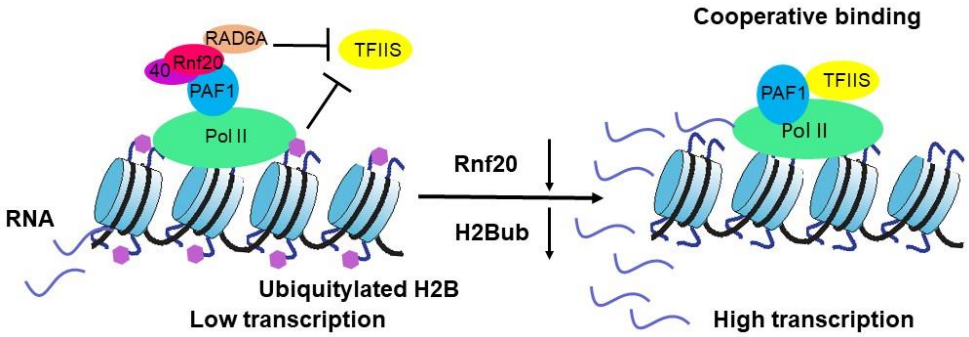

Figure 6. Proposed model for the regulation of a subset of genes by RNF20 and H2Bub (Adapted from Shiloh et al. FEBS lett. 2011). High levels of H2Bub (purple) are associated with RNF20-suppressed genes, which are transcribed with low efficiency due to inefficient elongation. TFIIS binding is inhibited in these cases, either by H2Bub or by additional RNF20/RNF40/RAD6A complex activities. When Rnf20 is inhibited, H2Bub levels decline, allowing TFIIS to be recruited to chromatin and co-operatively bind to the PAF1 complex and Pol II [105].

Chapter 2: AIMS OF THE STUDY

The role of epigenetic regulators is crucial in the initiation and progression of cancer. Among these regulators, RNF20 is an important one, but its specific function in lung cancer has not been thoroughly explored. Consequently, my doctoral research thesis aimed to address the following objectives:

(1) To investigate the impact of *Rnf20* gene disruption on tumorigenesis in *in vivo*. Given that *Rnf20* homozygous knockout (*Rnf20-/-* KO) mice are embryonically lethal, we aim to study whether *Rnf20* heterozygous KO (*Rnf20+/-*) mice develop tumors and assess the frequency and types of tumors formed at different stages of their life.

(2) To elucidate the function of RNF20 in essential cellular processes, such as cell migration, proliferation and morphology. By analyzing these aspects, we aim to understand how RNF20 influences cancer cell behavior and its possible involvement in lung cancer progression.

(3) To analyze the impact of RNF20 loss on genome stability and gene expression. Through in-depth analysis, we aim to identify potential changes in the gene regulatory networks that may arise due to RNF20 dysregulation. This objective will provide insights into the molecular mechanisms underlying RNF20's role in cancer development.

(4) The ultimate goal of this project is to unravel the molecular mechanism by which RNF20 regulates lung cancer growth. By integrating findings from the previous objectives and conducting further investigation, we aim to gain a comprehensive understanding of the specific pathways and processes influenced by RNF20 in the context of lung cancer. This knowledge can potentially lead to the identification of novel therapeutic targets for combating lung cancer and may have broader implications for cancer research and treatment.

Chapter 3: MATERIALS & METHODS

3.1 Methods

3.1.1 Mouse lines and animal experiments

All animal experiments were performed according to the institutional guidelines. The *Rnf20*tm1a (EUCOMM) Wtsi mouse line was utilized for these studies. While the *Rnf20* haploinsufficient mouse line was generated for the cardiology research in Prof. Dobreva laboratory, I utilized this already existing mouse line for my PhD thesis work. Animals were housed and bred under controlled temperature and lighting (12/12-h light/dark cycle), fed ad libitum with normal diet and water. Mouse work was performed in compliance with the German Law for Welfare of Laboratory Animals, which complies with international regulations. Mice were sacrificed at the age of 6 months and 1 year. Lungs were isolated, fixed with 3.7% formaldehyde, and embedded in the paraffin. 7µm thick paraffin sections were used for hematoxylin and eosin staining and IHC staining.

3.1.2 Immunohistochemistry and immunofluorescence staining

For immunohistochemical staining on paraffin sections, slides were heated at 55 °C for 10 min and submerged into xylene (Sigma), followed by serial deparaffinization steps 3x xylene, 100% ethanol, 80% ethanol, 70% ethanol and 50% ethanol and H2O subsequently. Antigen retrieval was done by microwave boiling in 10 mM citrate buffer for 10 min. The subsequent steps were done with the VECTASTAIN Universal Quick HRP Kit (PK-7800, Vector Laboratories) by incubating sections for about 10 minutes in prediluted blocking serum, blotting excess serum from sections, incubating primary antibody diluted in buffer containing 1.5% blocking serum overnight, followed by washing with PBS for 5minutes three times. Incubate sections in prediluted biotinylated secondary antibody for 10min and then washing the sections for 5 minutes each three times. Incubate sections in ready to use streptavidin solutions for 5 minutes each and then wash sections again for 5min each three times. Staining was developed with DAB Peroxidase (HRP) Substrate Kit (SK-4100, Vector Laboratories). Images were acquired by the

NanoZoomer 2.0-HT whole slide imager (Hamamatsu) and analyzed by the NDP.view2 Viewing software (Hamamatsu).

For immunofluorescence staining on paraffin sections, slides were deparaffinized, and antigen retrieval steps were performed as described for IHC staining on paraffin sections. Slides were then blocked with 10% FCS with 0.5% Triton X-100 (Sigma) in PBS for 1 hr and incubated with primary antibodies in blocking buffer at 4°C overnight. On the next day, slides were washed and secondary antibodies were added for 1hr. Slides were then washed and mounted in an anti-fade mounting medium. Images were acquired by the NanoZoomer 2.0-HT whole slide imager (Hamamatsu) and analyzed by the NDP.view2 Viewing software (Hamamatsu).

3.1.3 Human tissue microarray quantification of immunoreactivity

Human lung cancer tissue microarray slides, containing 168 cases of multiple types of lung cancer, 10 each of normal and cancer adjacent normal tissue, were purchased from US Biomax Inc (LC2085c). IHC staining was performed as described above. For semiquantitative analysis of immunoreactivity of RNF20, H-score of the nuclear staining signal of cells was quantified. Ten fields were randomly selected with at least 100 cells in each field, and the H-score was generated by adding the percentage of strongly stained (3×), the percentage of moderately stained (2×), the weakly stained (1×) cells, giving a range of 0-300. The differences were less than 5%, and the mean of the two values was used. At least 1000 cells in 10 random views were selected to analyze.

3.1.4 Cell culture, CRISPR/Cas9-*Rnf20* LOF MLE-12 cells and generation of stable cell lines

MLE12 and NCI-H82 (H82) were purchased from ATCC (CRL-2110, CRL-3216). MLE12 cells were cultured in DMEM/F12 medium supplemented with 10% fetal bovine serum (FCS) and penicillin/streptomycin/glutamine (PSG). H82 cells were cultured in RPMI1640 supplemented with 10% FCS and PSG.

3.1.4.1 Generation of stable cell lines by using CRISPR/Cas9-*Rnf20* LOF MLE-12 cells/ transgenic Rnf20+/- MLE-12 cells

Transgenic *Rnf20*+/- MLE-12 cells were generated using the CRISPR–Cas9 technology. For generating transgenic *Rnf20*+/- MLE-12 cells, sense and antisense oligos gRNA-1: 5′-CACCGGGCCACTGATGATGCCTCA-3′ and 5′-CTGAGGCATCATCAGTGGCCCAAA-3′; gRNA-2: 5′-CACCGGATAGTGGAGGAAGCAGTGC-3′ and 5′-CGCACTGCTTCCTCCACTATCCAAA -3′ are annealed by mixing 4 µl of 40 µM sense oligo with 4 µl of 40 µM antisense oligo and heating the mixture at 95°C for 2 minutes. The reaction is then diluted with 392 µl to reach a total volume of 400 µl, without vortexing. From this dilution, 6 µl is used for the ligation reaction. For the ligation, 1 µl of pSpCas9 (BB)-2A-puro (Px459)V2.0 plasmid (Addgene plasmid # 62988), previously digested and eluted in 15 µl, is combined with 6 µl of annealed oligo pairs, 2 µl of 10X buffer, 2 µl of ligase (5 units), and 9 µl of H2O. The mixture is then incubated at room temperature for 1 hour. Following ligation, the reaction is transformed into Top10 cells and incubated at 37°C overnight. Colonies are picked the next day for mini-prep analysis.

For transfection into MLE-12 cells, a 6-well plate is utilized. Firstly, 1 µg of the vector is mixed with 2 µg of empty vector. Lipofectamine is prepared at a ratio of 1 part DNA to 2 parts Lipofectamine. A) It involves mixing 3 µg of DNA with 125 µl of Opti-MEM and waiting for 5 minutes at room temperature. B) It requires mixing 6 µl of Lipofectamine with 125 µl of Opti-MEM and also waiting for 5 minutes at room temperature. Options A and B are then combined and left to incubate for 15 minutes at room temperature before being added to the MLE-12 cells. The following day, the media is replaced to include puromycin for selection, and positive clones are screened for in a 96-well plate. Positive cells were selected using puromycin (2 µg/ml) for 3 days prior to clonal expansion and single clone selection. Single-positive clones were isolated and genotyped. The sequences of primer pairs used for genotyping of transgenic *Rnf20*+/- MLE-12 cells are described in Material section.

3.1.4.2 Generation of Hif1a knockdown stable cell lines

For a generation of HIF1α knockdown stable cell line, $0.5X10^6$ HEK293T cells were seeded on a 6-well plate and transfected with 1.5 µg plasmids containing shRNA for *Hif1a* or control shRNA, along with packaging plasmids using X-tremeGENE DNA transfection reagent (Roche, 6366236001). Viral supernatant was collected 48h after transfection and used to transduce control and *Rnf20+/-* MLE12 cells in the presence of 0.1% polybrene. 48h after transduction, cells were selected with 5 µg/ml puromycin for two passages and were maintained in a normal medium containing 2 µg/ml puromycin.

3.1.4.3 Transient transfection of siRNA in NCI-H82 cells

Human *RNF20* siRNA and control siRNA were purchased from Horizon (ON-TARGET plus siRNA, SMART Pool, Cat#: L-007027-00-0005). 10^5 H82 cells in a 6-well plate and transfected them with 25nM siRNAs using Lipofectamine RNAiMax (Thermo Fisher Scientific, 13778-075). Following an overnight incubation with the transfection mix, medium was replaced and cells were harvested for RNA and protein isolation 72 hours post-transfection.

3.1.4.4 Cryopreservation and thawing of cells

Cultured cells were cryopreserved by resuspending the cell pellet in freezing medium containing 10% DMSO and put in freezing box which is placed immediately in -80°C freezer overnight and then placed in -195°C liquid nitrogen for long term storage.

3.1.5 Sample Size of *Rnf20+/- and control* mice lung tissues & *Rnf20* LOF and control cell lines for metabolomics analysis:

For the LC-MS based metabolomics analysis in *Rnf20*+/- and *WT* mice lung tissue, 25mg of lung tissue was sent for the analysis. The process involved sacrificing mice at 1 year of age. The lungs were harvested and washed with PBS three times to remove any

contaminants. Subsequently, 25mg of lung tissue was weighed and immediately transferred to test tubes, followed by snap-freezing in liquid nitrogen to preserve the metabolite profile. The tissue samples were then packaged in dry ice and sent for LC-MS based metabolomics analysis.

For the *Rnf20* LOF (loss-of-function) cell line and the control cell line, 5 million cells were counted for each before sending them for metabolomics analysis. The cell lysis process involved treating the cells with trypsin 0.25%, followed by resuspension in PBS and centrifugation to remove the supernatant. The cells were then suspended again in 10 ml of PBS, and 10µl of the cell suspension were counted under a microscope. Cells were centrifuged and supernatant were removed and immediately snap froze in liquid nitrogen and Subsequently, 5 million cells from each of three biological replicates of both the control and *Rnf20* LOF cell lines were counted and sent in dry ice for metabolomics analysis.

3.1.6 Lactate assay

For lactate assay, medium of the MLE-12 cells and H82 cells cultured for 24 hours is collected and passed through a 10KDa molecular spin filter to remove the LDH from the sample since LDH from the FBS containing medium could degrade the lactate and then proceed for assay according to manufacturer's instructions (K607).

MLE-12 cells were seeded at a density of 1500 cells per well in a 96-well plate and grown overnight. The supernatant of the cells is diluted directly with assay buffer. Added 2–50 µl of test samples to a 96-well plate. Adjust the volume to 50 µl/well with lactate assay buffer. Mixed enough reagents for the number of assays to be performed. For each well, prepare a total of 50 µl of reaction mix containing lactate assay buffer (46 µl), lactate enzyme mix (2 µl), and probe (2 µl) and mix well. Added 50 µl of the reaction mix to each well containing the lactate standards and test samples and mixed well. I incubated the reaction for 30 minutes at room temperature, protected from light. Measured absorbance at OD 570 nm.

3.1.7 Glucose uptake assay

For Glucose uptake assay, equal number of cells were seeded for 12 hours and next day proceeded for the assay according to manufacturers instructions (K676).

MLE-12 cells were seeded at a density of 1500 cells per well in a 96-well plate and grown overnight. Cells were washed twice with PBS and starved in 100µl serum free adipocyte medium overnight (to increase glucose uptake), then rewashed 3X with PBS. The cells were starved for glucose by preincubating with 100µl Krebs-Ringer-Phosphate-HEPES (KRPH) buffer containing 2% BSA for 40 min, then stimulated with 1µM insulin for 20min. 10µl of 10mM 2DG was added and then cells were incubated for 20 min. Washed cells 3X with PBS to remove exogenous 2-DG. To degrade endogenous NAD(P) and to denature enzymes, lysed cells with 80µl of extraction Buffer, frozen or thawed once, and heated at 85°C for 40 min. Cooled the lysate and neutralized by adding 10µl of Neutralization Buffer. & diluted 1:50 times. Added 1-50 µl sample per well. Adjusted the final volume to 50 µl with Assay Buffer. As a control, a parallel sample well was prepared and not treated with insulin or 2-DG. For the enzymatic reaction step, mix enough reagent for the number of assays (control, sample, and standard) to be performed. For each well, prepare 10µl Reaction Mix A (Assay Buffer: 8µl and Enzyme Mix: 2µl). Added 10µl Reaction Mix A into each well. Mix and incubate at 37°C for 1hr. To degrade unused NADP, added 90µl of extraction buffer to each well, sealed with aluminum sealing tape, and heated at 90°C for 40 min. Cool on ice for 5 minutes and 12µl of neutralization buffer. For each well, prepared 38ml recycling reaction Mix B (Glutathione Reductase: 20µl, Substrate (DNTB): 16µl, Recycling Mix 2µl). Add 38µl Reaction of reaction mix B into each well. Mixed well. For the standard curve, diluted 2-DG6P Standard to 0.1 mM (100 pmol/µl) by adding 10 µl of 10 mM 2-DG6P to 990 µl Assay Buffer and mixed well. Diluted further to 0.01 mM (10 pmol/µl) by adding 50 µl of 0.1 mM 2-DG6P to 450 µl assay buffer. Add 0, 2, 4, 6, 8 and 10 µl into a series of well on a 96 well plate in duplicate to generate 0, 20, 40, 60, 80, and 100 pmol/well of 2-DG6P Standard. Adjusted volume to 50 µl/well with the assay buffer. Measured absorbance at 412 nm in a microplate reader at 37°C every 5 min until the 100 pmol standard reaches 1.5–2.0 OD.

3.1.8 Boyden chamber migration and invasion assay

Boyden chamber inserts were placed on 24-well plates containing 10% FCS medium. $1x10^5$ MLE12 cells or 2 $x10^5$ H82 cells were seeded on top of the insert in a 0% FCS medium, overnight (for H82 cells, 24hrs later), the insert membranes were fixed with 3.7% formaldehyde for 10 min and washed 3 times with PBS. The upper surface of the membranes was cleaned by wiping with a piece of wet paper. Membranes were then stained with crystal violet for 10 minutes. Images of randomly selected areas were acquired with a 20x objective and the number of cells that had migrated to the lower surface of the membrane was quantified using ImageJ (http://imagej.nih.gov/ij/). The *in vitro* Matrigel invasion assay was essentially similar to the cell migration assay described above, except that the membrane filter was precoated with 50 µl diluted Matrigel (diluted with serum free culture medium, final working concentration 1 mg/ml) for 2 hrs before seeding the cells. 24 hrs later, the insert membranes were fixed. For each migration and invasion assay.

3.1.9 Soft agar colony formation assay

Cell proliferation was measured using CellTiter 96® AQueous One Solution Cell Proliferation Assay (MTS) according to manufacturer's protocol. Absorbance was measured at 490 nm. Absorbance is proportional to the number of living cells in culture. For soft agar colony formation assay, control and Rnf20 loss of function MLE12 cells were suspended in complete DMEM/F12 medium containing 0.3% low melting agarose, and plated onto solidified 0.6% agarose in complete DMEM/F12 medium in 12-well culture plates at a density of 5,000 cells per well. The colonies were stained with 0.005% Crystal Violet.

3.1.10 Sodium dodecyl sulfate-Polyacrylamide Gel electrophoresis (SDS PAGE)

5-15% separating gel were made (depending upon the size of the protein of interest) of 30% acrylamide/ 0.8% N, N' – methylene bisacrylamide solution. 5% stacking gels were made on the separating gels with comb lanes. Protein samples were mixed with loading dye and heated at 95°C for 10min and cooled down and loaded into the gel. Proteins were separated by applying 60V until the protein stacks and then 100V when the

protein reaches the separating gel and then run until the front dye reaches to the bottom of the gel and just before the front dye go out run is stopped. Prestained markers were loaded in parallel.

3.1.11 Western blotting analysis

After electrophoresis, the gel was transferred carefully to a nitrocellulose membranes using a wet transfer system at 100V for 1hour. After transfer the nitrocellulose membrane were blocked with 5% milk in PBS and 0.5% tween. The membranes were incubated with primary antibody with appropriate dilution for 1 hour. The membranes were then washed with washing buffer (PBS containing 0.5% tween) and then incubated with HRP conjugated secondary antibody for 1 hour.

3.1.12 Immunoprecipitation and immunoblotting

For immunoprecipitation, 50 µg whole cell lysate fraction of control and *Rnf20+/-* MLE12 cells were diluted with co-IP buffer (50 mM Tris pH7.5, 100 mM NaCl, 15 mM EGTA, 0.1% Triton-X100, protease inhibitors SET-I (Sigma) into 500 µl for each co-IP reaction. The lysates were then incubated with the indicated antibodies overnight at 4 °C followed by 3 hrs incubation with Protein-A/G-Sepharose beads (GE Healthcare). Immunoprecipitates were washed five times in co-IP buffer, dissolved in 2x SDS-PAGE sample buffer, and subjected to standard western blot analysis.

3.1.13 Seahorse Extracellular Acidification (ECAR) assay

Extracellular acidification (ECAR) and oxygen consumption (OCR) rates were measured using the Seahorse XFe96 analyzer (Seahorse Bioscience) following the manufacturer's protocols. Briefly, ECAR and OCR were measured 4 h after seeding MLE-12 cells (40.000 cells per well) on XFe96 microplates. MLE-12 cells were maintained in non-buffered assay medium in a non-CO_2 incubator for 1 h before the assay. The Glycolysis stress test kit (Seahorse Bioscience) was used to monitor the extracellular acidification rate under various conditions. Three baseline recordings were made, followed by sequential injection of glucose (10 mM), the mitochondrial / ATP synthase inhibitor oligomycin (3 µM), and the glycolysis inhibitor 2-deoxy-D-glucose (2-DG; 500

mM). The Mito stress test kit was used to assay the mitochondrial respiration rate under basal conditions, in the presence of the ATP synthase inhibitor oligomycin (3 μM), the mitochondrial uncoupler carbonyl cyanide-4-(trifluoromethoxy)phenyl-hydrazone (FCCP; 1 μM), and the respiratory chain inhibitors antimycin A (1.5 μM) and rotenone (3 μM).

3.1.14 RNA Isolation, RT-PCR and Real-Time PCR

RNA was isolated using the TRIzol RNA Isolation Reagent (Invitrogen). For real-time PCR analysis cDNA was synthesized with the High Capacity cDNA Reverse Transcription Kit (Applied Biosystems) and real-time PCR was performed using the SYBR GREEN PCR master mix (Applied Biosystems). Cycle numbers were normalized to those of HPRT.
For RNA-Seq, the RNA was isolated using RNeasy Microarray kit (Qiagen #73304).

3.1.15 Luciferase reporter Assay

Dual luciferase assays were performed following transient transfection of MLE-12 cells in 48 well plates with a total of 200ng of DNA per well, containing 158ng effector plasmid, 40ng Hypoxia regulatory element (HRE) luciferase reporter plasmid, 2ng *Renilla* luciferase plasmid. Luciferase activities were measured with Luciferase Assay system (Promega, E1500) by Tecan Spark microplate reader and the values were normalized to Renilla values.

3.2 Statistical analysis

Results from quantitative analyses are presented as mean +/- standard error of the mean (SEM) and Student T-test. Statistical analysis was performed using one way anova. Sample sizes were determined based on previous experience with analogous experiments. Statistical significance was defined as *$p<0.05$, **$p<0.01$, ***$p<0.001$, **** $p<0.0001$. Experiments are performed in 3 or more biological replicates.

3.3 Materials

3.3.1 Antibiotics

Name	Final conc	Source
Ampicillin	100µg/ml	sigma
Puromycin	4µg/ml	sigma
Penicillin/Streptomycin	50µg/ml	sigma

3.3.2 Cell culture media

Name	Source
DMEM, 4.5g/L D glucose GlutaMAX™	Gibco
DMEM/F12 1:1 mixture	Gibco
RPMI-1640	Gibco

3.3.3 Chemicals

Name	Source
2 log DNA ladder	New England Biolabs
BSA	NEB
Agarose, electrophoresis grade	Roth
Noble Agar	Sigma-Aldrich
Albumin fraction V (BSA)	Roth
Ammonium Persulphate (APS) $((NH_4)_2S_2O_8)$	Sigma-Aldrich
Ampicillin sodium salt	Sigma-Aldrich
Bradford reagent ready to use	Fermentas
Bradford reagent	Fermentas
Chloroform	Sigma

Citrate	Sigma
DMSO	Sigma
DTT	Roth, karlsruhe, Germany
Dry milk, non fat, blotting grade	Bio-rad
EDTA	Sigma
EGTA	Roth
Eosin, aqueous	Sigma
Ethanol, absolute	Roth
Ethidium bromide	Sigma
Formide	Sigma
Formaldehyde	Sigma
Glycine	Sigma
Glycerol	Roth
HCl	Sigma
Hematoxylin	Sigma
HEPES	Sigma
Isofluran CP	Cp-pharma
Isopropanol	Roth
KCl	Roth
Methanol	Roth
$MgCl_2$	Sigma
Na_2HPO_4	Sigma
NaCl	Sigma
NaOH	Sigma

3.3.4 Oligonucleotides

Oligos for qPCR	Sequence
q*POGLUT1*_F	TCTCCTTCAGTAAGACATCAGAGT
q*POGLUT1*_R	CTGTGCTGCTGACCTTACCA
q*LDHA*_F	CACGTCAGCAAGAGGGAGAA

q*LDHA*_R	ACTTGCAGTTCGGGCTGTAT
q*SLC2a1*_F	AGAACAAGCAAAGGCGTTCAA
q*SLC2a1*_R	CTAGCGCGATGGTCATGAGT
q*RNF20*_F	AGTTCTGCCTTGTCTCCGC
q*RNF20*_R	CATGGAGGTGCCAGGTTCTC
qHPRT_F	*AGGACTGAACGTCTTGCTCG*
qHPRT_R	*TCCAGCAGGTCAGCAAAGAA*
q*Ldha*_F	AACTTGGCGCTCTACTTGCT
q*Ldha*_R	TAGCCGCCTGAGGACTTACT
q*Pfkfb3*_F	AGGACACGCCTTCCTTTCAG
q*Pfkfb3*_R	ACTGACACTTGTTCTCCGCA
q*Hif1a*_F	GCGGCGAGAACGAGAAGAAA
q*Hif1a*_R	GGGGAAGTGGCAACTGATGA
q*Slc2a1*_F	AATGGCGGCGGTCCTATAAA
q*Slc2a1*_R	GCCAAACACCTGGGCAATAAG
qRnf20_F	CGAACACTGCAATCCAAGAA
qRnf20_R	TGACCTACTTTGGTTTGGCTACT
qPdk1_F	GTCTTTAACCAGGGGCGGTG
qPdk1_R	CAACCTGCGGCTGTATGCC
qEno1_F	GTCCACTGGCATCTACGAGG
qEno1_R	GCTGGTGCCAGGAACTCAT
qVegfa_F	TATTCAGCGGACTCACCAGC
qVegfa_R	AACCAACCTCCTCAAACCGT
qPoglut1_F	CCAGAAGGACTCAGGCTCAAA
qPoglut1_R	GGTCCTCTTCTATGACGCCG
qHprt_F	CAGTCCCAGCGTCGTGATTA
qHprt_R	TGGCCTCCCATCTCCTTCAT

3.3.5 Genotyping primers for generation of *Rnf20* LOF cell line

Forward Primer 1	CGAACACTGCAATCCAAGAA
Reverse Primer 1	CTCAAAGCAAAGTTCAACTTC
Reverse Primer 2	CTCTCAAAGTTCTCACAGTTC

3.3.6 Genotyping primers for Rnf20+/- mice

Rnf20_Forward Primer	CTAGCAGTATGGTGGAGCCTCAGG
Rnf20_Reverse Primer	CTTAACCGAGACTAAGGACACAGC
LAR3	CAACGGGTTCTTCTGTTAGTCC

3.3.7 Antibodies

Name	Source	Identifier
CD45 antibody	Abcam	Cat# ab10558, RRID:AB_442810
Ki67 antibody	Abcam	ab15580, RRID:AB_443209
E Cadherin antibody [DECMA-1]	Abcam	Cat# ab11512, RRID:AB_298118
Fibronectin antibody	Abcam	Cat# ab2413, RRID:AB_2262874
Mouse Anti-N-Cadherin Monoclonal Antibody	Sigma-Aldrich	Cat# C3865, RRID:AB_262097
Monoclonal Anti-alpha-Tubulin antibody produced in mouse	Sigma-Aldrich	Cat# T5168, RRID:AB_477579
PDK1	Cell signaling technology	Cat# 3062
Ldha	Cell signaling technology	Cat# 2012S

Rnf20	abcam	Cat# ab32629
Rnf20	Novus	Cat# NBP2-54995
Name	Source	Identifier
Glut1(mouse)	Alpha Diagnostics	Cat#GT11-A
Hif1alpha (C-Term) rabbit polyclonal	Caymann Chemicals	Cat# 10006421
V5	Invitrogen	R960-25

3.3.8 Enzymes

Name	Source
Red Taq DNA polymerase	Sigma
RNAseA	Roche
Proteinase K	Sigma
Restriction enzymes and buffers	NEB
Trypsin EDTA	Gibco

3.3.9 Commercial kits

Name	Source
Syber green PCR master mix	Applied biosystems
Red Taq PCR master mix	Invitrogen
High performance reverse transcriptase kit	Fermentas
Glucose uptake kit	Biovision
Lactate assay kit	Biovision

Gene elute plasmid miniprep kit	Sigma
Gene elute plasmid midiprep kit	Sigma
Gene elute PCR cleanup kit	Sigma
ECL western blotting detection kit	GE, USA

3.3.10 Eukaryotic cell lines

Cell line	Description
HEK293T	Human embryonic kidney cells expressing the large T antigen of the SV-40 virus
MLE-12	Murine lung epithelial 12 (MLE-12) cells
NCI-H-82	National Cancer Institute human-82

3.3.11 Solutions, reagents and media

Name	Composition or supplier
2x SDS PAGE sample buffer	150mM Tris pH 6.8, 1.2% (v/v) SDS, 30% (v/v) SDS, 30% (v/v) glycerol, 6.7% (v/v) β-mercaptoethanol, 1.8mg bromophenol blue
10x PBS	1.37M NaCl, 27mM KCl, 0.1M Na_2HPO_4. $12H_2O$, 17.6mM KH_2PO_4 (pH titrated to 7.4)
PBST	0.05% (v/v) Tween 20 in 1xPBS
Blotting buffer	20% (v/v) methanol, 192mM glycine, 25mM Tris
10x agarose gel sample buffer	250mg/100ml (w/v), bromophenol blue 250mg/100ml (w/v) xylene cyanol, 50mM Tris pH 7.6, 60% (v/v) glycerol
10x SDS PAGE running buffer	35mM SDS, 250mM TRIS, 0.86M glycine

2x RNA loading dye	40µl Formaldehyde, 100µl Formamide, 20µl 10x TBE, 2µl Ethidium bromide
10x TBE	0.89M Tris, 0.89M H_3BO_3, 20mM Na_2EDTA pH 8.0
Co-IP buffer	50mM Tris-HCl pH 7.5, 15mM EGTA, 100mM NaCl, 0.1% (v/v) Triton X-100
Stripping solution 1	200mM glycine, 500mM Nacl (pH titrated to 2.2)
Stripping solution 2	200mM glycine, 500mM NaCl (pH titrated to 7.4)
Sripping solution 3	200mM Tris-HCl (pH titrated to 7.4)
Washing buffer	0.1% (v/v) Tween 20 in PBS
L1 lysis buffer (ChIP)	50mM Tris pH 8, 2mM EDTA pH 8, 0.1% (v/v) NP40, 10% (v/v) glycerol
L2 nuclear resuspension buffer (ChIP)	50mM Tris pH=8, 5mM EDTA pH 8, 1% (w/v) SDS
DB dilution buffer (ChIP)	200mM NaCl, 50mM Tris pH 8, 5mM EDTA, 50mM 0.5% NP40
NaCl-washing buffer (ChIP)	500mM NaCl, 20mM Tris pH 8, 2mM EDTA, NP40 (v/v) 1%, 0.1% (w/v) SDS
LiCl-wasing buffer (ChIP)	500mM LiCl, 20mM Tris pH 8, 2mM EDTA, 1% (v/v) NP40, 0.1% (w/v) SDS
EB-extraction buffer (ChIP)	10mM Tris pH 8, 1mM EDTA, 2% (w/v) SDS
TE-buffer	10mM Tris pH 8, 1mM EDTA
Tail Lysis Buffer	100mM Tris pH 8.5, 5mM EDTA, 0.2% SDS, 200mM NaCl, 100µg/ml Proteinase K
Cytoskeletal (CSK) buffer	10mM PIPES, pH 6.8, 100mM NaCl, 300mM sucrose, 1mM EGTA, 1mM MgCl2
L-Glutamine	Gibco
β mercaptoethanol	Signa-Aldrich

Matrigel@ Growth Factor Reduced (GFR) Basement Membrane Matrix	Corning (354230)
Hematoxylin Solution	Sigma-Aldrich (GHS 116)
Eosin Y solution	Sigma-Aldrich (HT 110216)
Crystal violet solution	Sigma-Aldrich (HT901)
Fisher Chemical™ Permount™ Mounting Medium	Fisher Scientific
ProLong™ Gold Antifade Mountant	Thermo Fisher Scientific
Permount mounting media	Fischer scientific
Fluorsave reagent	Calbiochem
Paraformaldehyde	Sigma

Chapter 4: RESULTS

4.1 Deletion of one allele of *Rnf20* causes spontaneous lung tumor formation in mice

The exact mechanisms behind the development of spontaneous cancers when one allele of *Rnf20* is lost are not well understood. However, researchers have discovered that the loss of H2Bub, primarily catalyzed by RNF20, leads to adenocarcinomas with increased malignancy and poor differentiation. Additionally, immunohistochemistry analysis revealed that a significant majority of lung adenocarcinoma samples exhibit extremely low or undetectable levels of H2Bub [107]. Thus, my hypothesis was that *Rnf20* heterozygous knockout (*Rnf20*+/- KO) mice would develop spontaneous lung tumors. It is worth noting that global *Rnf20* homozygous knockout (*Rnf20*-/- KO) mice do not survive beyond the embryonic stage due to their lethal nature. Therefore, to study the role of RNF20 in lung cancer development, I kept *Rnf20*+/- and wild type mice on normal diet for 6 and 1 year. Mice were kept at an ambient temperature of 23 ± 2°C with constant humidity and a 12-hour light/12-hour dark cycle. Mice had free access to water and were fed ad libitum with normal diet.

At the final time points of 6 months and 1 year, I euthanized both the *Rnf20*+/- and wild-type mice (Fig 7A), and subsequently performed histological examinations on their tissues. In brief, lungs were isolated (Fig 7B), fixed with 3.7% formaldehyde, and embedded in the paraffin. 7µm thick paraffin sections were used for hematoxylin and eosin staining. I observed that 75% (6 out of 8) *Rnf20*+/- mice formed lung tumors at 6 months of age compared to 14.3% (1 out of 7) wild type (WT, +/+) mice and that 75% (15 out of 20) *Rnf20*+/- mice formed lung tumors at 1 year of age compared to 8.3% (1 out of 12) WT mice (Fig 7C). This indicated a significantly high incidence of spontaneous tumor formation in *Rnf20*+/- mice at 6 months and 1 year of age.

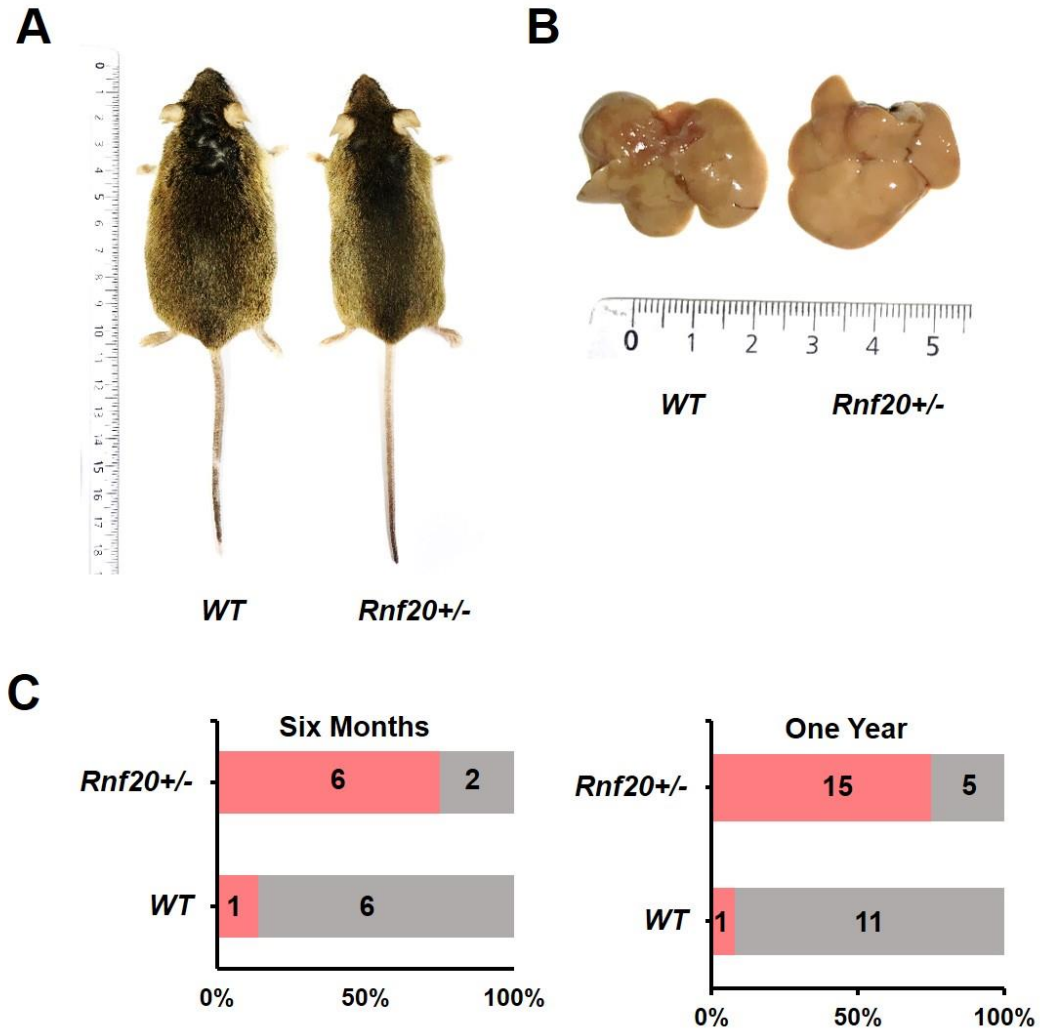

Figure 7. Loss of one allele of *Rnf20* causes spontaneous lung cancer. A, Representative image of wild type and *Rnf20+/-* mice. **B,** Representative image of wild type and *Rnf20+/-* mice lungs. **C,** *Rnf20+/-* mice have an extremely high tumorigenic incidence of 75% at six months and one year compared to WT mice. Compared to WT mice, which showed one out of seven mice had tumors at six months and one out of twelve mice at one year, Rnf20+/- mice showed six out of eight mice at six months and fifteen out of twenty mice had tumors at one year.

4.2 Loss of one allele of *Rnf20* causes spontaneous Adenocarcinoma in mice lung

There was little known about the type of tumors formed in *Rnf20+/-* mice lung. After analyzing the histology of the spontaneous lung tumors developed in *Rnf20+/-* mice, I observed the presence of large tumors exhibiting distinct characteristics of

adenocarcinoma (Fig 8). These tumors displayed enlarged nuclei and an ample amount of cytoplasm, which are typical features associated with adenocarcinoma.

To confirm whether these tumors were indeed adenocarcinoma, I conducted immunohistochemistry staining specifically for thyroid transcription factor 1 (TTF1), a well-established marker for adenocarcinoma. The results of the staining demonstrated that these tumors were positive for TTF1, confirming their adenocarcinoma nature.

Further investigation were carried out to assess tumor cell proliferation and immune cell infiltration within these tumors. For evaluating tumor cell proliferation, I utilized an antibody specific to Ki67, which is a commonly used marker for cell proliferation. Simultaneously, I used an antibody specific to CD45, a marker for immune cells, to examine the level of immune cell infiltration in the tumors (Fig 8). As anticipated, the immunohistochemical analysis revealed that the tumor cells positive for TTF1 exhibited Ki67-positive cells, indicating tumor cells undergoing proliferation. Nevertheless, number of TTF1 positive cells undergoing proliferation were low. Additionally, these tumors also showed CD45-positive cells, suggesting immune cell infiltration. However, the infiltrating CD45-positive cells were low in number.

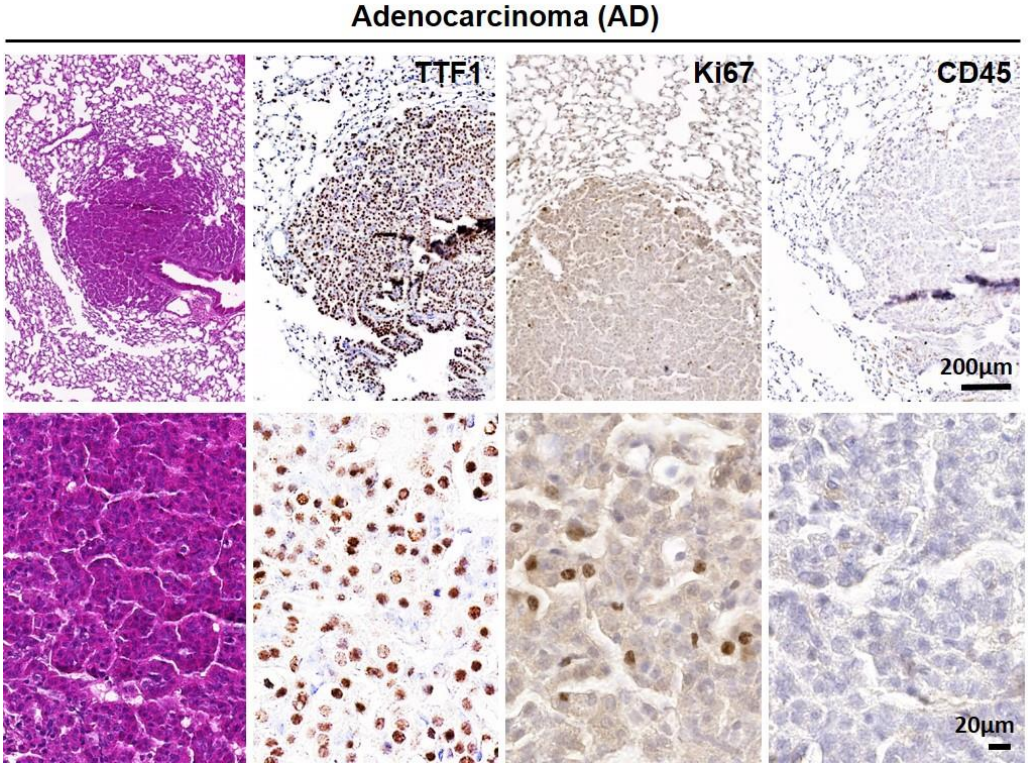

Figure 8. *Rnf20+/-* mice deciphers adenocarcinoma in lungs. Representative images (left to right) of H & E stainings and immunohistochemistry stainings for TTF1, Ki67 and CD45 of mouse lungs of Rnf20+/- mice. Scale bars, 200µm and 20µm.

4.3 *Rnf20* haplo-deficiency causes spontaneous small cell like lung carcinoma in mice lung

After analyzing the histology of the spontaneous lung tumors developed in *RNF20+/-* mice, I also observed the presence of tumors exhibiting distinct characteristics of small cell like lung carcinoma (Fig 9). These tumors displayed small nuclei with scant cytoplasm, which are typical features associated with SCLC.

To confirm whether these tumors were indeed SCLC, I conducted immunohistochemistry staining specifically for Synaptophysin (Syp), a well-established marker for SCLC. The results of the staining demonstrated that these tumors were positive for Syp, confirming their SCLC nature.

Further investigation were carried out to assess tumor cell proliferation and immune cell infiltration within these tumors. For evaluating tumor cell proliferation, I utilized an antibody specific to Ki67, which is a commonly used marker for cell proliferation. Simultaneously, I used an antibody specific to CD45, a marker for immune cells, to examine the level of immune cell infiltration in the tumors (Fig 9). As anticipated, the immunohistochemical analysis revealed that the tumor cells positive for Syp exhibited Ki67-positive cells, indicating tumor cells undergoing proliferation. Interestingly, number of Syp-positive cells undergoing proliferation were high when compared with TTF1-positive tumors. Additionally, these tumors also showed CD45-positive cells, suggesting immune cell infiltration. Unexpectedly, the infiltrating CD45-positive cells in Syp-positive tumor cells were high in number when compared with TTF1-positive tumors in the *Rnf20+/-* mice.

SCLC is a highly aggressive malignancy in humans with a poor prognosis [108]. Up until now, there have been no reports suggesting a connection between the depletion of *Rnf20* and the development of SCLC. Therefore, the discovery that *Rnf20+/-* mice exhibited SCLC is a novel and significant finding.

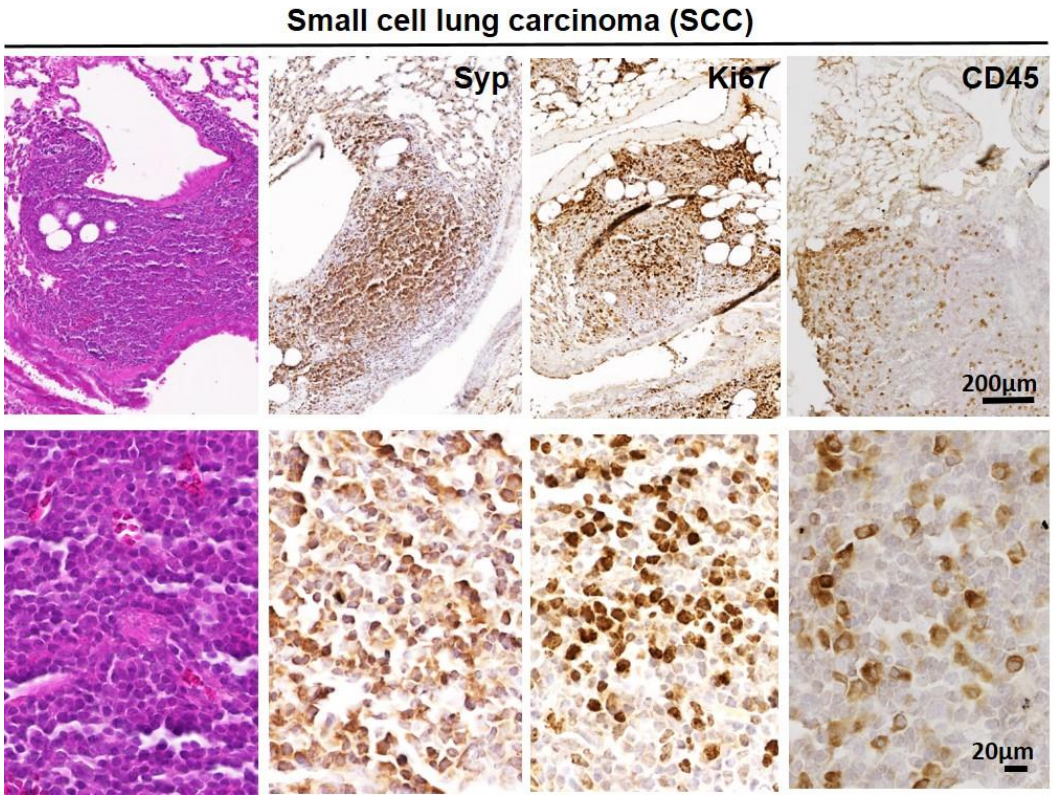

Figure 9. *Rnf20+/-* mice deciphers small cell like lung cancer phenotype. Representative images (left to right) of H & E stainings and immunohistochemistry stainings for Syp, Ki67 and CD45. Scale bars, 200µm and 20µm.

4.4 SCLC and AD patients exhibit lower levels of RNF20 and Human patients with low levels of RNF20 had a poorer survival rate than those with high levels of RNF20

To confirm the relevance of *Rnf20+/-* mice data, human patient samples were analysed. According to the analysis, RNF20 protein levels in patients with SCLC and a progressive loss in high-grade adenocarcinoma AD were significantly decreased (Fig 10A). Moreover, according to Kaplan-Meier plotter analysis, the lung cancer patients with low expression of *RNF20* had a poorer survival outcomes compared to patients with higher *RNF20* expression levels (Fig 10B). This finding suggested that RNF20 may play a crucial role in lung cancer progression and patient outcomes. However, it's important to note that correlation does not necessarily imply causation. While the study indicates an association between low *RNF20* expression and poor patient survival, further research

would be required to establish whether RNF20 itself directly influences patient outcomes or if it is simply a marker for other underlying factors that affect lung cancer progression.

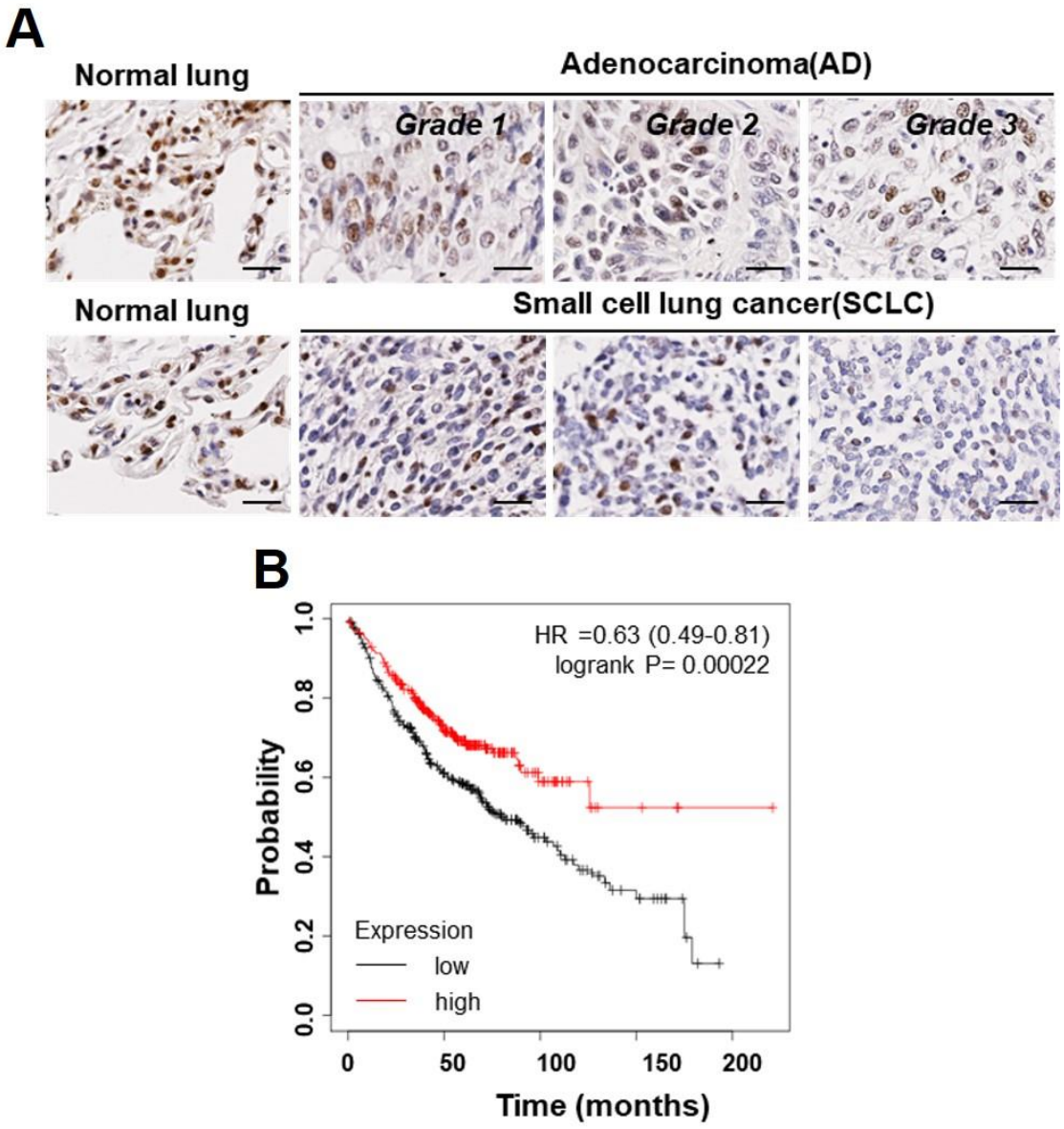

Figure 10. Human lung cancer showed a lower level of RNF20. **A,** Immunohistochemistry of representative tissue samples from different types and grades of lung tumors from a tissue microarray stained with an anti-RNF20 antibody. **B,** Kaplan-Meier plotter was used for the analysis: (https://kmplot.com/analysis/), showing human patients with low levels of *RNF20* had a poorer survival rate than those with high levels of *RNF20*.

4.5 Generation of *Rnf20* loss of function cell line in MLE-12 cells

For in vitro cell culture study of *Rnf20* in mouse lung epithelial cell line MLE-12, I depleted RNF20 in MLE12 cells using clustered regularly interspaced short palindromic repeats (Crispr)/Cas9 gene editing technology (Fig 11A, upper pannel). Genotyping results showing control and *Rnf20* loss of function cell populations (Fig4A bottom pannel), in line with the previous observation that global *Rnf20* KO mice are embryonically lethal. Genotyping result was further validated by RT-qPCR (Fig11B) and western blot (Fig11C). RT-qPCR and western blot results showed ~50% reduction in the level of RNF20 in *Rnf20* LOF MLE-12 cells when compared with control MLE-12 cells.

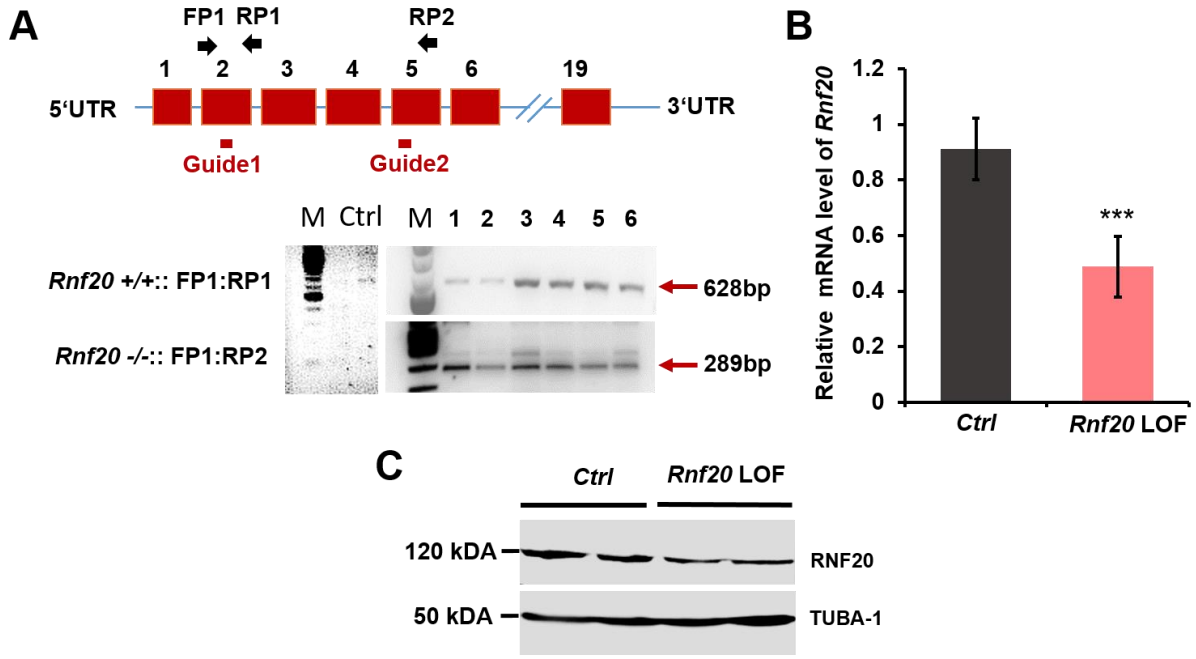

Figure 11. A, Schematic outline of knocking out of one allele of *Rnf20* gene in MLE-12 cells (Top) and Knockout verification by agarose gel and band size indicated by red arrow, guides are indicated by red bar, FP and RP represents forward primer and reverse primer **B,** mRNA expression upon depletion of *Rnf20* to around 50% level. (Data in B represents mean ± s.d., One way ANOVA. ***, P≤0.001, compared with MLE-12 control cells, (n=3). **C,** Western blot analysis of RNF20 and TUBA-1 (loading control).

4.6 *Rnf20*+/- mice lungs exhibit higher DNA damage and reduced P53 and RB levels

DNA damage-induced genome instability plays a pivotal role in the initiation and progression of tumors, making it a critical factor in understanding cancer development [109] [110]. There are several reports suggesting the RNF20 depletion leading to DNA damage [33]. In order to investigate the role of RNF20 in DNA damage in our mice model system, I isolated primary *Rnf20*+/- mouse embryonic fibroblasts from E13.5 embryos by disintegrating tissues with forceps and then growing isolated fibroblasts in petri-dishes with DMEM medium and washing the cells with PBS solution after the fibroblasts are attached to the petri-dish (4 hours). For this experiment, I have not immortalized the fibroblasts, I have used isolated mortal fibroblasts. Next, I analyzed the level of gamma H2Ax, a well-known marker for DNA damage, using immunostaining and western blot. Interestingly, I found that the level of gammaH2Ax was significantly high in *Rnf20*+/- mouse embryonic fibroblasts when compared with control fibroblasts (Fig12A & B). Importantly, without the use of any agents that cause DNA damage, Rnf20+/- MLE12 cells displayed an increase in the frequency of loci positive for the double-strand break marker H2AX (Figure 12C & 12D). Both control and Rnf20+/- MLE12 were treated with H2O2 to cause a significant increase in the H2AX loci, and labeling of H2AX at various time intervals following treatment revealed clear abnormalities in DNA repair (Fig 12A). In addition, I also analyzed the lung tissues of 6 months and 1-year-old *Rnf20*+/- mice. I observed that the level of gammaH2Ax was significantly high in both tumor and tumor adjacent tissues compared to the WT mice lung (Fig 12E). P53 and RB proteins are master regulators of genome stability [111] [112]. It was previously shown that inactivation of both P53 and RB induces small cell lung cancer in mouse model. Therefore, I analyzed the levels of P53 and RB proteins using western blot in *Rnf20*+/- MLE-12 cells. The result showed that the levels of P53 and RB proteins were significantly reduced in *Rnf20*+/- MLE-12 cells when compared with control cells (Fig 12F).

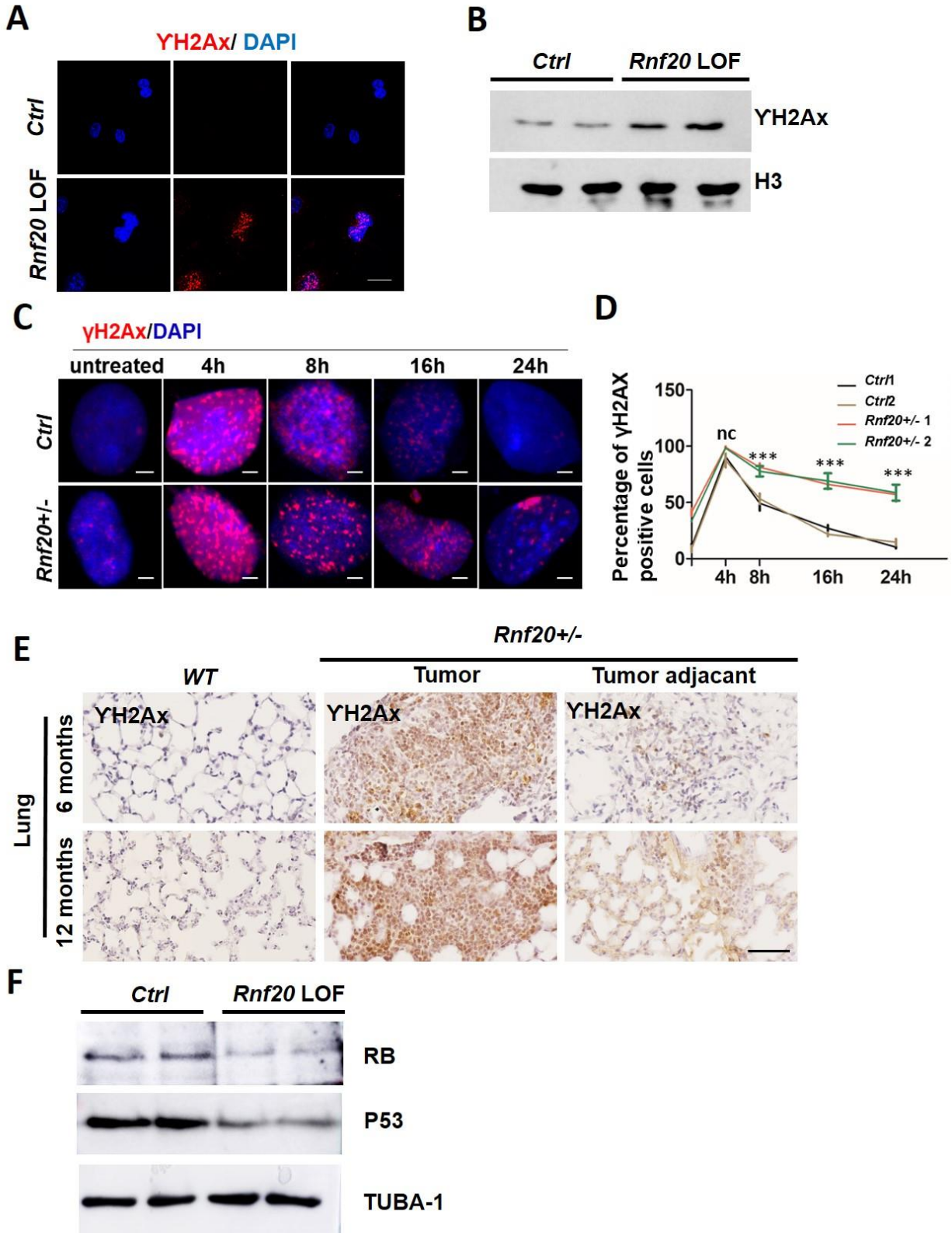

Figure 12. RNF20 depletion leads to DNA damage. A, Immunofluorescence representative pictures of control and *Rnf20* loss of function MLE-12 cells stained for γH2Ax. Scale bar, 20μm. **B,** Western blot

analysis of γH2Ax and α-Tubulin (loading control). **C,** Costaining for γH2AX (red) and DAPI (blue) of wild-type and *Rnf20*+/- MLE12 cells at the indicated time points after treatment with 0.5mM H2O2. Scale bar, 2 µm**. D,** Kinetics of γH2AX foci from (C). **E,** Representative Immunohistochemistry images of lung tumor sections for γH2Ax in WT and *Rnf20* loss of function groups at 6 months and 1 year. Scale bars, 100µm. **F,** Western blot analysis of RB, P53 and TUBA1 in control and *Rnf20* loss of function MLE-12 cells.

4.7 Haplo-deficiency of *Rnf20* causes splenomegaly and higher expression of inflammatory markers in lungs

According to recent reports, chromatin-targeting RNF20, driving histone H2B monoubiquitylation (H2Bub1), modulates inflammation and inflammation-associated cancer in mice and humans [94]. I also set out to determine whether it is true in our *Rnf20*+/- mice system in light of these observations.

At one year old, mice were sacrificed, and the spleen were harvested and imaged. I could clearly detect that the spleens of *Rnf20*+/- mice were larger than those of wild type mice (Fig 13A). Then, following standard procedure of fixing the spleen, serial dehydration, embedding the tissues, sectioning and H & E staining, I could see clear morphological abnormality in *Rnf20*+/- verses WT (Fig 13B). In order to further investigated, whether there is effect on the lungs, inflammatory markers were checked in *Rnf20*+/- lung tissues verses WT lung. Indeed, I could observe significant increase in inflammatory markers such as TNF- α and Chintinase and IL1-ß (Fig 13C & D).

According to these findings, *Rnf20*+/- mice exhibit splenomegaly and have higher levels of inflammatory markers in their lungs than wild-type mice.

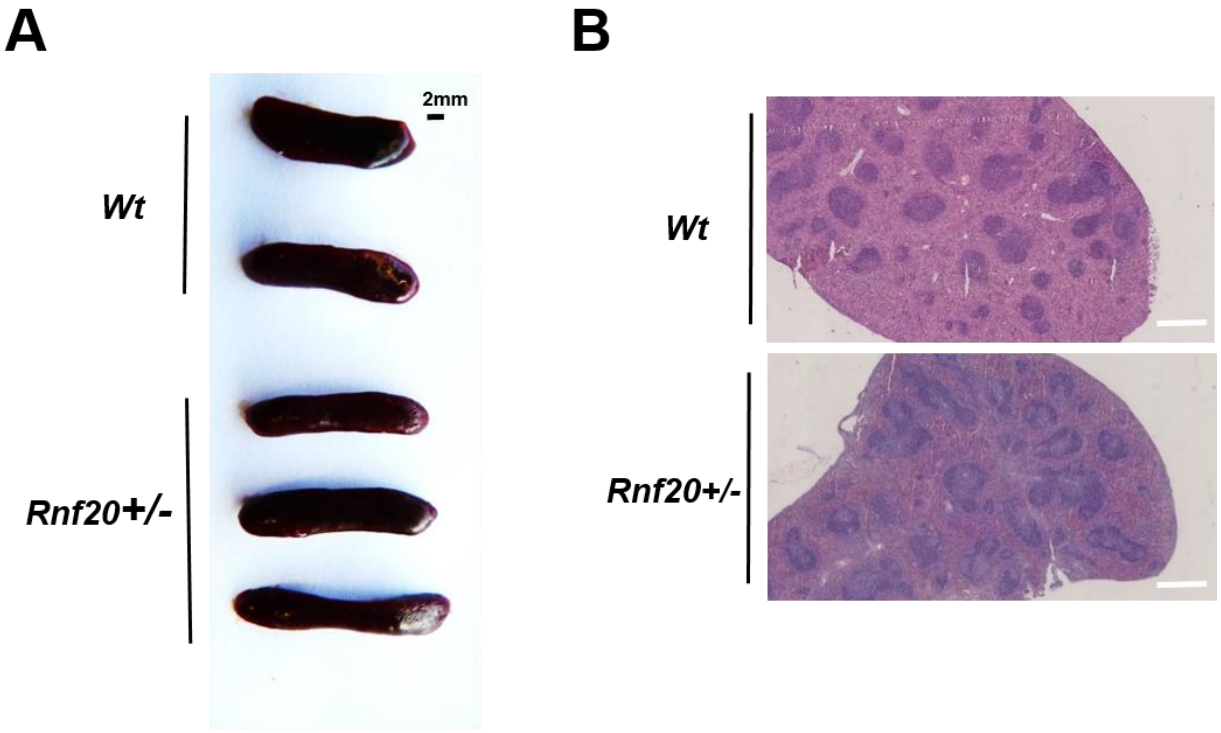
A
2mm
Wt
Rnf20+/-
B
Wt
Rnf20+/-

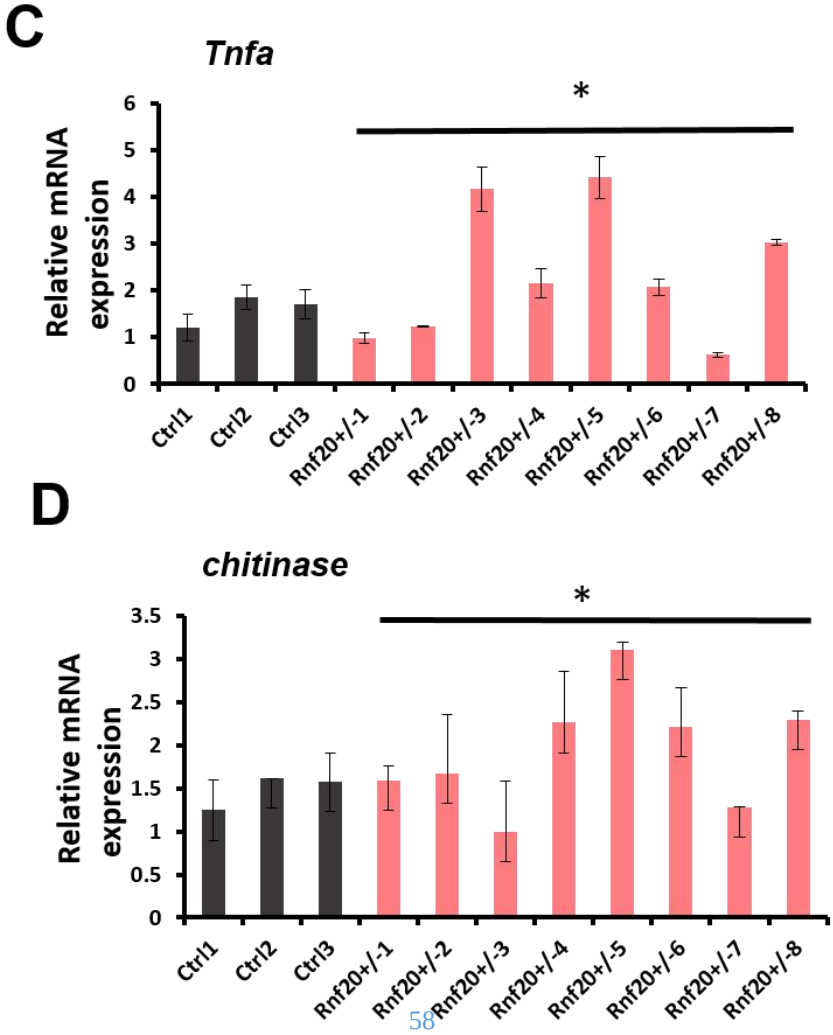
C
Tnfa
*
Relative mRNA expression
0
1
2
3
4
5
6
Ctrl1
Ctrl2
Ctrl3
Rnf20+/-1
Rnf20+/-2
Rnf20+/-3
Rnf20+/-4
Rnf20+/-5
Rnf20+/-6
Rnf20+/-7
Rnf20+/-8
D
chitinase
*
Relative mRNA expression
0
0.5
1
1.5
2
2.5
3
3.5
Ctrl1
Ctrl2
Ctrl3
Rnf20+/-1
Rnf20+/-2
Rnf20+/-3
Rnf20+/-4
Rnf20+/-5
Rnf20+/-6
Rnf20+/-7
Rnf20+/-8

Figure 13. Haplo-deficiency of *Rnf20* in mice causes inflammation and enlarged spleen. A, Representative image of spleen, wild type and *Rnf20*+/- mice (scale bar: 2mm). **B,** H & E stainings of spleen, wild type and *Rnf20*+/- mice (scale bar: 0,75mm). **C & D,** mRNA expression of TNF- α and Chitinase in lung tissues from Wild type (n=3) and *Rnf20*+/- mice (n=8) (Data in B represents mean ± s.d., One way ANOVA. ***, P≤0.001, compared with MLE-12 control cells).

4.8 *Rnf20* loss promotes epithelial mesenchymal transition and metastasis

Epithelial mesenchymal transition (EMT) is one of the important event during tumor progression, invasion and metastasis [113] [114] [115]. To determine whether RNF20 plays a role in EMT, I used *Rnf20* loss of function MLE-12 cells and control MLE-12 cells. While control MLE12 cells maintained a cobblestone-like, epithelial appearance in cell culture, *Rnf20* loss of function MLE-12 cells developed a spindle-shaped mesenchymal morphology (Fig14A). I used western blotting and mesenchymal marker like N cadherin and epithelial marker such as E cadherin to further my investigation into EMT in *Rnf20* loss of function cells. In fact, N-cadherin is increased whereas E cadherin is downregulated (Fig 14B). Additionally, I used confocal microscopy to do immunostaining on *Rnf20* loss of function cells vs WT and found that, when compared to control MLE-12 cells, *Rnf20* loss of function MLE-12 cells had a significant decrease in the epithelial marker E-cadherin and an increase in the mesenchymal markers N-cadherin and Fibronectin (Fig 14C). These findings demonstrate that, under cell culture conditions, *Rnf20* haplo deficiency causes EMT transition.

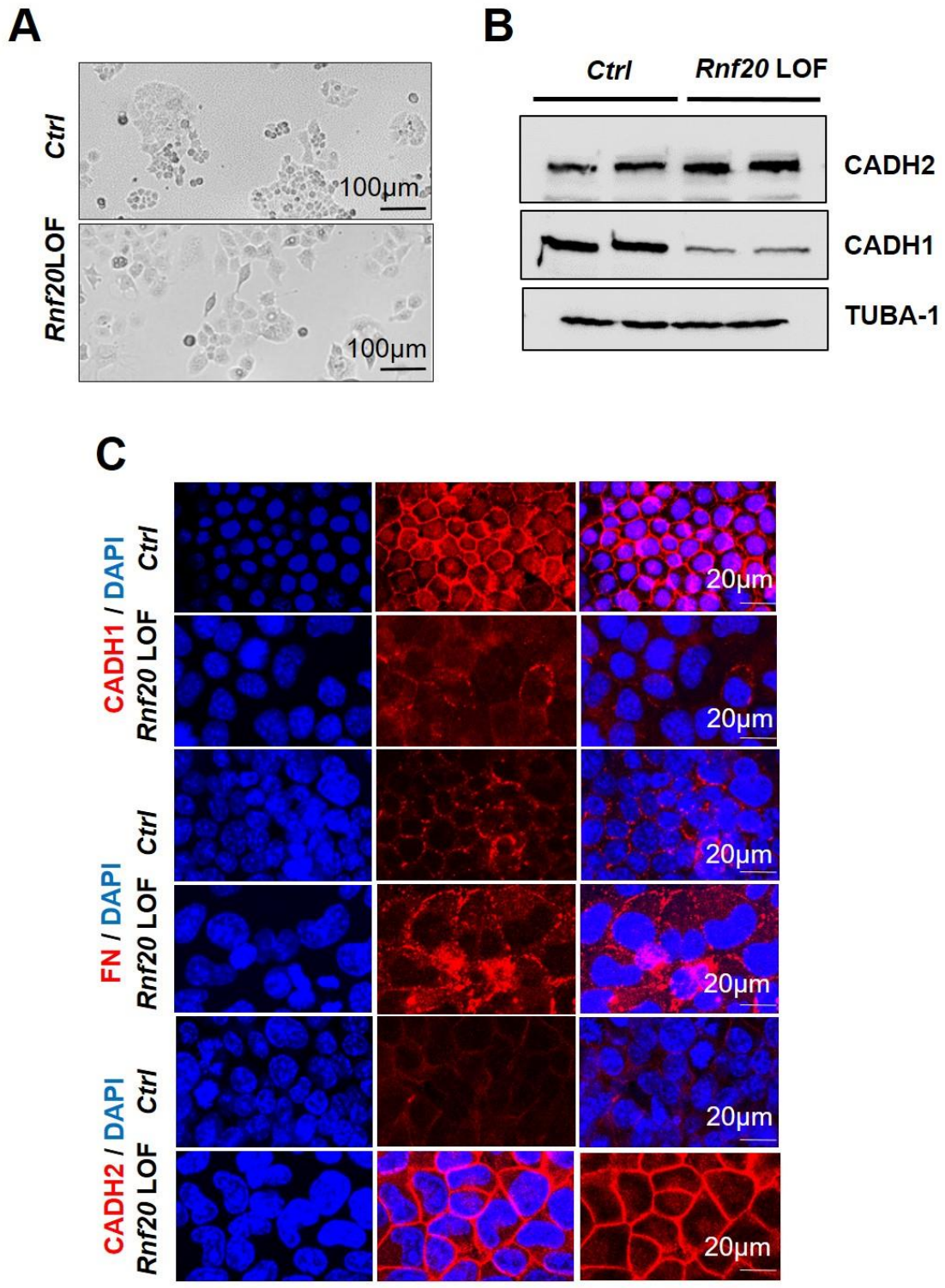

Figure 14. ***Rnf20*** **depletion induces morphological alterations and EMT in MLE-12 cells. A,** Representative microscopic images of MLE-12 control and MLE-12 *Rnf20* loss of function cells. Scale bar, 100µm. **B,** Western blot analysis CADH2, CADH1 and TUBA1 (loading control). C, Immunofluorescence representative pictures of control and *Rnf20* loss of function MLE-12 cells stained for CADH2, CADH1 and FN. Scale bar, 20µm.

4.9 *Rnf20* depletion promotes higher survival, migration and invasion in vitro

According to a previous study, *Rnf20* knockdown increases BEAS-2B cell proliferation and migration while decreasing the retinoic acid-induced squamous differentiation [107]. We used a plate colony formation experiment to examine cell survival following *Rnf20* haplo-deficency. In fact, I noticed a significantly larger number of colonies generated in an in vitro colony formation assay (Fig 15A).

In the Boyden chamber assay, MLE-12 cells were planted on top of the 24 well plate with 0% FCS. Overnight, cells were allowed to migrate through the Boyden chamber, which was put on top of the 24 well plate. As stated in methods section, cells were imaged and counted the next day. Boyden chamber experiment revealed that *Rnf20* loss of function cells had more migrated cells compared to control cells (Fig 15B). Moreover, I performed matrigel invasion assay and Rnf20 loss of function MLE-12 cells exhibit significantly higher invasive ability (15C). Similarly, I performed Boyden chamber migration assay in NCL- H 82 cells and observed more migrated cells in Rnf20 silenced cells verses control cells (15D).

Overall, our observations indicate that *Rnf20* promotes higher colony formation, migration.

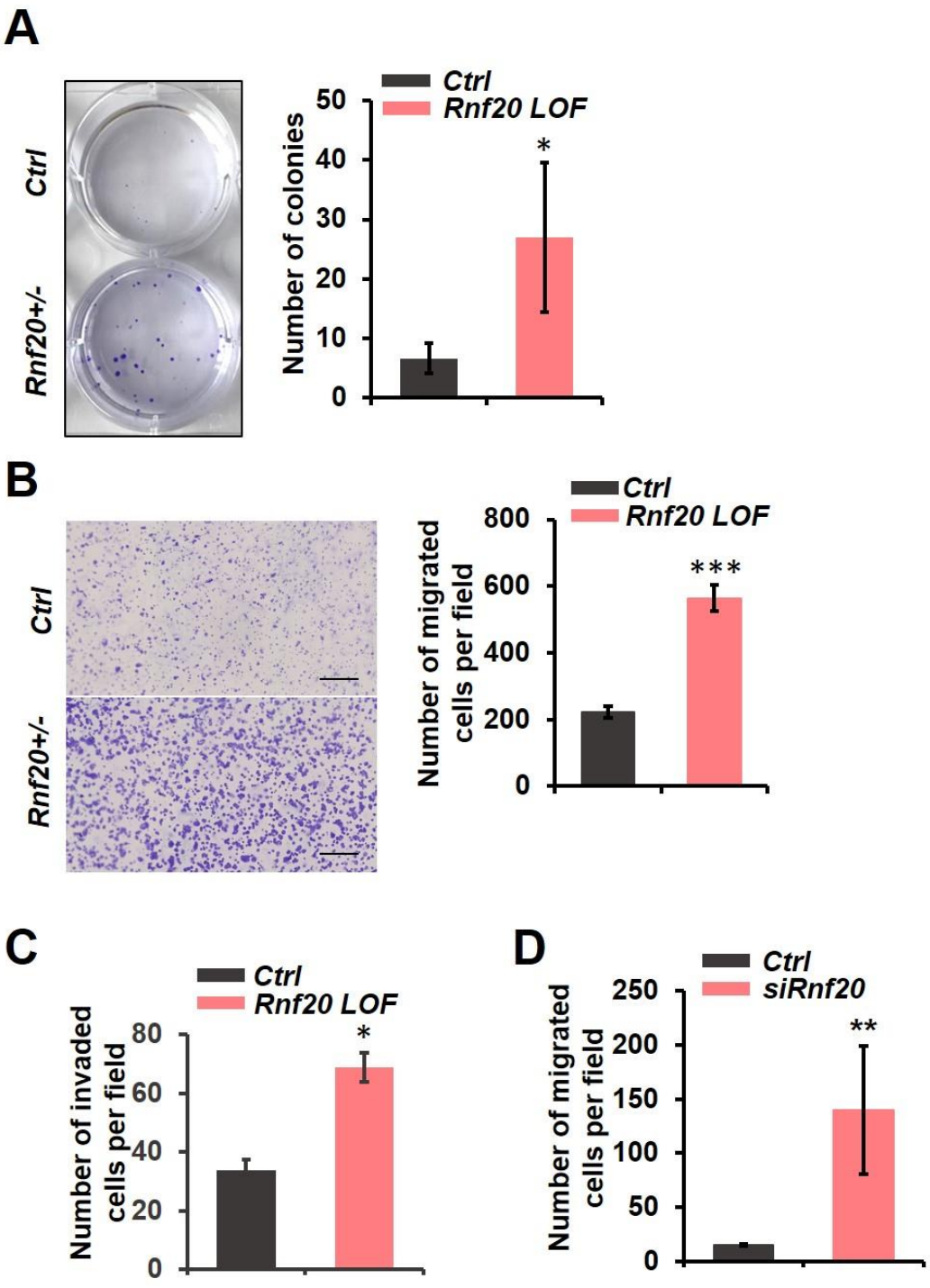

Figure 15. *Rnf20* depletion promotes cell proliferation and migration in vitro. A, Quantification of colonies formed in MLE-12 control and MLE-12 *Rnf20* loss of function cells (n=3) (*, P≤0.1 compared with MLE-12 control). **B,** Quantification of migration of MLE-12 control and MLE-12 *Rnf20* loss of function cells (n=3) (***, P≤0.001 compared with MLE-12 control cells). **C,** Quantification of invasion of MLE-12 control and MLE-12 *Rnf20* loss of function cells (n=3) **D,** Quantification of migration of NCI-H82 control cells and

siRNA mediated silencing of Rnf20 in NCL-H82 (n=3) (Data in A, B & C represent mean ± s.d., One Way ANOVA. **, P≤0.01 compared with MLE-12 control cells).

4.10 *Rnf20* deficiency leads to higher expression of metabolic genes

I sought to research the mechanism of lung cancer development in vitro. As a result, I performed RNA seq analysis. Interestingly, I discovered that the Hif1a signaling pathways and glycolysis/gluconeogenesis were the key elevated pathways (Fig 16A). Additionally, heat map analysis was able to clearly display several of the major metabolic genes that were elevated (Fig 16B). Volcano plot also shows the distribution of differentially expressed genes *Rnf20* loss of function versus control MLE12 cells (Fig 16C). I carried out qPCR analysis in *Rnf20* loss of function verses control MLE-12 cells to further validate findings from RNA seq analysis. All significant genes identified by RNAseq screening, including Ldha, pfkfb3, Poglut1, Pdk1, Eno1, Vegfa, Hif1a, and Slc2a1, were elevated as anticipated (16D). Additionally, I further validated RNAseq data using qPCR analysis via RNF20's siRNA-mediated silencing, and discovered that some important metabolic genes, including Poglut1, Slc2a1, and Ldha, were elevated (Fig 16E). Additionally, I discovered using a western blot that *Rnf20* loss of function cells have higher levels of certain crucial metabolic proteins than control cells, including Pdk1 and Ldha (Fig 16F).

Overall, my findings indicate that RNF20 depletion increases the expression of glycolytic target genes.

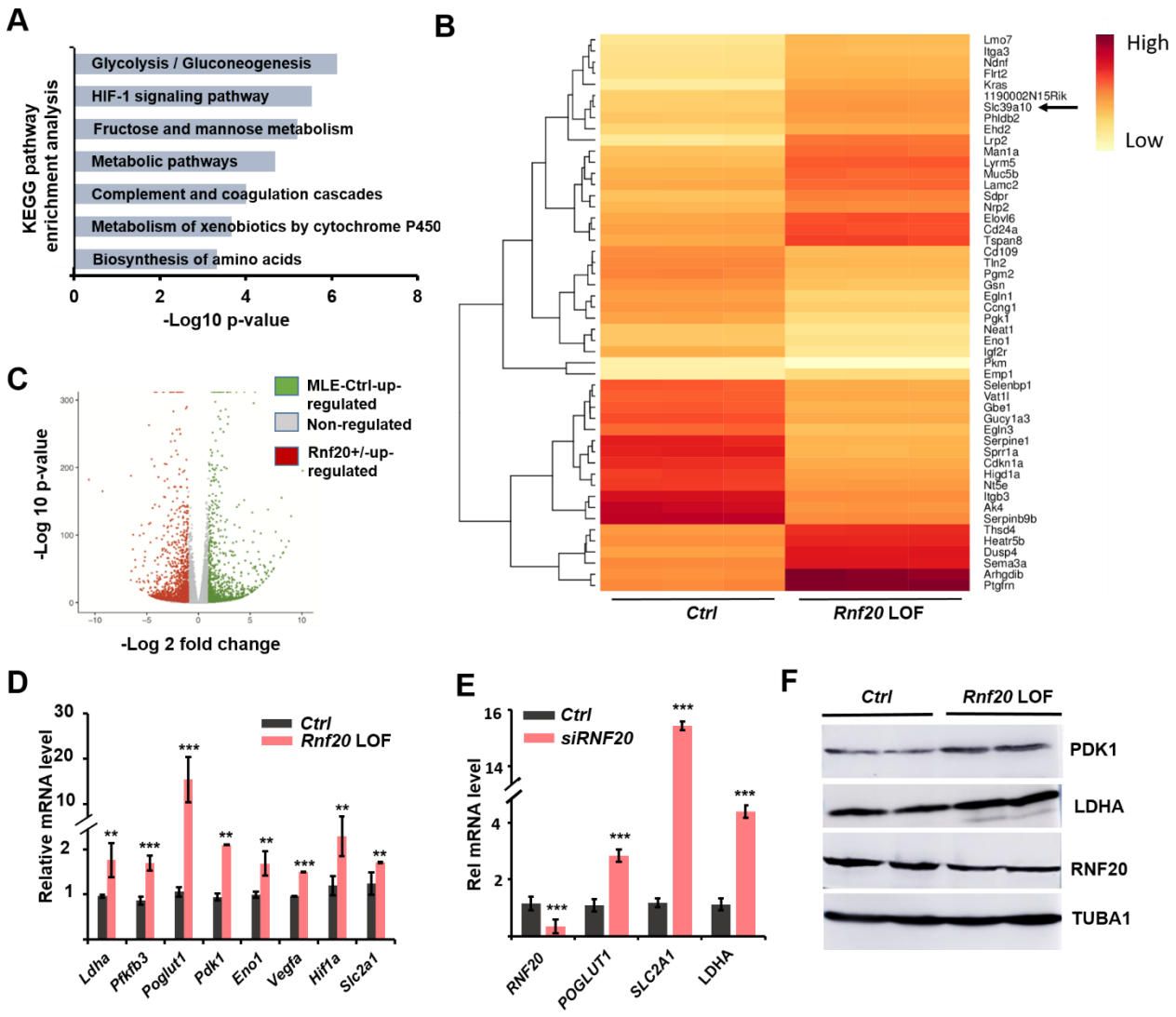

Figure 16. A, KEGG-based enrichment analysis of transcripts upregulated in *Rnf20* loss of function cells (n=3) compared to control (n=3) using DAVID bioinformatics tool and plotted by highest significance (-log10 of modified Fisher's exact P-value). **B,** Heat map depicting differentially expressed genes in *Rnf20* loss of function verses control MLE-12 cells (n=3) **C,** Volcano plot showing the distribution of differentially expressed genes in *Rnf20* loss of function verses control MLE-12 cells (n=3); log2 fold change ≤ -1; p-value < 0.05. **D,** mRNA expression of *Rnf20* depletion associated genes obtained in RNA-seq gene enrichment analysis (*Ldha*, Pfkfb3, Poglut1, Pdk1, Eno1, Vegfa, Hif1a and Slc2a1) in MLE-12 cells (n=3). **E,** mRNA expression of siRNA mediated *RNF20* depletion associated genes (POGLUT1, SLC2a1 and LDHA) in NCI-H82 cells. (Data in B represent mean ± s.d., One Way ANOVA. **, P≤0.01, ***, P≤0.001, compared with MLE-12 control cells (n=3). **F,** Western blot showing pdk1 and Ldha upregulation in MLE-12 cells.

4.11 Depletion of *Rnf20* leads to higher glycolysis in vitro

Based on my previous RNA-seq data, I observed that the depletion of *Rnf20* in MLE-12 cells led to a significant increase in the glycolysis pathway. To further investigate this functional impact, I conducted Seahorse ECAR (extracellular acidification rate) analysis. This experimental technique allows for the assessment of glycolysis-related changes in cellular metabolism. As expected, the Seahorse ECAR analysis revealed a substantial rise in glucose uptake when compared to control cells after the addition of glucose. This suggests that the glycolytic pathway is indeed enhanced in *Rnf20*-loss of function conditions. However, when oligomycin was added, there was not a significant difference in glycolytic rate compared to the control cells. This finding implies that the maximum glycolytic rate remains relatively unchanged despite the increase in glucose uptake caused by the depletion of RNF20 (as shown in Fig 17A & B). In summary, these results indicate that the depletion of RNF20 leads to an increase in the glycolytic rate specifically in response to glucose availability. However, the overall maximum glycolytic capacity seems unaffected by the absence of RNF20. These findings shed light on the functional impact of RNF20 depletion on cellular metabolism, particularly in the context of glycolysis, and provide valuable insights into the role of RNF20 in regulating metabolic pathways in MLE-12 cells.

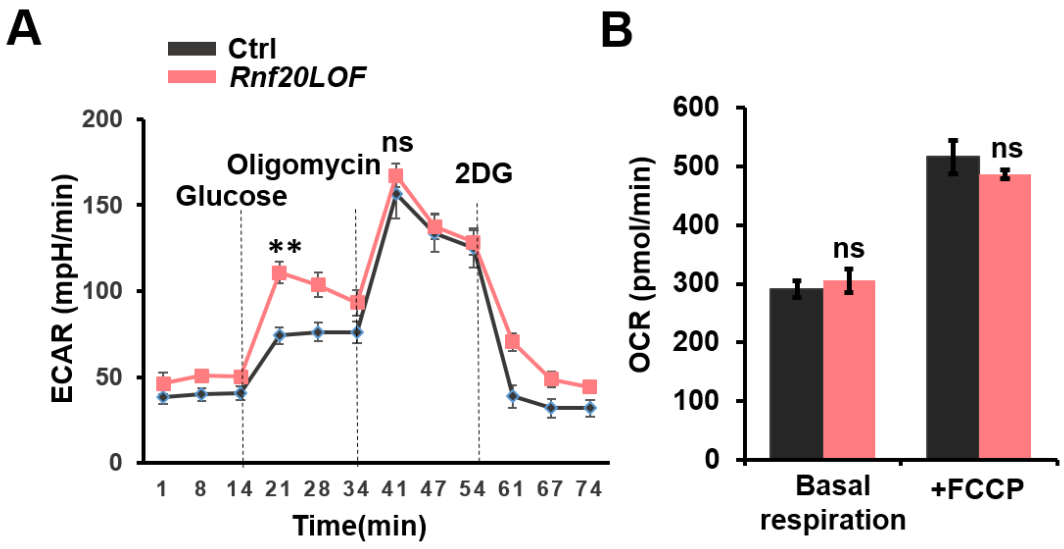

Figure 17. RNF20 depletion is critical for enhanced glycolytic activity in MLE-12 cells. A, B, Extracellular acidification rate (ECAR) in MLE-12 cells treated with or without oligomycin (Oligo) showing

increased basal glycolytic activity and no significant (ns) change in maximal glycolytic activity in control and *Rnf20* loss of function cells (n=3) (**, P≤0.01 compared with MLE-12 control cells).

4.12 In vitro, RNF20 depletion results in increased glucose uptake and lactate secretion

As it was shown in earlier results, *Rnf20* deficiency increases the rate of extracellular acidification. I examined glucose uptake in control and *Rnf20* loss of function cells in order to further validate how RNF20 depletion affects glycolysis. I discovered that there is, in fact, an increase in glucose uptake in RNF20 loss of function cells. In this experiment, 2-DG can be converted to 2-DG-6-phosphate (2-DG6P) via glucose transporters. However, 2-DG6P cannot be metabolized any further and builds up in the cells. The cells absorption of 2-DG (or glucose) is inversely correlated with the amount of accumulated 2-DG6P. Glucose uptake were analyzed in RNF20 loss of function MLE-12 cells verses control cells and I found out that there is significant increase in Glucose uptake upon depletion of RNF20 in MLE-12 cells (Fig 18A). I questioned whether a lack of RNF20 also affected lactate secretion, a crucial measure that illustrates the impact of glycolysis. In order to test the lactate secretion in two cell lines—*Rnf20*-loss of function MLE-12 cells vs control cells and *Rnf20*-silenced NCL-H82 cells versus control cells—I used the lactate secretion assay. For this assay, I used supernatant of the cells. The primary stereoisomer of lactate generated in human intermediate metabolism is L(+)-Lactate, which is found in blood. D(-)-Lactate is also found, but its concentration is only between 1 and 5 percent that of L(+)-Lactate. In the Lactate Assay Kit, a particular reaction between lactate and an enzyme mixture results in a product that causes the lactate probe to produce color through interaction. According to expectations, RNF20-loss of function cells produce more lactate than control cells, both in *Rnf20*-loss of function MLE-12 cells compared to control cells and in *Rnf20*-silenced NCL-H82 cells compared to control cells (Fig 18B & C).

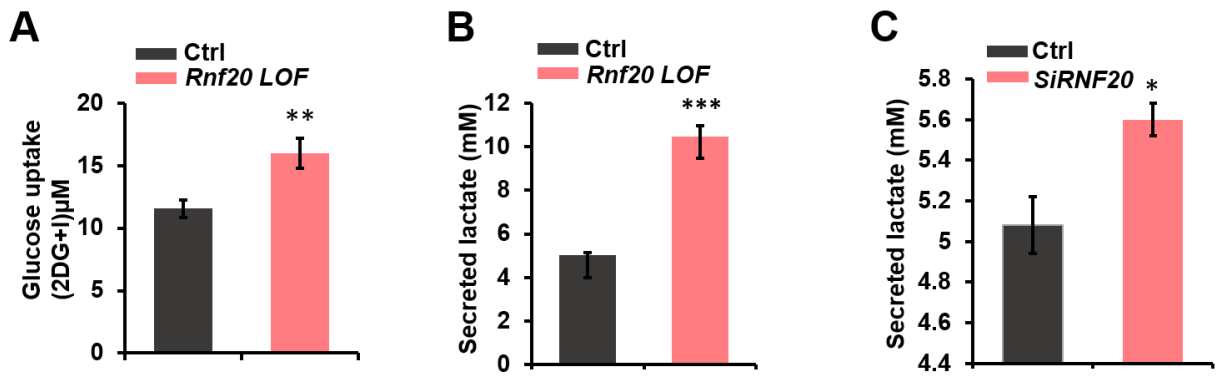

Figure 18. Depletion of RNF20 results increases glucose uptake and lactate secretion in vitro. A, Glucose uptake in *Rnf20* loss of function and control cells (n=3) starved overnight with serum free medium and then treated with 10µl of 10mM 2-deoxyglucose (2-DG) and incubated for 20min and stimulated with 1µM of insulin for 20min. **B,** Secreted lactate level in supernatant of *Rnf20* loss of function and control MLE-12 cells. **C**, Secreated lactate level in siRNA mediated silencing in Ctrl (n=3) and *RNF20* in NCL - H82 cells (n=3). (Data in A & B represent mean ± s.d., One Way ANOVA. (*, P≤0.05, **, P≤0.01, ***, P≤0.001, compared with MLE-12 control cells).

4.13 RNF20 depletion leads to changes in metabolites of Glycolytic and Krebs cycle pathway

From my previous findings, it has become evident that cells depleted of RNF20 display increased expression of metabolic genes, along with higher rates of glucose uptake and lactate secretion. These observations led me to wonder whether there were changes in the levels of metabolites within the glycolytic pathway. To investigate this further, I conducted a targeted LC-MS/MS based metabolomics analysis focused on glycolysis and Krebs cycle. For this experiment, wild type and *Rnf20+/-* mice were sacrificed, and their lung tissues were isolated and 30 mg weighed before being subjected to metabolomics analysis.

The results of the targeted metabolomics study revealed that many metabolites within the glycolytic and Krebs cycles showed significantly higher levels in the RNF20 depleted cells. A heat map representation (Fig 19A) clearly indicated this substantial increase in metabolite levels. Notably, the levels of Glucose-6-phosphate and Fructose-6-phosphate were particularly elevated, indicating a higher rate of glucose absorption in these cells.

While lactate levels were also found to be high, the difference was not statistically significant. One plausible explanation for this observation is that the lactate is predominantly secreted by the cells and therefore may accumulate more in the supernatant rather than remaining within the cells, making it difficult to detect significant changes in intracellular lactate levels.

To provide a visual representation of the key metabolites and their upregulated levels, a schematic diagram was created, with all important metabolites marked in red. Corresponding graph (Fig 19 B) further illustrated the observed upregulation of these metabolites.

These findings shed light on the metabolic alterations that occur in RNF20 depleted cells, particularly in relation to glycolysis and the Krebs cycle. The increased levels of specific metabolites indicate a shift in cellular metabolism, likely driven by the absence of RNF20.

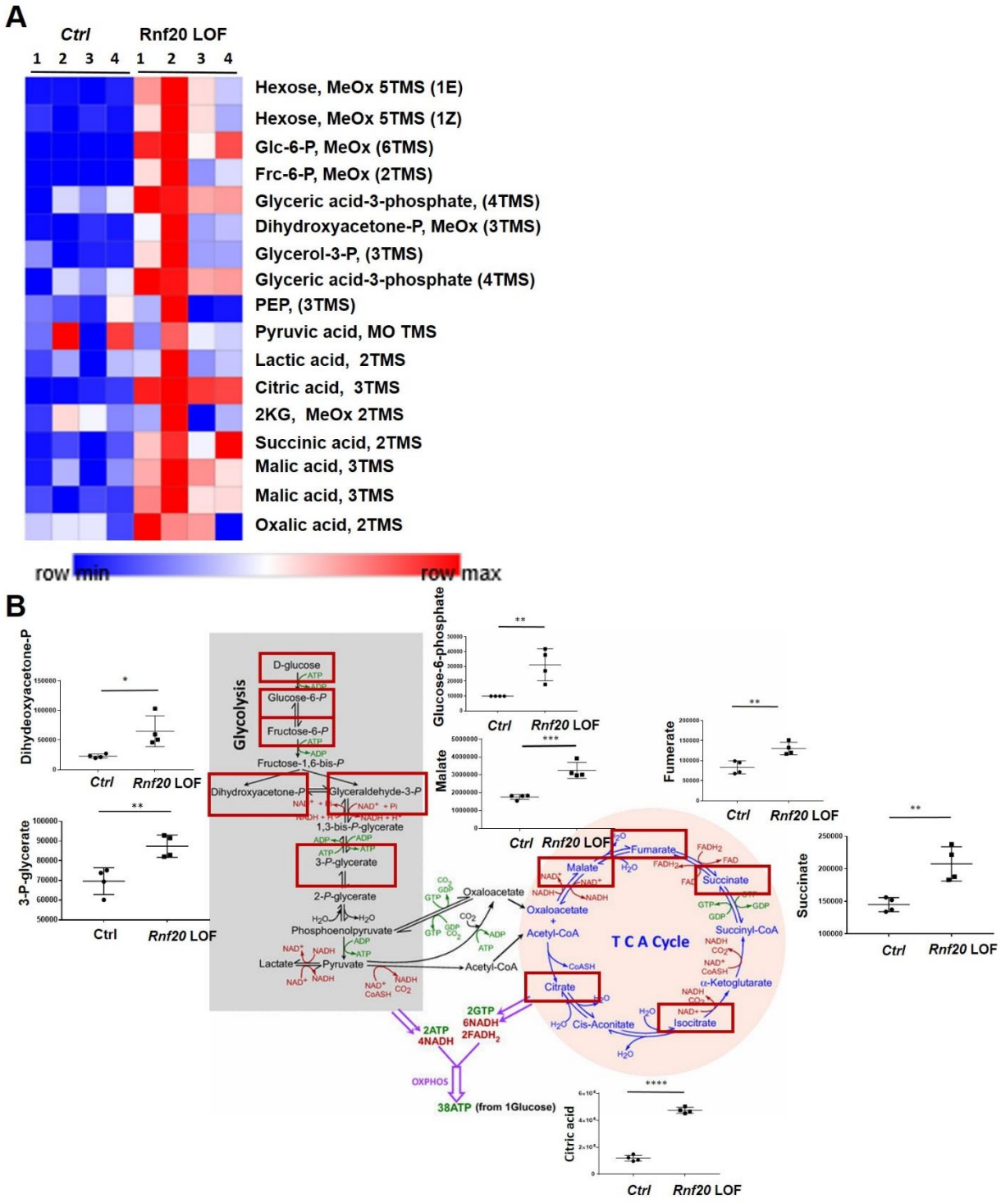

Figure 19. Critical enhancement in level of metabolites upon depletion of RNF20. A, Heat map of upregulated metabolites of glycolysis and kreb's cycle in *Rnf20* loss of function MLE-12 cells verses control cells (n=3). **B,** Schematic diagram of glycolytic and Krebs cycle with significantly enhanced metabolites from targeted LC-MS/MS based metabolomics analysis , metabolites marked in red box upon *Rnf20* loss of function MLE-12 cells verses control MLE-12 cells, backbone of glycolytic pathway modified from Alam

et al, 2016, Clin Transl Med. (Data in dot plot represents mean ± SEM, Student T-test, ****, P≤0.0001, ***, P≤0.001, **, P≤0.01, *, P≤0.05, compared with MLE-12 control cells).

4.14 *Rnf20* loss of function cells have poor ATP/AMP ratio signifying metabolic stress

Cells with a defective *Rnf20* gene displayed increased glucose uptake and metabolic gene expression, which has been established in my previous shown data. To further investigate the metabolic changes caused by *Rnf20* deficiency, I compared the metabolic data of *Rnf20*-loss of function MLE-12 cells to that of control cells. In this comparison, it was discovered that several nucleotides showed elevated levels in the *Rnf20*-loss of function cells (Fig 20A). Additionally, a striking observation was made regarding the ATP/AMP ratio, which was dramatically lower in the *Rnf20*-loss of function cells compared to the control cells (Fig 20B). This significant reduction in the ATP/AMP ratio is indicative of metabolic stress in the Rnf20-loss of function cells. These findings collectively suggest that in vitro depletion of RNF20 leads to metabolic changes that are characterized by higher metabolic gene expression, increased glucose uptake, and elevated lactate secretion in the cells. Moreover, the observed decrease in the ATP/AMP ratio serves as further evidence of the metabolic stress experienced by the *Rnf20*-loss of function cells compared to the control cells.

This study provides important insights into the role of RNF20 in cellular metabolism and highlights its potential impact on metabolic homeostasis. The altered nucleotide levels and the impaired ATP/AMP ratio signify a shift in energy metabolism in the absence of RNF20, possibly affecting cellular energy production and utilization.

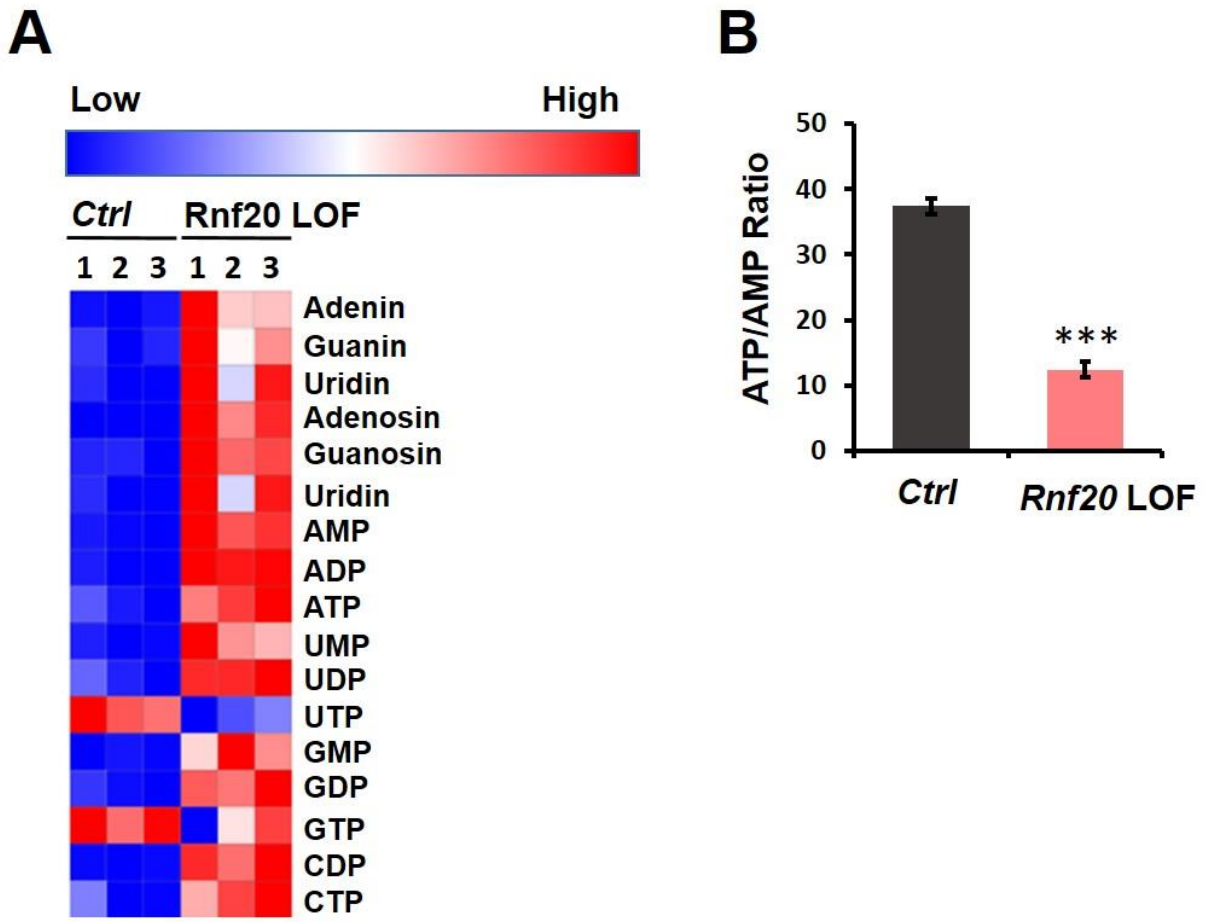

Figure 20. A, RNF20 depletion leads to enhancement of several of nucleotides and poor ATP/AMP ratio thereby shows metabolic stress. **B,** Ratio of ATP to ADP in *Rnf20* LOF MLE-12 cells verses control cells (n=3). (Data in B represents mean ± s.d., One way ANOVA. ***, P≤0.001, compared with MLE-12 control cells).

4.15 *Rnf20* deficiency exhibits higher expression and activity of Hif1a both in normoxia and hypoxia

In my RNA-seq experiment comparing *Rnf20* loss of function cells to control cells, I observed an upregulation of the HIF1a signaling pathway. This led me to further validate the expression of HIF1a using both western blot and immunostaining techniques. Through these analyses, I discovered that HIF1a levels were significantly elevated in *Rnf20* loss of function MLE-12 cells compared to control cells, regardless of whether they were under normal oxygen conditions (normoxia) or deprived of oxygen (hypoxia) (Fig

21A & B). To gain more insights, I wanted to determine whether the increased HIF1a levels were accompanied by enhanced activity. To address this question, I conducted a dual luciferase assay, which allowed me to assess the activity of HIF1a in both normoxia and hypoxia. The results were striking – *Rnf20* loss of function cells exhibited substantially higher levels of HIF1a activity compared to control cells, regardless of the oxygen conditions (Fig 21C), which may have important implications for understanding the molecular mechanisms underlying RNF20's role in regulating HIF1a signaling-mediated glucose metabolism.

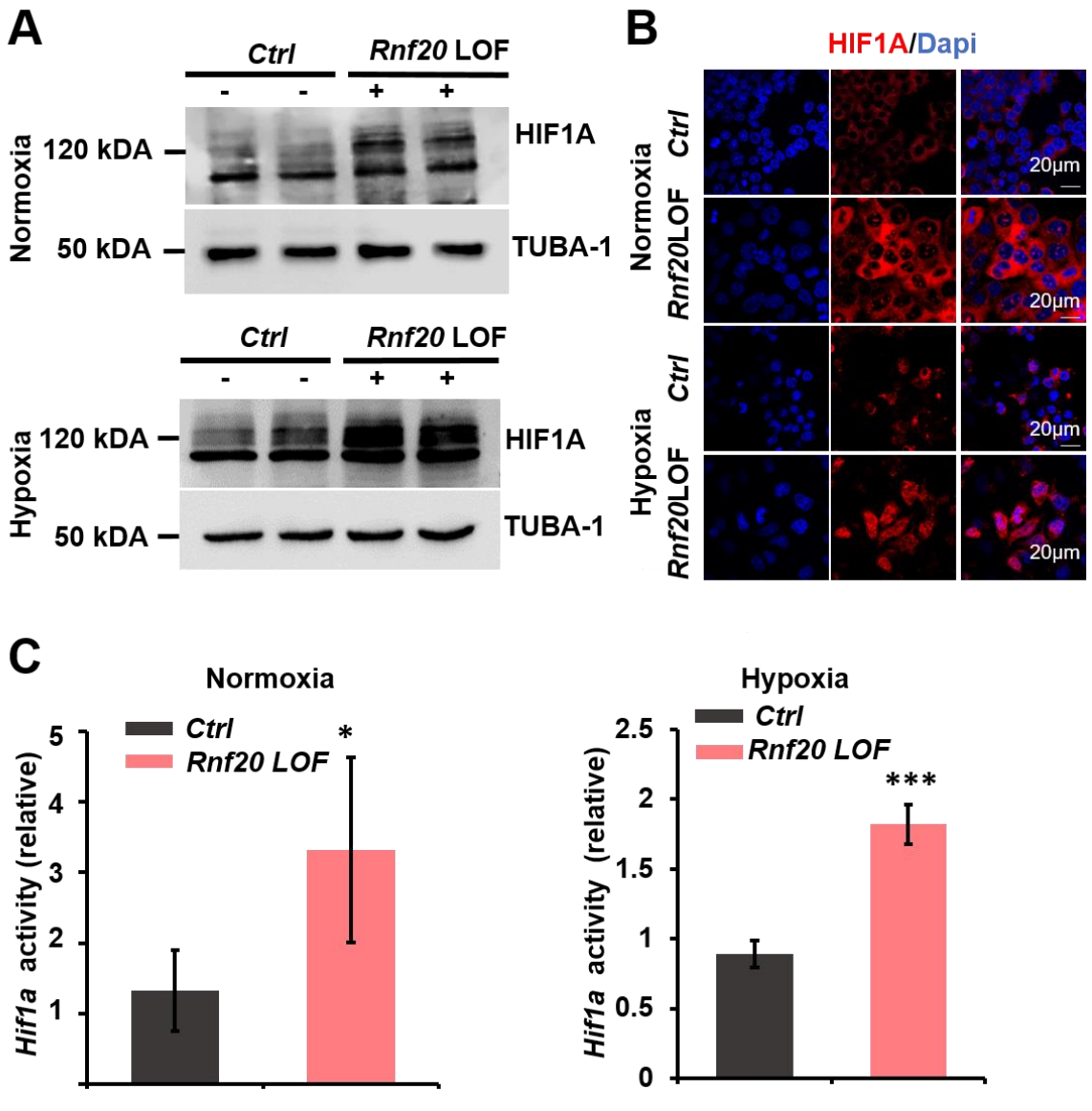

Figure 21. HIF1a is significantly upregulated upon depletion of RNF20. A, Western blot analysis of HIF1a and α-Tubulin (loading control) under normoxia (top) and hypoxia (bottom) (24 hours with 5% O_2) conditions. **B,** Immunofluorescence representative pictures of control and *Rnf20* loss of function MLE-12 cells in normoxia and hypoxia stained with anti-HIF1a antibody. Scale bars, 20μm. **C,** Relative Luciferase activity of *Hif1a* in *Rnf20* loss of function cells vs control cells (n=3) under normoxia and hypoxia (Data in C represent mean ± s.d., One way ANOVA, ***, P≤0.001, *, P≤0.05, compared with control cells).

4.16 *Rnf20+/-* mice lungs exhibit higher expression of metabolic genes

In my previous results, I have already demonstrated that the deficiency of RNF20 leads to increased expression of metabolic genes *in vitro*. To further establish the significance of this finding, I decided to investigate whether the same effect occurs in vivo using *Rnf20+/-* mice. I conducted a qPCR analysis targeting important metabolic genes, including *Ldha, Pfkfb3, Poglut1, Pdk1, Eno1,* and *Vegfa* (Fig 22A). The qPCR results revealed significant differences in the mRNA levels of these metabolic genes between the *Rnf20+/-* mice and the WT mice. These findings strongly indicate that the *Rnf20+/-* mice exhibit a distinct pattern of gene expression related to metabolism compared to the WT mice. To further investigate this, I performed immunohistochemistry to examine the expression of an important glucose transporter, GLUT1, in lung sections from both *Rnf20+/-* and WT mice. Remarkably, the immunohistochemistry results showed considerably higher expression of GLUT1 in the lungs of *Rnf20+/-* mice compared to the WT mice (Fig 22B).

Our data collectively suggests that the lungs of *Rnf20+/-* mice exhibit increased expression of metabolic genes, including GLUT1, indicating a potentially altered metabolic profile in these mice compared to the WT counterparts. These findings provide further evidence supporting the role of RNF20 in regulating metabolic gene expression, both *in vitro* and *in vivo*, and highlight its significance in the context of metabolic regulation.

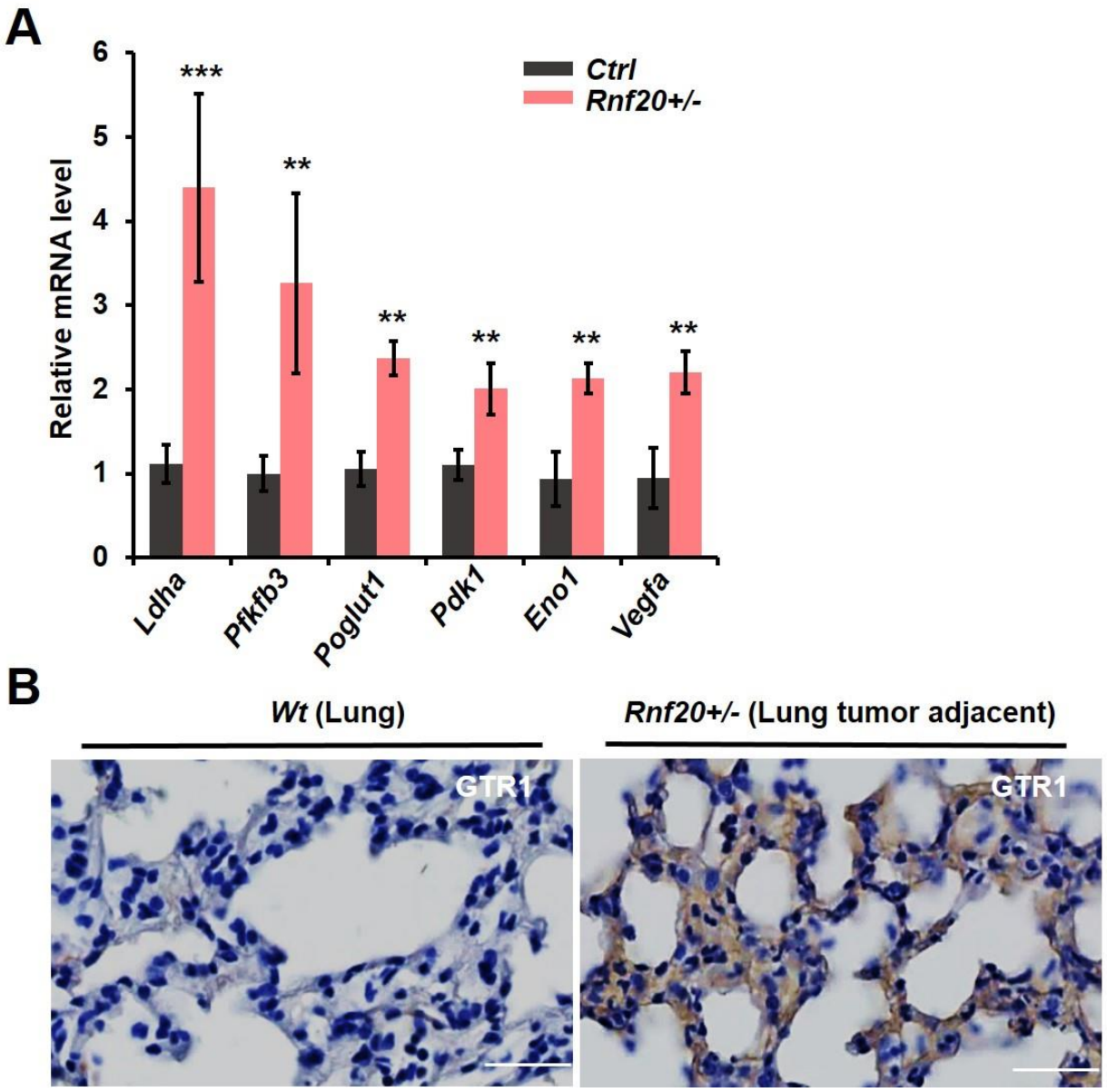

Figure 22. The lungs of *Rnf20* haploinsufficient mice showed significantly higher levels of metabolic genes. A, mRNA expression of *Rnf20* depletion associated genes obtained in RNA-seq gene enrichment analysis (*Ldha, Pfkfb3, Poglut1, Pdk1, Eno1, Vegfa, Hif1a* and *Slc2a1*) in mouse lung (n=3). **B,** Immunohistochemistry stainings for Glucose transporter-1 (GTR1) in wild type and control mouse lungs. (*, P≤0.05, **, P≤0.01, ***, P≤0.001 compared with MLE-12 control cells).

4.17 The lungs of *Rnf20+/-* mice have greater glucose uptake and lactate secretion

Since our previous findings showed that *Rnf20+/-* mice have higher metabolic, specifically glycolytic gene expression in the lungs, I set out to determine whether these mice have higher glucose uptake than wild type mice. I thus carried out targeted metabolomics analysis and discovered that the levels of the metabolites glucose-6-phosphate and fructose-6-phosphate were greater in the lungs of *Rnf20+/-* mice compared to WT mice (Fig 23A & B). For this experiment, *Rnf20+/-* and WT mice were sacrificed and lungs were isolated, 30mg of tissue is weighed and put in Eppendorfs and flash frozen in liquid nitrogen and sent for metabolomics. I also performed lactate assay in blood serum from *Rnf20+/-* mice blood and Wild type mice. As expected lactate levels were significantly higher in *Rnf20+/-* mice compared to wild type mice (Fig 23C).

In summary, our data reveal that *Rnf20+/-* mice lungs have higher glucose absorption and have higher blood lactate levels than wild type mice.

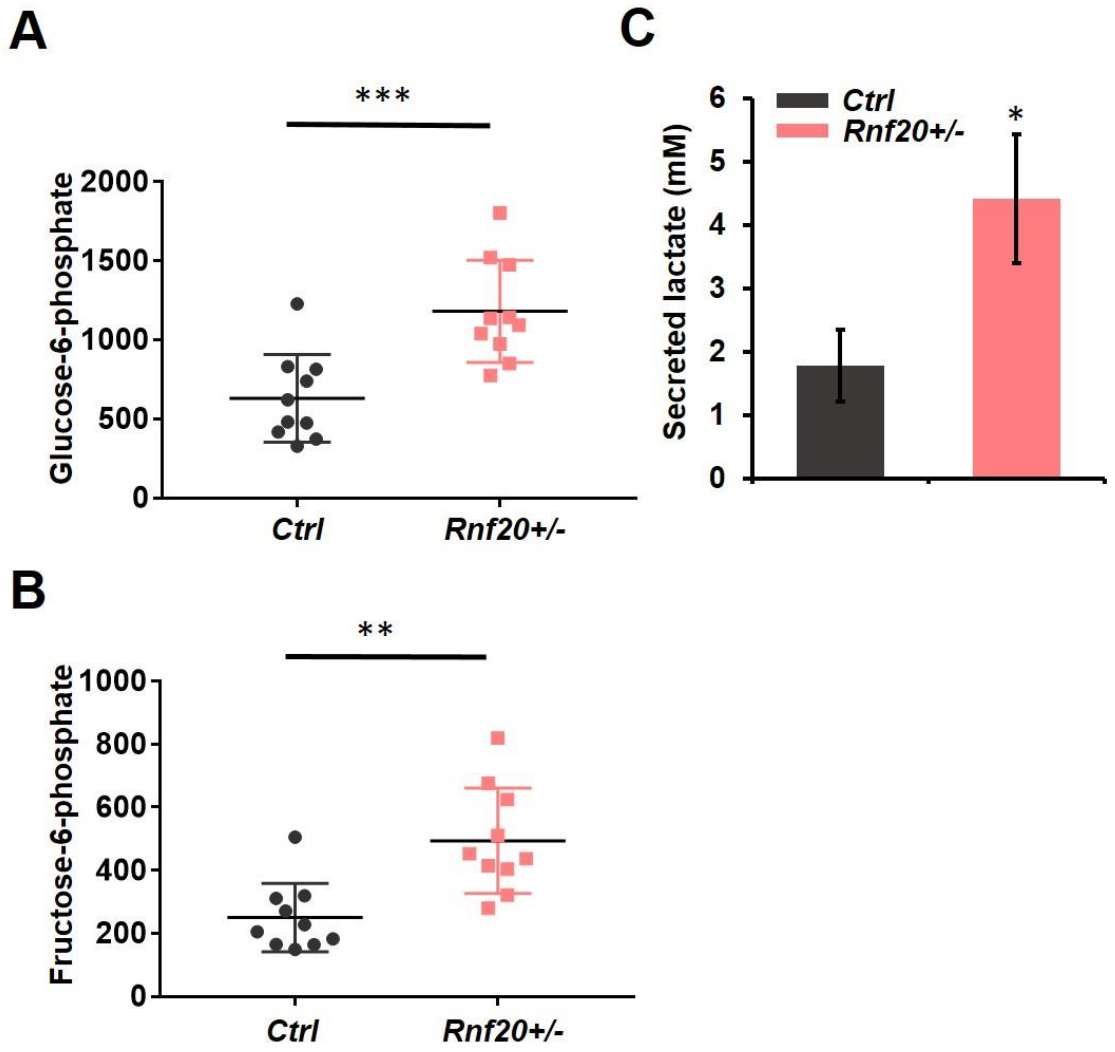

Figure 23. *Rnf20+/-* mice has higher glucose uptake as indicated by enhanced uptake of Glucose-6 phosphate and Fructose-6-phosphate and higher lactate secretion. A & B, Glucose-6-phospate and Fructose-6-phosphate level in lung homogenates of wild type and *Rnf20+/-* mice (n=10) (Data in dot plot represents mean ± SEM, Student T-test, ***, P≤0.001, **, P≤0.01, *, P≤0.05, compared with MLE-12 control cells). Y-axis represents peak values generated from LS-MS based metabolomics. **C,** Lactate secretion in wild type and Rnf20+/- mice (n=5) blood serum.

4.18 *Hif1a* loss partially rescues glycolytic rate of *Rnf20* loss of function cells

In order to investigate the specificity of the higher levels and activity of HIF1a in *Rnf20* loss of function cells, I conducted a rescue experiment. In this experiment, I knocked down *Hif1a* in both *Rnf20* loss of function cells and control cells (Fig 24A). Subsequently, I performed seahorse analysis to measure the extracellular acidification

rate in both control and *Rnf20* loss of function MLE-12 cells. The results of the seahorse analysis revealed that when *Hif1a* was knocked down, there was a partial rescue of the glycolytic rate that was previously observed in *Rnf20* loss of function MLE-12 cells (Fig 24B & C). This implies that HIF1a plays a significant role in mediating the higher glycolytic rate seen in RNF20-loss of function cells.

In summary, the rescue experiment provided evidence that the increased glycolytic rate in RNF20-loss of function cells is specifically attributed to the activity of HIF1a. This suggests a direct link between RNF20 and HIF1a in regulating glycolysis and sheds light on the underlying molecular mechanisms that contribute to altered metabolic pathways in *Rnf20*-loss of function cells.

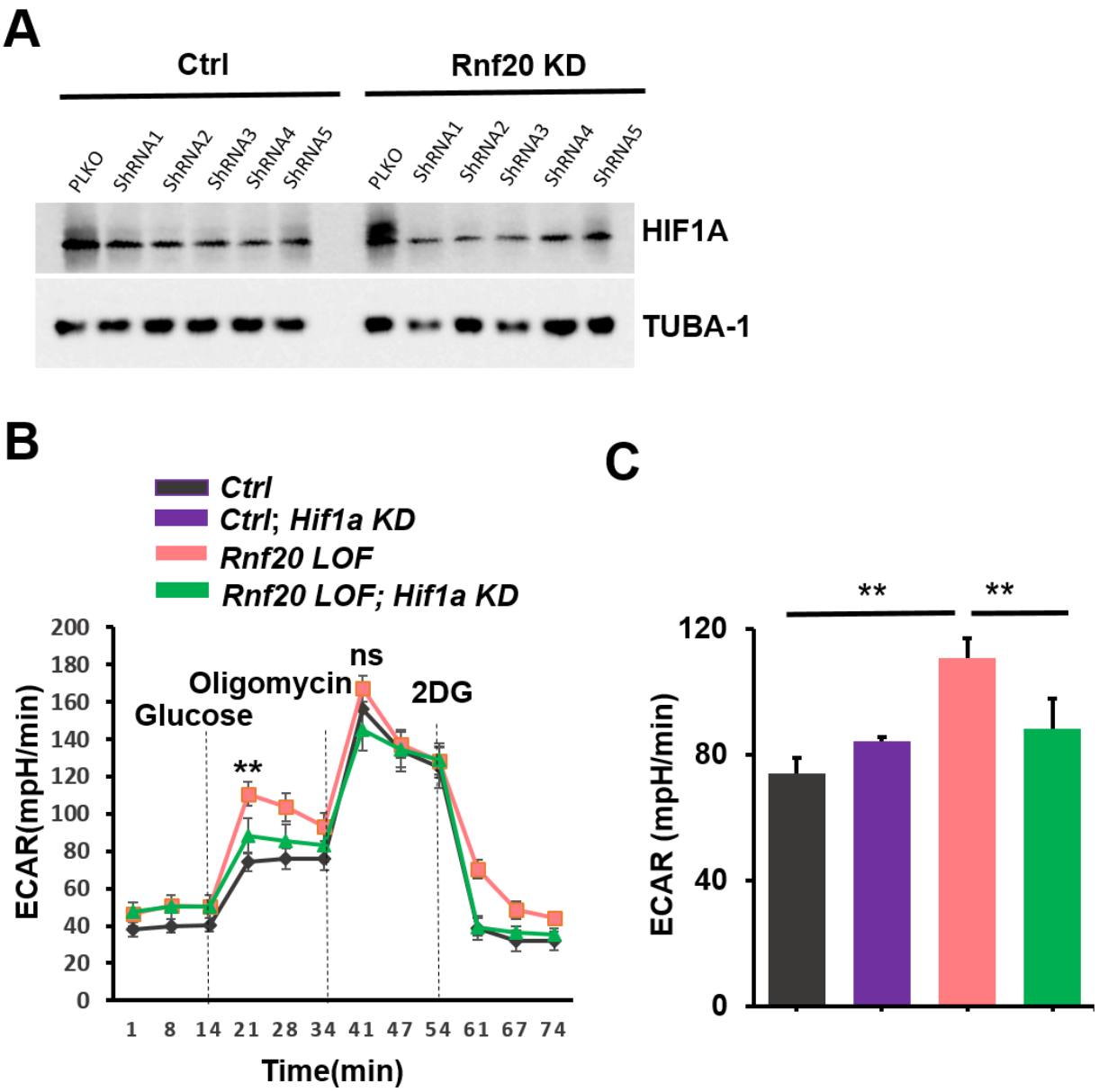

Figure 24. Knockdown of *Hif1a* results in rescue in basal glycolysis in *Rnf20* LOF MLE-12 cells. A, Western blot analysis of HIF1a and α-Tubulin (loading control) in *Rnf20* LOF and control MLE-12 cells upon shRNA mediated knockdown of *Hif1a*. **B & C,** Extracellular acidification rate (ECAR) in MLE-12 cells treated with or without oligomycin (Oligo) showing partial rescue of increased basal glycolytic activity of *Rnf20* loss of function cells upon knockdown of *Hif1a* and no significant (ns) change in maximal glycolytic activity upon knockdown of *Hif1a* in *Rnf20* LOF cells (Data in B represents mean ± s.d., One Way ANOVA. **, P≤0.01 compared with MLE-12 control cells).

4.19 *Hif1a* loss partially rescues glucose uptake and lactate secretion in RNF20 loss of function cells

In continuation of the results obtained in RNF20 loss of function cells that glycolytic rate is somewhat restored when *Hif1a* was knocked down in *Rnf20* depleted cells, I ran rescue experiments for glucose uptake and lactate secretion. Interestingly, I discovered that knocking down of *Hif1a* in RNF20-depleted cells partially restored glucose uptake and lactate production (Fig 25A & B).

Based on these findings, I infer that HIF1a plays a crucial role in restoring glucose uptake and lactate secretion, two of the most critical parameters characterizing glycolysis, in RNF20 loss of function situations.

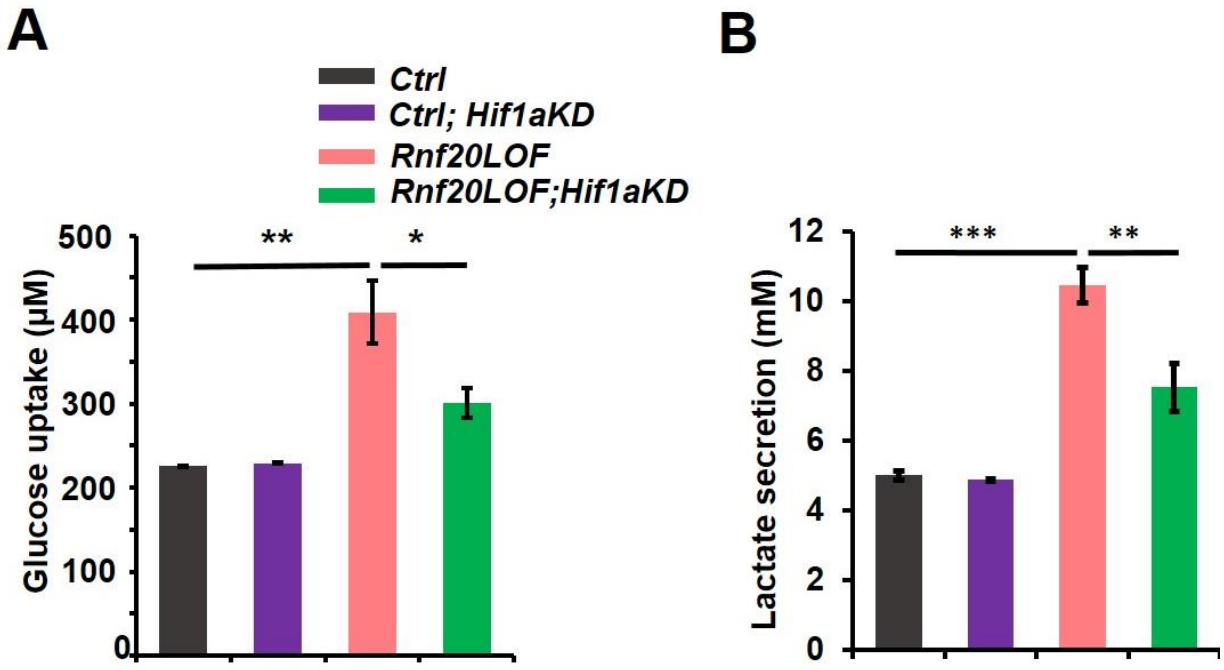

Figure 25. Knockdown of *Hif1a* results in rescue in glucose uptake and lactate secretion in *Rnf20* LOF MLE-12 cells. A, Glucose uptake in RNF20 LOF and control MLE-12 cells upon shRNA mediated knockdown of *Hif1a* (n=3) **B,** Lactate secretion in RNF20 LOF and control MLE-12 cells upon shRNA mediated knockdown of *Hif1a* (n=3) (Data represents mean ± s.d., One way ANOVA,*, P≤0.05, **, P≤0.01, ***, P≤0.001 compared with MLE-12 control cells).

4.20 *Hif1a* loss partially rescues cell migration, invasion and colony formation in RNF20 loss of function cells

In keeping with prior rescue findings that *Hif1a* knockdown rescues glucose uptake and lactate secretion in RNF20 loss of function cells, I wanted to see if HIF1a could also rescue cell survival, migration, and invasion which are hallmarks of cancer in RNF20 loss of function cells. The results showed that depletion of HIF1a significantly reduced the colony formation ability of the *Rnf20* loss of function MLE-12 cells (Fig 26A). Importantly, the migratory and invasive property of *Rnf20* loss of function MLE-12 cells were also significantly reduced (Fig 26B & C).

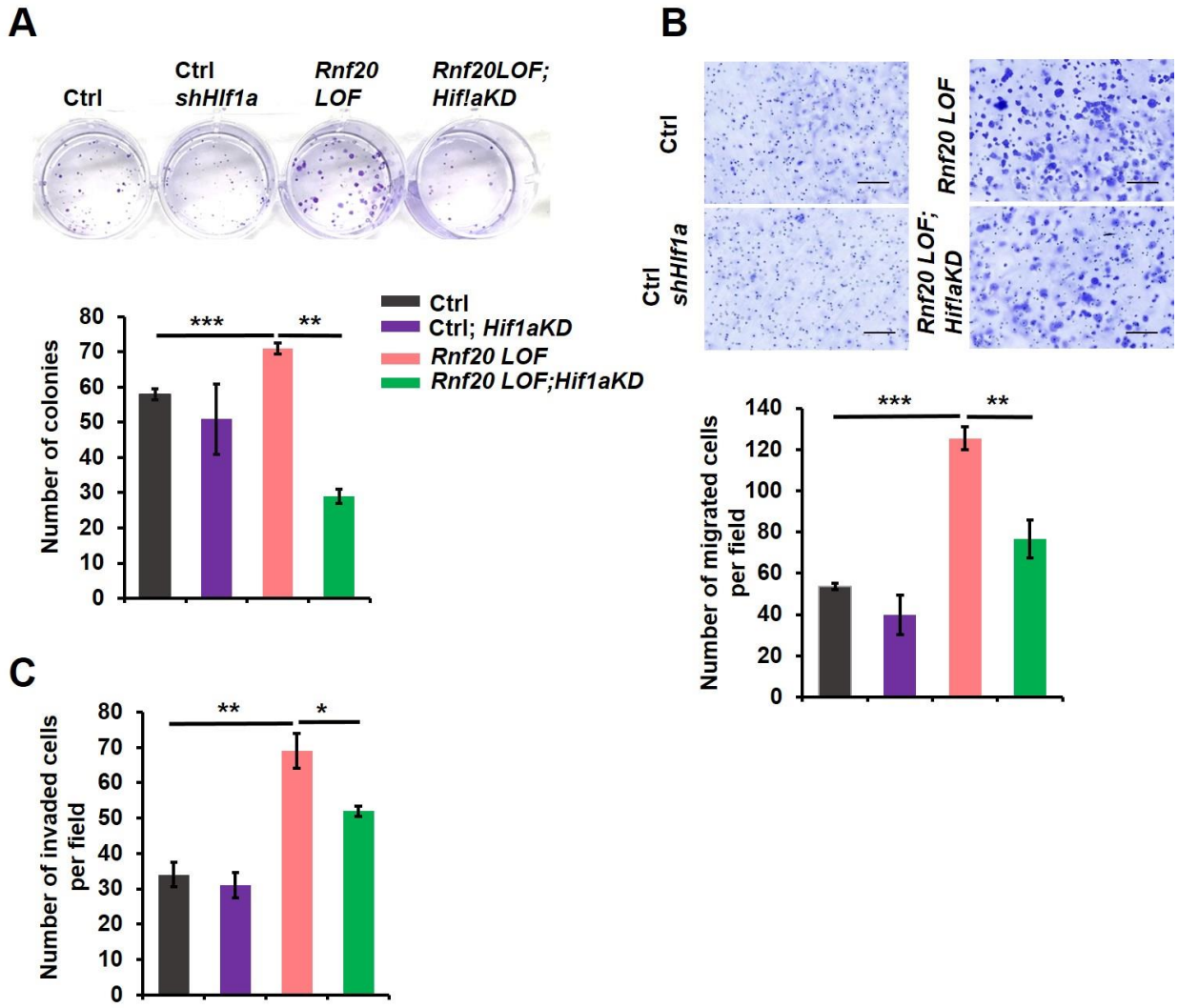

Figure 26. **Knockdown of *Hif1a* results in rescue of cell proliferation, migration and invasion in *Rnf20* loss of function cells. A, B & C,** Quantification of colonies formed, migration and invasion in MLE-12 control, MLE-12 *Rnf20* loss of function (n=3) and upon knockdown of *Hif1a* in these cell lines (Data in **A, B & C** represent mean ± s.d., One Way ANOVA. *, P≤0.05, **, P≤0.01, ***, P≤0.001, compared with MLE-12 control cells).

4.21 Increased glycolysis by *Rnf20* loss is not due to mitochondrial functional damage

It is well known that mitochondrial damage can result in increased glycolysis in the cells because the cells compensates for the energy production by using a low efficient glycolytic method [116]. Therefore, I measured the oxygen consumption rate (OCR) using seahorse in control and *Rnf20* loss of function MLE-12 cells. When *Rnf20* loss of function MLE-12 cells were compared to control MLE-12 cells, there was no significant difference in OCR at the basal level or after the addition of an un-coupler for mitochondria FCCP (Fig 27A & B).

These findings demonstrate that the glycolytic phenotype found in RNF20 loss of function cells is not due to mitochondrial damage, with OCR being one means for detecting this.

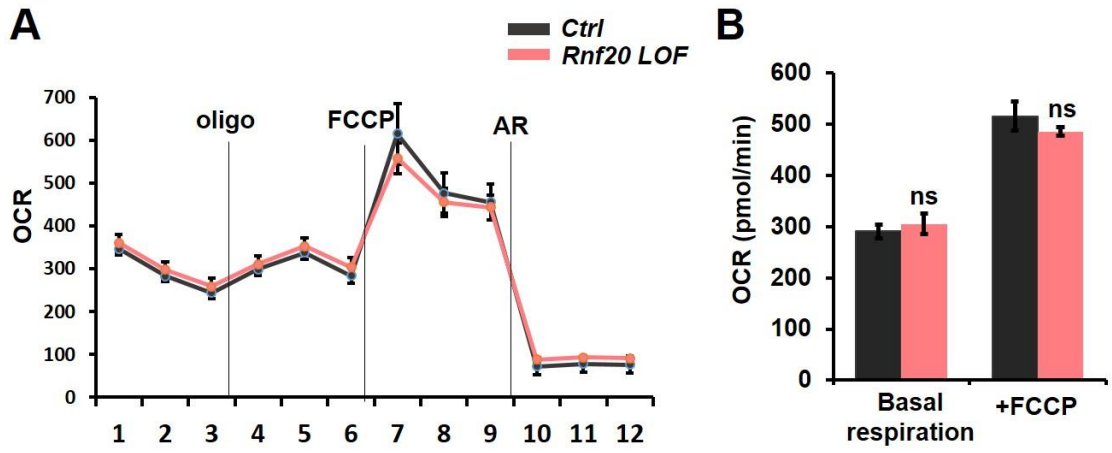

Figure 27. **A & B,** Oxygen consumption rates (OCR) in control and RNF20 loss of function MLE-12 cells (n=3) under basal conditions. (Data in B represents mean ± s.d., One way ANOVA. ns: not significant, compared with MLE-12 control cells).

4.22 Increased glycolysis by *Rnf20* loss is not due to mitochondrial functional damage

As previously noted in Figure 27, there is no damage in mitochondria function shown by OCR, in *Rnf20* loss of function settings compared to control cells, thus I set out to investigate if there could be an accumulation of reactive oxygen species due to mitochondrial damage. To this end, I stained control and *Rnf20* loss of function MLE-12 cells with mitosox red to determine the level of reactive oxygen species/mitochondrial damage. As a positive control, cells treated with antimycin A were used (Fig 28). While I detected strong fluorescent signal in the positive control, I did not find any staining and thus mitochondrial functional damage in *Rnf20* loss of function MLE-12 cells when compared with control cells.

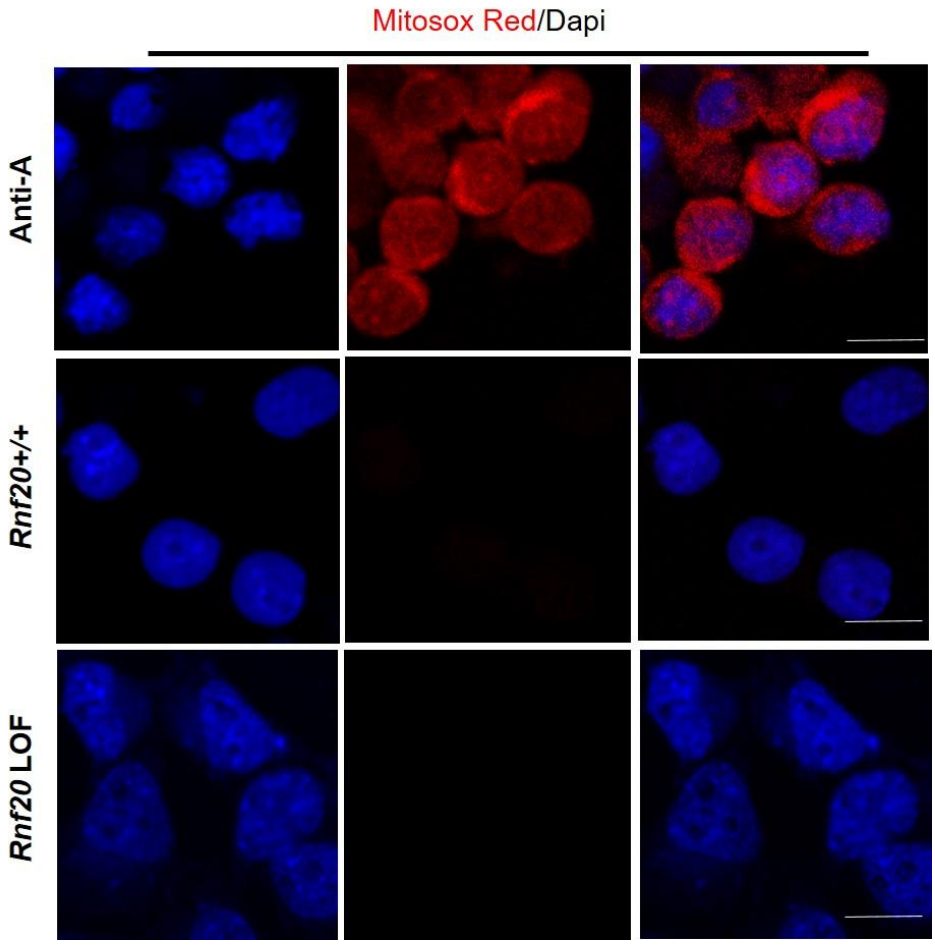

Figure 28. Increased glycolysis is not attributed to mitochondrial damage in RNF20 loss of function cells. Immunofluorescence representative images of control and RNF20 loss of function MLE-12 cells treated with 1.25μM mitosox red, 20nM treatment with antimycin A for 10min at 37°C in CO_2 incubator before treating with mitosox red was used as positive control.

Chapter 5: DISCUSSION & CONCLUSION

Loss of *Rnf20* has been shown to play a role in a number of cancers [1] [94] [107]. Several studies have indicated that RNF20 appear to act as tumor suppressor in mammalian cells [1] [94] [107]. Reduction of RNF20 has been observed in prostate cancer [117], [118], [119], colorectal cancer [94], lung cancer [120] [107], and due to promoter hypermethylation in breast cancers [1]. Several studies have also found that RNF20 downregulation promotes cell proliferation, cell migration, anchorage independence, and tumorigenesis in mammalian cells [1] [94] [107]. Furthermore, H2Bub1 deficiency has also been linked to a malignant phenotype [121] [1] [94]. H2Bub1 was found to be highly expressed in normal mammary epithelium and benign mammary tumors, but undetectable in the vast majority of malignant breast cancers [121]. Consistent with these observations, I found that *Rnf20* haplodeficient mice developed spontaneous lung tumors in the lungs, with histological characteristics of SCLC and Adenocarcinoma.75% of mice had the detected tumors. SCLC were highly proliferative with very few immune cells infiltrating, however those of adenocarcinoma were less proliferative and with very few immune immune cell infiltrating.

The TCGA data analysis of human lung cancer patient's revealed lower survival in patients with lower *Rnf20* expression compared to higher expressing counterparts (Fig 10), demonstrating clinical relevance of the data obtained from haplodeficient *Rnf20* mice.

Furthermore, RNF20 deficiency promoted epithelial mesenchymal transition (EMT) phenotype in lung cells. RNF20 loss in mouse lung epithelial cells caused increased colony formation and migratory ability, which is consistent with the EMT phenotype. In addition, I discovered a critical link between RNF20 and HIF1a in tumorigenesis. My *in vitro* experiments revealed that the loss of RNF20 increased glycolysis and gluconeogenesis in line with the Warburg effect. Above interpretation was further supported by physiological seahorse assays and measuring the extracellular acidification rate of the cells following RNF20 loss, which was further supported by higher glucose uptake in these cells. Silencing of *Hif1a* was sufficient to reduce the increased growth, migration and glycolytic activity of *Rnf20* loss of function cells. .

5.1 Critical role of RNF20 in tumor initiation, proliferation and migration

In this study, I describe RNF20's critical role in lung cancer initiation, proliferation and metastasis. Fundamentally, I have employed three model systems *Rnf20* heterozygous mouse model system for in vivo studies. For in vitro studies I have used *Rnf20* loss of function cells in which from start site exon 2 to exon 5 were deleted resulting in level of *Rnf20* reduced to 50%. Also, I used *Hif1a* KD stable cell lines in which Hif1a was knockdown by lentiviral transfection. Moreover, *RNF20* silenced NCl-H82 cells were used for the silencing *Rnf20* by transient transfection of siRNA. Changes in expression of RNF20 have been linked to various types of tumors, though the relationship appears to be complex and tumor type-specific. RNF20 functions as a tumor suppressor in a variety of cancers e.g. breast cancer, kidney cancer [1] [122] [92]. Clear cell renal carcinoma (ccRCC) is a common type of renal cancer characterized by aberrant lipid accumulation, indicating increased lipid metabolism promotes the proliferation of cancer cells [92]. Lee et al discovered that RNF20 overexpression represses lipogenesis and cell proliferation by inhibiting sterol regulatory element-binding protein 1c (SREBP1c). Furthermore, RNF20 inhibits tumor growth and lipid storage in xenografts [92]. Depending on the breast cancer subtype, their clinical outcome and response to therapy defers. My study underlies key role of RNF20 acting as tumor suppressor in lung cancer is in line with the previous findings. In addition I observed that lower RNF20 expression correlates with higher tumor incidence. The role of RNF20 in lung cancer initiation and progression were further corroborated by our results that loss of since functional allele of *Rnf20* is sufficient to dramatically elevate the occurrence of spontaneous lung tumors in mice. Additionally, the tumor promoting role of *Rnf20* in lung cancer initiation and progression is further supported by cell culture studies.

The role of *Rnf20* in cell proliferation is complex and cell type specific. It was shown that *Rnf20* depletion leads to breast cancer proliferation. Similarly, Rnf20 overexpression reduces cell proliferation in Clear cell renal cell carcinoma [92]. In mouse cells, *Rnf20* silencing upregulated colony formation indicating neoplastic transformation of cells [93]. However silencing of *Rnf20* in leukemia cells leads to cell proliferation inhibition in cell

culture studies [99]. In addition, it was observed that *Rnf20* knockdown and downregulation of H2Bub1 significantly increases the proliferation of cisplatin resistant lung cancer cells [107]. In line with lung cancer cell specific studies, we observed that *Rnf20* silencing lead to increased proliferation in colony formation assay. Furthermore, the individual colonies were markedly increased by *Rnf20* depletion. It is noteworthy that tumor suppressive role of *Rnf20* seems to be tissue specific and several publications suggest that tumor promoting role of *Rnf20* eg. in MLL rearranged leukemia. Mixed lineage leukemia (MLL) are group of strong oncogenes which initiates aggressive form of acute leukemia. In this study they found that *Rnf20* is required for proliferation of MLL-fusion leukemia cells. Suppressing the expression of *Rnf20* in different models of MLL-rearranged leukemia leads to inhibition of cell proliferation both in tissue culture and in vivo models [99]. Phenotypic characterization is an important aspect to understand the type of tumor. Here in our study we investigated in detail type of tumors formed in case of *Rnf20* haplosufficient mice and we found that majority of the tumors formed have small cell lung cancer phenotype and some of them have adenocarcinoma phenotype. Since most of the small cell lung cancer tumors have TP53 and Rb mutations, therefore we investigated level of these two proteins in our cell culture and mouse model showing significant decrease in level of these two protein in *Rnf20* depleted condition. These results shows that *Rnf20* depletion resulting in tumorigenesis works on two point control that TP53 and RB mutations and alterations in metabolic genes resulting in tumor progression in lungs. Interestingly, silencing of *Rnf20* in basal like stem cells increased their proliferation and migration, and their tumorigenicity and metastatic capacity partly through upregulation of inflammatory cytokines however in luminal breast cancer cells *Rnf20* silencing reduces proliferation, migration, tumorigenic and metastatic capacity [123]. Similar observation was also made by another study showing that RNF20 depletion increases the transcriptional effect of epidermal growth factor (EGF) resulting in higher cell migration and tumorigenesis [1].

The mechanism by which RNF20 depletion leads to lung cancer initiation needs to be investigated further. Studies found that RNF20 depletion leads to increased accumulation of DNA damage and genomic instability [31]. Putting in consideration that DNA damage and genomic instability together with genetic mutations are considered the major

contributor of tumorigenesis. Currently some recent publications are also reporting that lipogenesis and metabolic changes to be one of the contributors for tumorigenesis in RNF20 depletion. In our study we also find an important link between RNF20 depletion and changes in glycolysis and other dramatic changes in metabolism. It would be interesting to find out the relationship between DNA damage phenotype and metabolic phenotype and whether they are consequential or subsequent events. The phenotypic characterization of the *Rnf20*+/- mice revealed that the majority of tumors formed in the lungs had mixed tumor characteristics with SCLC and adenocarcioma phenotypes and some having adenocarcinoma characteristics. According to other report using comprehensive genetic profiles of SCLC, loss of TP53 and RB1 is required for the development of SCLCs [124]. I also found that when one allele of *Rnf20* was lost, the expression of TP53 and Rb1 was reduced. To survive, certain non-small cell lung cancers (NSCLC) can adopt many of the molecular and phenotypic characteristics of more resistant small lung neuroendocrine tumors [3]. As an illustration, Tyrosine kinase inhibitors work well in NSCLCs with epidermal growth factor receptor (EGFR) mutations. Relapse, on the other hand, occurs after one year of continuous therapy in a majority of cases. A fundamental histological transformation from NSCLC to SCLC is observed in a subset of resistant cancers, but the molecular changes associated with this transformation are unknown. These newly transformed SCLC tumors also have Rb mutations and increased neuroendocrine markers, as seen in classical SCLC [125]. As a result, it must be investigated further whether NSCLC transforms to SCLC in *Rnf20*+/- mice lung tumors.

In addition, I discovered kidney and liver tumors. Immunohistological examination of the liver and kidney revealed the presence of SCLC-like tumors in these organs. However, whether these tumors do indeed metastasize from the lung requires additional evidence and investigation. In addition, I observed splenic inflammation, splenomegaly, which is consistent with previous research [94]. I hypothesized that inflammation seen in the *Rnf20*+/- mice spleen is secondary. To investigate this, I performed RT-qPCR on wild type and *Rnf20*+/- mice spleen for several inflammatory markers, but I found no evidence of significant deregulation of these inflammatory markers. As a result, I conclude that the phenotype I observed in the spleen in Rnf20+/- mice is secondary due to lung cancer.

According to a recent study [94], RNF20 modulates inflammation and inflammation-related colon cancer. They focused on inflammation and inflammation-induced colon cancer in *Rnf20*+/- mice, as well as the underlying mechanism. They only see colonic inflammation in Rnf20+/- mice when they are given dextran sodium sulphate (DSS). They also observed that DSS treatment caused spleen inflammation in *Rnf20*+/- mice. However, the phenotype observed in my study for *Rnf20*+/- mice is much stronger, and I observed distinct spontaneous tumors in lungs, liver, and kidney, but no abnormality or inflammation in the colon of *Rnf20*+/- mice. Although the knockout strategy was different in their case as the ring domain is deleted compared to complete one allele deletion of Rnf20 in our model system. Different knockout strategy implies independent functions. , it is important to note that they did not discuss lung, liver or kidney tumors in their study, so the phenotype in the colon after DSS treatment may be tissue specific in their context. Another possibility is that different animal facilities resulted in *Rnf20*+/- mice with a mild phenotype, or that different mutations have varying degrees of phenotypic penetrance depending on how mice were generated.

5.2 *Rnf20* haplo-deficiency leads to epithelial to mesenchymal transition

In epithelial mesenchymal transition (EMTs), the acquisition of mesenchymal characteristics from epithelial cells occurs in embryonic development, adult tissue regeneration, cancer, etc [126]. For epithelial cells, various adhesion molecules, including E-cadherin, attach to the basement membrane and adjacent cells to maintain an epithelial phenotype. The main molecular events of EMT are reduced expression of epithelial markers like E-cadherin and increased expression of mesenchymal markers like vimentin, fibronectin and N-cadherin, etc. HIF1a Regulates the Transforming Growth Factor 1/SMAD Family Member 3 Pathway, which plays central role in EMT, to Promote Breast Cancer Progression [127]. TGF1 promotes the stability of hypoxia-inducible factor-1 (HIF-1) by selectively inhibiting PHD2 expression [128]. Wnt/-catenin signaling promotes hypoxia-induced epithelial-mesenchymal transition in hepatocellular cancer via hif-1 signaling crosstalk [129]. Hypoxia promotes fibrogenesis in vivo by stimulating the

epithelial-to-mesenchymal transition via HIF-1 [130]. In this study, I found that RNF20 haplo-deficiency could lead to upregulation of HIF1a and hence create a pseudo hypoxic environment. This pseudo hypoxic environment could lead to EMT in *Rnf20* loss of function cells. I found a dramatic loss of the cell-cell adhesion molecule E-cadherin as well as changes in morphology in mouse lung epithelial cells (MLE-12) after RNF20 haplo-deficiency, from cobblestone-like appearance to spindle shaped morphology, suggesting *Rnf20* loss of function cells undergo EMT. Since EMT is considered a major contributor to cancer cell migration and metastasis, RNF20 haplo-deficiency mediated EMT may play a key role in facilitating migration and metastasis in *Rnf20* loss of function cells. However, the molecular mechanism needs to be investigated in detail in a context of lung cancer. In line, it has recently been shown that RNF20 is critical for SNAIL mediated E-cadherin repression in human breast cancer [122].

5.3 *Rnf20* silencing alters metabolism resulting in lung carcinogenesis

In this study, targeted metabolomics analysis in MLE-12 cells revealed that *Rnf20* loss of function cells exhibited dramatic changes in metabolites of glycolytic pathway as well as Tricarboxylic acid (TCA) cycle. RNF20 has previously been shown to promote adipogenesis by regulating transcriptional activity of peroxisome proliferator-activated receptor-γ (PPARγ) [131]. *Rnf20* defective (adipose specific)mice developed lower fat mass with smaller adipocytes when fed a standard chow diet, compared to wildtype littermates [131]. Moreover, high-fat diet-fed *Rnf20+/-* mice developed insulin resistance accompanied by reduced fat tissues. Mechanistically, RNF20 functioned as a transcriptional co-activator for $PPAR_Y$ by promoting NCoR1 degradation in adipocytes [131]. In line, another report showed that RNF20 overexpression represses lipogenesis and cell proliferation by inhibiting sterol regulatory element binding protein 1c (SREBP1c) [92]. Since glucose metabolism and lipid metabolism are linked, it is possible that RNF20 haplo-deficiency results in alteration of glucose metabolism and subsequently lipid metabolism, or that alteration of glucose metabolism is tissue specific and independent of alteration in lipid metabolism in the case of *Rnf20* haplo-deficient mice.Previous report

[131] has revealed an interesting RNF20-NCoR1 axis in adipocyte biology through fine-tuning of transcriptional activity of PPARγ and suggested a role of RNF20 in lipid metabolism in a tissue-specific context but provided no evidence for the apparent higher glucose metabolism after depletion of RNF20 or the possible link between glucose metabolism and lipid metabolism. In their model system, Rnf20 depletion is adipocyte specific compared global depletion of one allele of *Rnf20* in our case, this could explain no apparent evidence of change in glucose metabolism. In our Rnf20 heterozygous mouse model system, we observe increase in glucose uptake and lactate secretion. In my cell culture model, I found that *Rnf20* loss of function cells exhibit dramatic changes in metabolites and the major pathway upregulated was related to glycolysis. Further validation showed that most of the glycolytic genes are upregulated. In addition, there was higher glucose uptake and higher lactate secretion both in cell culture. These changes are coupled to increase in metabolic enzymes. . This finding is interesting since, so far, there is no direct evidence about it. Both glucose and lipids play an important role in energy metabolism. Metabolic processes of glucose and lipids is intractably linked. As a result, further research is needed to determine whether there is correlation or crosstalk between increased glycolysis and increased lipid metabolism upon depletion of RNF20 *in vitro* and *in vivo*.

5.4 Increased glycolysis in *Rnf20* loss of function cells is not due to mitochondrial damage

Glycolysis plays an important role in tumor progression and metastasis. In recent years, it has been given a lot of importance along with other metabolic pathways in cancer and other diseases [132]. HIF1a acts as a transcriptional master regulator of oxygen homeostasis in all metazoan species. HIF1a binds to Von hippel Lindau (VHL) protein, a part of the ubiquitin degradation system that degrades HIF1a. In most human renal carcinomas, VHL gene is inactivated by mutation or epigenetic silencing, leading to dysregulated HIF1a transcriptional activity [133]. Under normoxia, VHL loss of function leads to Hif1a-dependent reprogramming of glucose and energy metabolism that includes increased glucose uptake, increased glycolysis and decreased mitochondrial respiration, underlying the Warburg effect [134]. Alternate mechanism has also been reported by

which Hif1a actively reprograms metabolism through trans-activating gene encoding pyruvate dehydrogenase kinase 1 (PDK1). PDK1 inactivates the TCA cycle enzyme, pyruvate dehydrogenase (PDH), which converts pyruvate to acetyl CoA, thereby causing a hypoxia induced metabolic switch that shunts glucose metabolites from mitochondria to glycolysis [135]. In my study, the increase in glycolysis in Rnf20 loss of function cells is not due to mitochondrial damage, unlike other ubiquitin ligase e.g. VHL. When pVHL is re-expressed in pVHL-deficient 786O and RCC10 renal cancer cells, it regulates mitochondrial function independently of HIF-. pVHL re-expression increased expression of CHCHD4, a key component of the disulphide relay system (DRS) involved in mitochondrial protein import within the intermembranous space (IMS), as well as complex I (NDUFB10) and complex IV (mtCO-2 and COX IV) respiratory chain subunits. These modifications were associated with higher OCR and dynamic changes in glucose and glutamine metabolism [136]. Importantly, I found that there was no change in oxygen consumption rate, indicating intact mitochondrial function (Fig 27). Furthermore, I confirmed it by MitoSox staining that there was no mitochondrial damage (Fig 28). Hence, the observed increase in glycolysis was not due to mitochondrial damage. These observations were further confirmed by metabolomics studies where data showed an increase in glycolytic metabolites as well as respiratory metabolites in *Rnf20* loss of function cells. It indicates that haplo-deficiency of RNF20 causes a metabolic switch that shunts glucose metabolites from mitochondria to glycolysis potentially due to stabilization of Hif1a and following alternate mechanism.

5.5 RNF20-HIF1a axis fine-tunes glycolytic gene expression patterns

HIF1a's role in the regulation of cancer cell metabolism has long been discussed [137]. Intratumoral hypoxia induces HIF1a expression, resulting in dramatic changes in cancer cell metabolism, including increased glycolysis and decreased mitochondrial metabolism and mass [138]. In lung cancer, HIF-1 is required for the activation and tumor-promoting impact of cancer-associated fibroblasts [139] [140]. HIF1A, also known as hypoxia-inducible factor 1-alpha, plays a crucial role in the progression of lung cancer

cells. HIF1A regulates metabolic reprogramming in cancer cells, enabling them to adapt to the hypoxic conditions. It promotes the witch from oxidative phosphorylation to glycolysis, even in the presence of oxygen, a phenomenon known as the Warburg effect. [141] [142]. This metabolic shift provides energy and metabolic intermediates required for rapid cell proliferation and survival. HIF1A enhances the invasiveness and metastatic potential of lung cancer cells. It promotes the expression of matrix metalloproteinases (MMPs), which are enzymes that degrade the extracellular matrix and facilitate cancer cell invasion into surrounding tissues. HIF1A also induces the expression of genes involved in epithelial-mesenchymal transition (EMT), a process through which cancer cells acquire a more mesenchymal phenotype, allowing them to detach from the primary tumor and invade distant organs [143]. RNA-seq based gene ontology analysis in *Rnf20* loss of function and WT MLE-12 cells revealed that the major pathways upregulated after RNF20 haplo-deficiency are HIF1a signaling and glycolytic pathways. RNF20 depletion leads to higher levels of *Hif1a* both in normoxia and hypoxia. Given that HIF1a is a major transcription regulator for glycolytic gene expression, one can hypothesize that RNF20 loss may have an effect on glycolytic pathways via HIF1a. When I knocked down HIF1a in *Rnf20* loss of function cells, I discovered that glycolysis, proliferation and migration were partially rescued. Based on these findings, it would be fascinating to learn how Rnf20 affects Hif1a levels and the expression of other glycolytic genes.

5.6 Based on my result, I conclude that

1) RNF20 acts as a tumor suppressor for lung cancer.
2) *Rnf20* haplodeficient mice develop spontaneous lung cancer.
3) Spontaneous lessions developed in *Rnf20* haplo-deficient mice show lung adenocarcinoma and SCLC-like characteristics.
4) *Rnf20* haplo-deficiency causes DNA damage and delayed repair.
5) RNF20 loss promotes EMT.
6) RNF20 loss stabilizes HIF1a.
7) RNF20 regulates HIF1a target genes at transcription level.
8) RNF20 loss induces higher glycolysis partially through activation of Hif1a signaling.
9) Increased glycolysis by RNF20 loss is not due to reactive oxygen species accumulation or mitochondrial function damage.
10) HIF1a loss partially rescues the increase glycolysis in cells.
11) Mechanistically, dysregulation of RNF20-HIF1a axis potentially triggers Warburg effect and genome instability for lung cancer initiation and growth. Therefore, RNF20-HIF1a axis could be a potential therapeutic target for lung cancer.

5.7 Outlook

Previous studies have shown that the loss of RNF20 is associated with various types of cancers, including prostate cancer, colorectal cancer, lung cancer, and breast cancer. RNF20 acts as a tumor suppressor in mammalian cells, and its reduction promotes cell proliferation, migration, and tumorigenesis. In the current study, I utilized an *Rnf20* heterozygous mouse model and observed spontaneous lung tumors in the mice with histological characteristics of small cell lung cancer (SCLC) and adenocarcinoma. TCGA data analysis of human lung cancer patients also revealed lower survival in patients with lower *Rnf20* expression, highlighting the clinical relevance of the findings.

Our mice model study reveals that *Rnf20+/-* mice have tumors in the lung that exhibit small cell lung cancer characteristics. Therefore, it is important to sequence the lung cell population and check for mutations in *RB* and *TP53*, as these mutations are present in small cell lung cancer patients. In our data, we observed that *Rnf20+/-* mice develop tumors in the liver and kidney as well. After immunohistochemical analysis, we found that these tumors also have small cell lung cancer characteristics. Therefore, it is important to conduct lineage tracing experiments to determine whether these tumors metastasize from the lungs.

Interestingly, I discovered a critical link between RNF20 and HIF1a in promoting tumorigenesis. The loss of RNF20 led to increased glycolysis and gluconeogenesis, as well as increased growth, migration, and glycolytic activity of cells. Knocking down of HIF1a reduced these effects, suggesting the involvement of the RNF20-HIF1a axis in tumor initiation and growth. A noteworthy experiment would be to compare the survival of Rnf20+/-KO mice to control mice after Hif1a loss of function in order to increase the relevance of our cell culture data. It would also be important to know whether the uptake of glucose in Rnf20+/-KO mice is decreased upon Hif1a loss of function.

This study demonstrated the critical role of RNF20 in lung cancer initiation, proliferation, and metastasis. RNF20 acts as a tumor suppressor in lung cancer, and its loss leads to increased proliferation and colony formation in vitro. Additionally, I found that RNF20 haplo-deficiency promoted EMT in lung cells. Loss of RNF20 resulted in reduced expression of the cell-cell adhesion molecule E-cadherin and changes in cell morphology, suggesting the occurrence of EMT. EMT is known to contribute to cancer

cell migration and metastasis. In order to investigate cell migration and metastasis in vivo, tail vein injection and subcutaneous injections could be done Rnf20 loss of function cells and control cells.

Overall, the findings suggest that RNF20 plays a critical role in lung cancer initiation, proliferation, migration, and EMT. This study highlights the interaction between RNF20 and HIF1a in lung cancer cells and its potential implications for cancer cell metabolism. HIF1a plays a crucial role in metabolic reprogramming, promoting the switch to facilitate glycolysis and facilitating cancer cell proliferation, invasion, and metastasis. Propose experiments to study how Rnf20 regulates Hif1a level: via monoubiquitination, regulating the stability of VHL, through altered succinate levels, etc.

Interestingly, the study also observed increased glucose uptake, lactate secretion, and upregulation of glycolytic genes in *Rnf20* loss of function cells and in *Rnf20+/-* lung cells. This indicates a potential link between RNF20 and glucose metabolism, raising questions about potential correlations with increased lipid metabolism upon RNF20 depletion or not. Investigating glycolytic metabolites in real time by radiolabeling them, and using PET scanning to analyze their breakdown in mouse models would be fascinating. Further research is needed to elucidate the mechanisms by which RNF20 affects HIF1a levels and the expression of glycolytic genes. Understanding these interactions could provide insights into the regulation of cancer cell metabolism and potential therapeutic targets of lung cancer.

Chapter 6: REFERENCES

1. Shema, E., et al., *The histone H2B-specific ubiquitin ligase RNF20/hBRE1 acts as a putative tumor suppressor through selective regulation of gene expression.* Genes Dev, 2008. **22**(19): p. 2664-76.
2. Bade, B.C. and C.S. Dela Cruz, *Lung Cancer 2020: Epidemiology, Etiology, and Prevention.* Clin Chest Med, 2020. **41**(1): p. 1-24.
3. Chen, Z., et al., *Non-small-cell lung cancers: a heterogeneous set of diseases.* Nat Rev Cancer, 2014. **14**(8): p. 535-46.
4. Sher, T., G.K. Dy, and A.A. Adjei, *Small cell lung cancer.* Mayo Clin Proc, 2008. **83**(3): p. 355-67.
5. Travis, W.D., *Classification of lung cancer.* Semin Roentgenol, 2011. **46**(3): p. 178-86.
6. Travis, W.D., *Pathology of lung cancer.* Clin Chest Med, 2011. **32**(4): p. 669-92.
7. Travis, W.D., et al., *The 2015 World Health Organization Classification of Lung Tumors: Impact of Genetic, Clinical and Radiologic Advances Since the 2004 Classification.* J Thorac Oncol, 2015. **10**(9): p. 1243-1260.
8. Guo, R., et al., *Use of dual-marker staining to differentiate between lung squamous cell carcinoma and adenocarcinoma.* J Int Med Res, 2020. **48**(4): p. 300060519893867.
9. Ginn, L., et al., *LncRNAs in Non-Small-Cell Lung Cancer.* Noncoding RNA, 2020. **6**(3).
10. Biberman, R., et al., *Increased risk for small cell lung cancer following residential exposure to low-dose radon: a pilot study.* Arch Environ Health, 1993. **48**(4): p. 209-12.
11. Sun, S., J.H. Schiller, and A.F. Gazdar, *Lung cancer in never smokers--a different disease.* Nat Rev Cancer, 2007. **7**(10): p. 778-90.
12. Gridelli, C., et al., *Non-small-cell lung cancer.* Nat Rev Dis Primers, 2015. **1**: p. 15009.
13. Gazdar, A.F., *Activating and resistance mutations of EGFR in non-small-cell lung cancer: role in clinical response to EGFR tyrosine kinase inhibitors.* Oncogene, 2009. **28 Suppl 1**: p. S24-31.
14. Chen, Y.L., et al., *Development of a novel ALK rearrangement screening test for non-small cell lung cancers.* PLoS One, 2021. **16**(9): p. e0257152.
15. Uras, I.Z., H.P. Moll, and E. Casanova, *Targeting KRAS Mutant Non-Small-Cell Lung Cancer: Past, Present and Future.* Int J Mol Sci, 2020. **21**(12).
16. Salgia, R., et al., *The improbable targeted therapy: KRAS as an emerging target in non-small cell lung cancer (NSCLC).* Cell Rep Med, 2021. **2**(1): p. 100186.
17. Xiang, L., et al., *A Potential Biomarker of Combination of Tumor Mutation Burden and Copy Number Alteration for Efficacy of Immunotherapy in KRAS-Mutant Advanced Lung Adenocarcinoma.* Front Oncol, 2020. **10**: p. 559896.
18. Rudin, C.M., et al., *Small-cell lung cancer.* Nat Rev Dis Primers, 2021. **7**(1): p. 3.
19. Meuwissen, R., et al., *Induction of small cell lung cancer by somatic inactivation of both Trp53 and Rb1 in a conditional mouse model.* Cancer Cell, 2003. **4**(3): p. 181-9.
20. Harbour, J.W., et al., *Abnormalities in structure and expression of the human retinoblastoma gene in SCLC.* Science, 1988. **241**(4863): p. 353-7.
21. Sriuranpong, V., et al., *Notch signaling induces cell cycle arrest in small cell lung cancer cells.* Cancer Res, 2001. **61**(7): p. 3200-5.
22. Lim, J.S., et al., *Intratumoural heterogeneity generated by Notch signalling promotes small-cell lung cancer.* Nature, 2017. **545**(7654): p. 360-364.
23. Saunders, L.R., et al., *A DLL3-targeted antibody-drug conjugate eradicates high-grade pulmonary neuroendocrine tumor-initiating cells in vivo.* Sci Transl Med, 2015. **7**(302): p. 302ra136.
24. Negrini, S., V.G. Gorgoulis, and T.D. Halazonetis, *Genomic instability--an evolving hallmark of cancer.* Nat Rev Mol Cell Biol, 2010. **11**(3): p. 220-8.
25. Rao, C.V., et al., *Enhanced genomic instabilities caused by deregulated microtubule dynamics and chromosome segregation: a perspective from genetic studies in mice.* Carcinogenesis, 2009. **30**(9): p. 1469-74.
26. Loeb, L.A., *Mutator phenotype may be required for multistage carcinogenesis.* Cancer Res, 1991. **51**(12): p. 3075-9.
27. Primo, L.M.F. and L.K. Teixeira, *DNA replication stress: oncogenes in the spotlight.* Genet Mol Biol, 2019. **43**(1 suppl 1): p. e20190138.
28. Abbas, T., M.A. Keaton, and A. Dutta, *Genomic instability in cancer.* Cold Spring Harb Perspect Biol, 2013. **5**(3): p. a012914.

29. Moyal, L., et al., *Requirement of ATM-dependent monoubiquitylation of histone H2B for timely repair of DNA double-strand breaks.* Mol Cell, 2011. **41**(5): p. 529-42.
30. Han, Y.G., et al., *TRAIP regulates Histone H2B monoubiquitination in DNA damage response pathways.* Oncol Rep, 2019. **41**(6): p. 3305-3312.
31. Nakamura, K., et al., *Regulation of homologous recombination by RNF20-dependent H2B ubiquitination.* Mol Cell, 2011. **41**(5): p. 515-28.
32. Hung, S.H., et al., *Monoubiquitylation of histone H2B contributes to the bypass of DNA damage during and after DNA replication.* Proc Natl Acad Sci U S A, 2017. **114**(11): p. E2205-E2214.
33. So, C.C., S. Ramachandran, and A. Martin, *E3 Ubiquitin Ligases RNF20 and RNF40 Are Required for Double-Stranded Break (DSB) Repair: Evidence for Monoubiquitination of Histone H2B Lysine 120 as a Novel Axis of DSB Signaling and Repair.* Mol Cell Biol, 2019. **39**(8).
34. Keijer, J. and D.A. van Dartel, *Reprogrammed metabolism of cancer cells as a potential therapeutic target.* Curr Pharm Des, 2014. **20**(15): p. 2580-94.
35. Hay, N., *Reprogramming glucose metabolism in cancer: can it be exploited for cancer therapy?* Nat Rev Cancer, 2016. **16**(10): p. 635-49.
36. Kroemer, G. and J. Pouyssegur, *Tumor cell metabolism: cancer's Achilles' heel.* Cancer Cell, 2008. **13**(6): p. 472-82.
37. Vander Heiden, M.G., L.C. Cantley, and C.B. Thompson, *Understanding the Warburg effect: the metabolic requirements of cell proliferation.* Science, 2009. **324**(5930): p. 1029-33.
38. Ward, P.S. and C.B. Thompson, *Metabolic reprogramming: a cancer hallmark even warburg did not anticipate.* Cancer Cell, 2012. **21**(3): p. 297-308.
39. DeBerardinis, R.J. and N.S. Chandel, *Fundamentals of cancer metabolism.* Sci Adv, 2016. **2**(5): p. e1600200.
40. McCracken, A.N. and A.L. Edinger, *Nutrient transporters: the Achilles' heel of anabolism.* Trends Endocrinol Metab, 2013. **24**(4): p. 200-8.
41. Cairns, R.A., I.S. Harris, and T.W. Mak, *Regulation of cancer cell metabolism.* Nat Rev Cancer, 2011. **11**(2): p. 85-95.
42. Clavell, L.A., et al., *Four-agent induction and intensive asparaginase therapy for treatment of childhood acute lymphoblastic leukemia.* N Engl J Med, 1986. **315**(11): p. 657-63.
43. Yan, H., et al., *IDH1 and IDH2 mutations in gliomas.* N Engl J Med, 2009. **360**(8): p. 765-73.
44. King, A., M.A. Selak, and E. Gottlieb, *Succinate dehydrogenase and fumarate hydratase: linking mitochondrial dysfunction and cancer.* Oncogene, 2006. **25**(34): p. 4675-82.
45. Trachootham, D., et al., *Selective killing of oncogenically transformed cells through a ROS-mediated mechanism by beta-phenylethyl isothiocyanate.* Cancer Cell, 2006. **10**(3): p. 241-52.
46. Wang, J., et al., *Inhibition of cancer growth in vitro and in vivo by a novel ROS-modulating agent with ability to eliminate stem-like cancer cells.* Cell Death Dis, 2017. **8**(6): p. e2887.
47. Zhang, W., et al., *Stromal control of cystine metabolism promotes cancer cell survival in chronic lymphocytic leukaemia.* Nat Cell Biol, 2012. **14**(3): p. 276-86.
48. Fantin, V.R., J. St-Pierre, and P. Leder, *Attenuation of LDH-A expression uncovers a link between glycolysis, mitochondrial physiology, and tumor maintenance.* Cancer Cell, 2006. **9**(6): p. 425-34.
49. Jozwiak, P., et al., *O-GlcNAcylation and Metabolic Reprograming in Cancer.* Front Endocrinol (Lausanne), 2014. **5**: p. 145.
50. Patra, K.C. and N. Hay, *The pentose phosphate pathway and cancer.* Trends Biochem Sci, 2014. **39**(8): p. 347-54.
51. Lucarelli, G., et al., *Metabolomic profile of glycolysis and the pentose phosphate pathway identifies the central role of glucose-6-phosphate dehydrogenase in clear cell-renal cell carcinoma.* Oncotarget, 2015. **6**(15): p. 13371-86.
52. Amelio, I., et al., *Serine and glycine metabolism in cancer.* Trends Biochem Sci, 2014. **39**(4): p. 191-8.
53. Dang, L., et al., *Cancer-associated IDH1 mutations produce 2-hydroxyglutarate.* Nature, 2009. **462**(7274): p. 739-44.
54. Fathi, A.T., et al., *Biochemical, Epigenetic, and Metabolic Approaches to Target IDH Mutations in Acute Myeloid Leukemia.* Semin Hematol, 2015. **52**(3): p. 165-71.
55. Baysal, B.E., et al., *Mutations in SDHD, a mitochondrial complex II gene, in hereditary paraganglioma.* Science, 2000. **287**(5454): p. 848-51.
56. Hao, H.X., et al., *SDH5, a gene required for flavination of succinate dehydrogenase, is mutated in paraganglioma.* Science, 2009. **325**(5944): p. 1139-42.

57. Baysal, B.E., *A recurrent stop-codon mutation in succinate dehydrogenase subunit B gene in normal peripheral blood and childhood T-cell acute leukemia.* PLoS One, 2007. **2**(5): p. e436.
58. Vanharanta, S., et al., *Early-onset renal cell carcinoma as a novel extraparaganglial component of SDHB-associated heritable paraganglioma.* Am J Hum Genet, 2004. **74**(1): p. 153-9.
59. Selak, M.A., et al., *Succinate links TCA cycle dysfunction to oncogenesis by inhibiting HIF-alpha prolyl hydroxylase.* Cancer Cell, 2005. **7**(1): p. 77-85.
60. Xiao, M., et al., *Inhibition of alpha-KG-dependent histone and DNA demethylases by fumarate and succinate that are accumulated in mutations of FH and SDH tumor suppressors.* Genes Dev, 2012. **26**(12): p. 1326-38.
61. Letouze, E., et al., *SDH mutations establish a hypermethylator phenotype in paraganglioma.* Cancer Cell, 2013. **23**(6): p. 739-52.
62. Sciacovelli, M., et al., *Fumarate is an epigenetic modifier that elicits epithelial-to-mesenchymal transition.* Nature, 2016. **537**(7621): p. 544-547.
63. Grasmann, G., et al., *Gluconeogenesis in cancer cells - Repurposing of a starvation-induced metabolic pathway?* Biochim Biophys Acta Rev Cancer, 2019. **1872**(1): p. 24-36.
64. Smolle, E., et al., *Distribution and prognostic significance of gluconeogenesis and glycolysis in lung cancer.* Mol Oncol, 2020. **14**(11): p. 2853-2867.
65. Lee, J.V., et al., *Akt-dependent metabolic reprogramming regulates tumor cell histone acetylation.* Cell Metab, 2014. **20**(2): p. 306-319.
66. Wellen, K.E., et al., *ATP-citrate lyase links cellular metabolism to histone acetylation.* Science, 2009. **324**(5930): p. 1076-80.
67. Mentch, S.J., et al., *Histone Methylation Dynamics and Gene Regulation Occur through the Sensing of One-Carbon Metabolism.* Cell Metab, 2015. **22**(5): p. 861-73.
68. Ulanovskaya, O.A., A.M. Zuhl, and B.F. Cravatt, *NNMT promotes epigenetic remodeling in cancer by creating a metabolic methylation sink.* Nat Chem Biol, 2013. **9**(5): p. 300-6.
69. Abdel-Wahab, O., et al., *Genetic characterization of TET1, TET2, and TET3 alterations in myeloid malignancies.* Blood, 2009. **114**(1): p. 144-7.
70. Yang, H., et al., *Tumor development is associated with decrease of TET gene expression and 5-methylcytosine hydroxylation.* Oncogene, 2013. **32**(5): p. 663-9.
71. Li, X. and N. Kazgan, *Mammalian sirtuins and energy metabolism.* Int J Biol Sci, 2011. **7**(5): p. 575-87.
72. Bungard, D., et al., *Signaling kinase AMPK activates stress-promoted transcription via histone H2B phosphorylation.* Science, 2010. **329**(5996): p. 1201-5.
73. Fujiki, R., et al., *GlcNAcylation of histone H2B facilitates its monoubiquitination.* Nature, 2011. **480**(7378): p. 557-60.
74. Wellen, K.E., et al., *The hexosamine biosynthetic pathway couples growth factor-induced glutamine uptake to glucose metabolism.* Genes Dev, 2010. **24**(24): p. 2784-99.
75. Lopez-Serra, P., et al., *A DERL3-associated defect in the degradation of SLC2A1 mediates the Warburg effect.* Nat Commun, 2014. **5**: p. 3608.
76. Chen, M., et al., *Promoter hypermethylation mediated downregulation of FBP1 in human hepatocellular carcinoma and colon cancer.* PLoS One, 2011. **6**(10): p. e25564.
77. Dong, C., et al., *Loss of FBP1 by Snail-mediated repression provides metabolic advantages in basal-like breast cancer.* Cancer Cell, 2013. **23**(3): p. 316-31.
78. Desai, S., et al., *Tissue-specific isoform switch and DNA hypomethylation of the pyruvate kinase PKM gene in human cancers.* Oncotarget, 2014. **5**(18): p. 8202-10.
79. Vanharanta, S., et al., *Epigenetic expansion of VHL-HIF signal output drives multiorgan metastasis in renal cancer.* Nat Med, 2013. **19**(1): p. 50-6.
80. Sebastian, C., et al., *The histone deacetylase SIRT6 is a tumor suppressor that controls cancer metabolism.* Cell, 2012. **151**(6): p. 1185-99.
81. Watanabe, H., et al., *Sirt2 facilitates hepatic glucose uptake by deacetylating glucokinase regulatory protein.* Nat Commun, 2018. **9**(1): p. 30.
82. Pezzuto, A. and E. Carico, *Role of HIF-1 in Cancer Progression: Novel Insights. A Review.* Curr Mol Med, 2018. **18**(6): p. 343-351.
83. Fong, G.H. and K. Takeda, *Role and regulation of prolyl hydroxylase domain proteins.* Cell Death Differ, 2008. **15**(4): p. 635-41.
84. Kaelin, W.G., Jr., *Molecular basis of the VHL hereditary cancer syndrome.* Nat Rev Cancer, 2002. **2**(9): p. 673-82.

85. Kaelin, W.G., Jr., *The von Hippel-Lindau tumor suppressor protein and clear cell renal carcinoma.* Clin Cancer Res, 2007. **13**(2 Pt 2): p. 680s-684s.
86. Ravi, R., et al., *Regulation of tumor angiogenesis by p53-induced degradation of hypoxia-inducible factor 1alpha.* Genes Dev, 2000. **14**(1): p. 34-44.
87. Hayashi, Y., et al., *Hypoxia/pseudohypoxia-mediated activation of hypoxia-inducible factor-1alpha in cancer.* Cancer Sci, 2019. **110**(5): p. 1510-1517.
88. Baysal, B.E., *On the association of succinate dehydrogenase mutations with hereditary paraganglioma.* Trends Endocrinol Metab, 2003. **14**(10): p. 453-9.
89. Rezaeian, A.H., et al., *A hypoxia-responsive TRAF6-ATM-H2AX signalling axis promotes HIF1alpha activation, tumorigenesis and metastasis.* Nat Cell Biol, 2017. **19**(1): p. 38-51.
90. Foglizzo, M., A.J. Middleton, and C.L. Day, *Structure and Function of the RING Domains of RNF20 and RNF40, Dimeric E3 Ligases that Monoubiquitylate Histone H2B.* J Mol Biol, 2016. **428**(20): p. 4073-4086.
91. Cole, A.J., R. Clifton-Bligh, and D.J. Marsh, *Histone H2B monoubiquitination: roles to play in human malignancy.* Endocr Relat Cancer, 2015. **22**(1): p. T19-33.
92. Lee, J.H., et al., *RNF20 Suppresses Tumorigenesis by Inhibiting the SREBP1c-PTTG1 Axis in Kidney Cancer.* Mol Cell Biol, 2017. **37**(22).
93. Shema, E., et al., *Corrigendum: The histone H2B-specific ubiquitin ligase RNF20/hBRE1 acts as a putative tumor suppressor through selective regulation of gene expression.* Genes Dev, 2017. **31**(18): p. 1926.
94. Tarcic, O., et al., *RNF20 Links Histone H2B Ubiquitylation with Inflammation and Inflammation-Associated Cancer.* Cell Rep, 2016. **14**(6): p. 1462-1476.
95. Duan, Y., et al., *Ubiquitin ligase RNF20/40 facilitates spindle assembly and promotes breast carcinogenesis through stabilizing motor protein Eg5.* Nat Commun, 2016. **7**: p. 12648.
96. Blank, M., et al., *A tumor suppressor function of Smurf2 associated with controlling chromatin landscape and genome stability through RNF20.* Nat Med, 2012. **18**(2): p. 227-34.
97. Sarno, F., A. Nebbioso, and L. Altucci, *DOT1L: a key target in normal chromatin remodelling and in mixed-lineage leukaemia treatment.* Epigenetics, 2020. **15**(5): p. 439-453.
98. Srinivasan, R.S., A.C. de Erkenez, and C.S. Hemenway, *The mixed lineage leukemia fusion partner AF9 binds specific isoforms of the BCL-6 corepressor.* Oncogene, 2003. **22**(22): p. 3395-406.
99. Wang, E., et al., *Histone H2B ubiquitin ligase RNF20 is required for MLL-rearranged leukemia.* Proc Natl Acad Sci U S A, 2013. **110**(10): p. 3901-6.
100. Garrido Castro, P., et al., *The HDAC inhibitor panobinostat (LBH589) exerts in vivo anti-leukaemic activity against MLL-rearranged acute lymphoblastic leukaemia and involves the RNF20/RNF40/WAC-H2B ubiquitination axis.* Leukemia, 2018. **32**(2): p. 323-331.
101. Zhang, F. and X. Yu, *WAC, a functional partner of RNF20/40, regulates histone H2B ubiquitination and gene transcription.* Mol Cell, 2011. **41**(4): p. 384-97.
102. Lee, J.H., et al., *Ring finger protein20 regulates hepatic lipid metabolism through protein kinase A-dependent sterol regulatory element binding protein1c degradation.* Hepatology, 2014. **60**(3): p. 844-57.
103. Shema, E., et al., *RNF20 inhibits TFIIS-facilitated transcriptional elongation to suppress pro-oncogenic gene expression.* Mol Cell, 2011. **42**(4): p. 477-88.
104. Murawska, M., et al., *The Chaperone FACT and Histone H2B Ubiquitination Maintain S. pombe Genome Architecture through Genic and Subtelomeric Functions.* Mol Cell, 2020. **77**(3): p. 501-513 e7.
105. Shiloh, Y., et al., *RNF20-RNF40: A ubiquitin-driven link between gene expression and the DNA damage response.* FEBS Lett, 2011. **585**(18): p. 2795-802.
106. Ran, F.A., et al., *Genome engineering using the CRISPR-Cas9 system.* Nat Protoc, 2013. **8**(11): p. 2281-2308.
107. Zhang, K., et al., *Loss of H2B monoubiquitination is associated with poor-differentiation and enhanced malignancy of lung adenocarcinoma.* Int J Cancer, 2017. **141**(4): p. 766-777.
108. Wang, S., et al., *Current Diagnosis and Management of Small-Cell Lung Cancer.* Mayo Clin Proc, 2019. **94**(8): p. 1599-1622.
109. Lok, B.H. and C.M. Rudin, *Epigenetic targeting of DNA repair in lung cancer.* Proc Natl Acad Sci U S A, 2019. **116**(45): p. 22429-22431.
110. Arroyo, R., et al., *Systematic identification of molecular links between core and candidate genes in breast cancer.* J Mol Biol, 2015. **427**(6 Pt B): p. 1436-1450.
111. Toufektchan, E. and F. Toledo, *The Guardian of the Genome Revisited: p53 Downregulates Genes Required for Telomere Maintenance, DNA Repair, and Centromere Structure.* Cancers (Basel), 2018. **10**(5).

112. van Harn, T., et al., *Loss of Rb proteins causes genomic instability in the absence of mitogenic signaling.* Genes Dev, 2010. **24**(13): p. 1377-88.
113. Tsai, J.H. and J. Yang, *Epithelial-mesenchymal plasticity in carcinoma metastasis.* Genes Dev, 2013. **27**(20): p. 2192-206.
114. Khan, M.I., et al., *Role of epithelial mesenchymal transition in prostate tumorigenesis.* Curr Pharm Des, 2015. **21**(10): p. 1240-8.
115. Zhang, Y. and R.A. Weinberg, *Epithelial-to-mesenchymal transition in cancer: complexity and opportunities.* Front Med, 2018. **12**(4): p. 361-373.
116. Semenza, G.L., *Hypoxia-inducible factor 1: regulator of mitochondrial metabolism and mediator of ischemic preconditioning.* Biochim Biophys Acta, 2011. **1813**(7): p. 1263-8.
117. Jaaskelainen, T., et al., *Histone H2B ubiquitin ligases RNF20 and RNF40 in androgen signaling and prostate cancer cell growth.* Mol Cell Endocrinol, 2012. **350**(1): p. 87-98.
118. Chernikova, S.B., et al., *Deficiency in mammalian histone H2B ubiquitin ligase Bre1 (Rnf20/Rnf40) leads to replication stress and chromosomal instability.* Cancer Res, 2012. **72**(8): p. 2111-9.
119. Wang, Z.J., et al., *Decreased histone H2B monoubiquitination in malignant gastric carcinoma.* World J Gastroenterol, 2013. **19**(44): p. 8099-107.
120. Urasaki, Y., L. Heath, and C.W. Xu, *Coupling of glucose deprivation with impaired histone H2B monoubiquitination in tumors.* PLoS One, 2012. **7**(5): p. e36775.
121. Prenzel, T., et al., *Estrogen-dependent gene transcription in human breast cancer cells relies upon proteasome-dependent monoubiquitination of histone H2B.* Cancer Res, 2011. **71**(17): p. 5739-53.
122. Wang, D., et al., *RNF20 Is Critical for Snail-Mediated E-Cadherin Repression in Human Breast Cancer.* Front Oncol, 2020. **10**: p. 613470.
123. Tarcic, O., et al., *RNF20 and histone H2B ubiquitylation exert opposing effects in Basal-Like versus luminal breast cancer.* Cell Death Differ, 2017. **24**(4): p. 694-704.
124. George, J., et al., *Comprehensive genomic profiles of small cell lung cancer.* Nature, 2015. **524**(7563): p. 47-53.
125. Niederst, M.J., et al., *RB loss in resistant EGFR mutant lung adenocarcinomas that transform to small-cell lung cancer.* Nat Commun, 2015. **6**: p. 6377.
126. Kim, D.H., et al., *Epithelial Mesenchymal Transition in Embryonic Development, Tissue Repair and Cancer: A Comprehensive Overview.* J Clin Med, 2017. **7**(1).
127. Peng, J., et al., *Hypoxia-Inducible Factor 1alpha Regulates the Transforming Growth Factor beta1/SMAD Family Member 3 Pathway to Promote Breast Cancer Progression.* J Breast Cancer, 2018. **21**(3): p. 259-266.
128. McMahon, S., et al., *Transforming growth factor beta1 induces hypoxia-inducible factor-1 stabilization through selective inhibition of PHD2 expression.* J Biol Chem, 2006. **281**(34): p. 24171-81.
129. Zhang, Q., et al., *Wnt/beta-catenin signaling enhances hypoxia-induced epithelial-mesenchymal transition in hepatocellular carcinoma via crosstalk with hif-1alpha signaling.* Carcinogenesis, 2013. **34**(5): p. 962-73.
130. Higgins, D.F., et al., *Hypoxia promotes fibrogenesis in vivo via HIF-1 stimulation of epithelial-to-mesenchymal transition.* J Clin Invest, 2007. **117**(12): p. 3810-20.
131. Jeon, Y.G., et al., *RNF20 Functions as a Transcriptional Coactivator for PPARgamma by Promoting NCoR1 Degradation in Adipocytes.* Diabetes, 2020. **69**(1): p. 20-34.
132. Phan, L.M., S.C. Yeung, and M.H. Lee, *Cancer metabolic reprogramming: importance, main features, and potentials for precise targeted anti-cancer therapies.* Cancer Biol Med, 2014. **11**(1): p. 1-19.
133. Schodel, J., et al., *Hypoxia, Hypoxia-inducible Transcription Factors, and Renal Cancer.* Eur Urol, 2016. **69**(4): p. 646-657.
134. Semenza, G.L., *HIF-1 mediates the Warburg effect in clear cell renal carcinoma.* J Bioenerg Biomembr, 2007. **39**(3): p. 231-4.
135. Kim, J.W., et al., *HIF-1-mediated expression of pyruvate dehydrogenase kinase: a metabolic switch required for cellular adaptation to hypoxia.* Cell Metab, 2006. **3**(3): p. 177-85.
136. Briston, T., et al., *VHL-Mediated Regulation of CHCHD4 and Mitochondrial Function.* Front Oncol, 2018. **8**: p. 388.
137. Infantino, V., et al., *Cancer Cell Metabolism in Hypoxia: Role of HIF-1 as Key Regulator and Therapeutic Target.* Int J Mol Sci, 2021. **22**(11).
138. Semenza, G.L., *Regulation of the breast cancer stem cell phenotype by hypoxia-inducible factors.* Clin Sci (Lond), 2015. **129**(12): p. 1037-45.

139. Zhang, Y., et al., *HIF-1alpha is necessary for activation and tumour-promotion effect of cancer-associated fibroblasts in lung cancer.* J Cell Mol Med, 2021. **25**(12): p. 5457-5469.
140. Maxwell, P.H., et al., *Hypoxia-inducible factor-1 modulates gene expression in solid tumors and influences both angiogenesis and tumor growth.* Proc Natl Acad Sci U S A, 1997. **94**(15): p. 8104-9.
141. Denko, N.C., *Hypoxia, HIF1 and glucose metabolism in the solid tumour.* Nat Rev Cancer, 2008. **8**(9): p. 705-13.
142. Lu, H., R.A. Forbes, and A. Verma, *Hypoxia-inducible factor 1 activation by aerobic glycolysis implicates the Warburg effect in carcinogenesis.* J Biol Chem, 2002. **277**(26): p. 23111-5.
143. Sun, S., et al., *Hypoxia-inducible factor-1alpha induces Twist expression in tubular epithelial cells subjected to hypoxia, leading to epithelial-to-mesenchymal transition.* Kidney Int, 2009. **75**(12): p. 1278-1287.

Chapter 7: APPENDIX

Table 1. List of Abbreviations

Abbreviations	Term
AD	Adenocarcinoma
Anti-A	Antimycin-A
ccRCC	Clear Cell Renal Cell Carcinoma
2DG	2-Deoxy-D-Glucose
CIN	Chromosomal Instability
DAPI	4,6-diamidino-2-phenylindole
DSBs	Double Strand Breaks (DSBs)
ECAR	Extracellular acidification rate
EGTA	Ethylenglycol-bis(aminoethylether)
FCS	Fetal Calf Serum
FP	Forward Primer
h	Hour
H & E	Hemotoxylin and Eosin
HIF1a	Hypoxia Inducible Factor 1 Subunit Alpha
LOF	Loss of Function
LC-MS/MS	Liquid chromatography-mass spectrometry/mass spectrometry
LCNEC	Large Cell Neuroendocrine Carcinoma of the Lung
LOF	Loss of Function
µg	Microgram
µl	Microliter

µm	Micrometer
MDS	Myelodysplastic Syndrome
mg	Milligram
MIN	Microinstability
ml	Millileter
mm	Millimeter
MTS	3-(4,5-dimethylthazol-2-yl)-5-(3-carboxylmethoxyphenyl-2-(4-sulfophenyl)-2H-tetrazolum)
NaCl	Sodium Chloride
NADPH	Nicotinamide Adenine Dinucleotide Phosphate
NHEJ	Non-Homologous End Joining
nm	Nanometer
NSCLC	Non-Small Cell Lung Carcinoma
OCR	Oxygen Consumption Rate
OD	Optical Density
Oligo	Oligonucleotide
PBS	Phosphate Buffer Saline
PET	Positron Emission Tomography
PPP	Pentose Phosphate Pathway
qPCR	Quantitative Polymerase Chain Reaction
Rnf20	Ring Finger Protein 20
ROS	Reactive Oxygen Species
RPA	Replication Protein A
RT-qPCR	Reverse Transcriptase – Quantitative Polymerase Chain Reaction

SCC	Squamous Cell Carcinoma
SCLC	Small Cell Lung Carcinoma
shRNA	Short hairpin RNA
siRNA	Small interfering RNA
TCA	Tricarboxylic acid cycle
TCGA	The Cancer Genome Atlas Program
WHO	World Health Organisation
WT	Wild Type
+/-	Heterozygous
°C	Degree Centrigrade
µg	Microgram
µl	Microliter
µm	Micrometer

ACKNOWLEDGEMENT

I would like to offer my heartfelt gratitude to everyone who has supported and assisted me throughout my PhD journey.

I would like to acknowledge and give my warmest thanks to my supervisor Prof. Dr. Gergana Dobreva for allowing me to complete my thesis work at her Laboratory at the Max Planck Institute for Heart and Lung Research, Bad Nauheim and the Centre for Biomedicine and MedicineTechnique, Mannheim, Germany. I admire her positive attitude and drive, which reflected upon me during my PhD studies. I would like to thank her for constant support, helpful suggestions, critical thinking and advice. Without her support, it would have been tough for me to finish my PhD studies and dissertation.

I would like to express my gratitude to Prof. Dr. Reinhard Dammann, Institute for Genetics, Justus-Liebig-University Giessen for his valuable suggestions and feedback for my thesis work on a regular basis.

I would like to specially thank Dr. Michael Potente, Aniogenesis and Metabolism Laboratory, Max Planck Institute for Heart and Lung Research for providing me opportunity to perform Seahorse metabolic experiments in his Laboratory. I would also like to thanks Dr. Anuradha Doddabalapur for aquainting me with this technique.

I would like to show my gratitude to the Metabolomics Core Technology Platform at COS University of Heidelberg for metabolomics measurements and analysis.

I would also like to thank my former collegue Dr. Luca Caputo for helping me with suggestions and support during the first year of my PhD.

I would also want to thank my lab members and all the other members of the institute and collaborating groups for who helped me and contributed to this project.

I would also like to thank Dr. Natalia Fontagnier, my Deutsch language teacher, for grammar corrections in the Abstract of my thesis.

In the end I would like to thank my family members, especially my parents Mr. Ashok Singh and Mrs. Suman Singh as well as my brother Mr. Abhishek Kumar Singh. They constantly inspired, supported and encourage me though all walks of life during my PhD journey. I would want to express my gratitude to my spouse, Dr. Indrabahadur Singh, for

his inspiration, drive and support. I would also like to thank my daughter Arika Singh, who motivates me to work harder and be a better role model for her.

This work was supported by a grant from ‘’LOEWE-Initiative der Landesförderung“ (Wiesbaden Germany) (III L 4 – 518/15.004 2009) and the ‘’Deutsche Forschungsgemeinschaft“ (DFG, Bonn, Germany) (BA 4036/1-1).

EIDESSTATTLICHE **E**RKLÄRUNG

„Ich erkläre: Ich habe die vorgelegte Dissertation selbständig und ohne unerlaubte fremde Hilfe und nur mit den Hilfen angefertigt, die ich in der Dissertation angegeben habe. Alle Textstellen, die wörtlich oder sinngemäß aus veröffentlichten Schriften entnommen sind, und alle Angaben, die auf mündlichen Auskünften beruhen, sind als solche kenntlich gemacht. Bei den von mir durchgeführten und in der Dissertation erwähnten Untersuchungen habe ich die Grundsätze guter wissenschaftlicher Praxis, wie sie in der „Satzung der Justus-Liebig-Universität Gießen zur Sicherung guter wissenschaftlicher Praxis“ niedergelegt sind, eingehalten.“